AN OPTICAL STUDY OF CHALCOGENIDE GLASSES USING UV-VIS-NIR SPECTROSCOPY

by

Pankaj Sharma

**A THESIS SUBMITTED IN FULFILLMENT OF THE REQUIREMENTS
FOR THE DEGREE OF**

DOCTOR OF PHILOSOPHY

IN

PHYSICS

**JAYPEE UNIVERSITY OF INFORMATION TECHNOLOGY
WAKNAGHAT
MAY 2008**

CERTIFICATE

This is to certify that the thesis entitled, "**AN OPTICAL STUDY OF CHALCOGENIDE GLASSES USING UV-VIS-NIR SPECTROSCOPY**" which is being submitted by *Mr. Pankaj Sharma* in fulfillment for the award of degree of **Doctor of Philosophy** in **Physics** by **Jaypee University of Information Technology**, is the record of candidate's own work carried out by him under my supervision. This work has not been submitted partially or wholly to any other University or Institute for the award of this or any other degree or diploma.

Date: May 31, 2008

Prof. (Dr.) S. C. Katyal
Head
Department of Physics

To my parents, for their never ending support…………….

Acknowledgements

Date: May 31, 2008   (*Pankaj Sharma*)

Abstract

The work reported in this thesis is concerned with the study of optical properties of Ge-Se-Te system and the effect of metal impurities (Bi, Cd, Pb and Sn) on the optical properties of As-Se-Ge system. Various bulk samples and their thin films prepared and studied are:

1. $Ge_{10}Se_{90-x}Te_x$; x = 0, 10, 20, 30, 40, 50.
2. $(As_2Se_3)_{90}Ge_{10}$
3. $[(As_2Se_3)_{90}Ge_{10}]_{95}M_5$; M = Bi, Cd, Pb and Sn.

Bulk samples were prepared by melt quench technique. Thin films of prepared samples were deposited using thermal evaporation technique at base pressure of $\sim 10^{-4}$ Pa. X-ray diffraction technique has been used to know the nature (amorphous or crystalline) of bulk and deposited films. Far-infrared transmission spectra have been obtained from FT-IR spectrophotometer to study the bonding arrangements in Ge-Se-Te system. The optical properties (refractive index and extinction coefficient) have been estimated by analyzing the transmission spectra (200 – 2400 nm) obtained from ultraviolet-visible-near infrared spectrometer. Swanepoel's method has been used to determine refractive index and extinction coefficient. Optical band gap has been determined using Tauc extrapolation. The effect of deposition parameters (type of substrates, thickness and substrate temperature) has been examined on the refractive index and optical energy gap of Ge-Se-Te thin films. Physical properties (coordination number, density, compactness, theoretical energy gap, cohesive energy and heat of atomization) of Ge-Se-Te glassy alloys have also been determined. The effect of metal impurities (Bi, Cd, Pb and Sn) on the optical properties has been studied for As-Se-Ge thin films.

A brief description of the thesis, which has been divided into seven chapters, is given below.

General introduction of amorphous semiconductors and their classification, historical development of chalcogenide glasses (ChG), their binary and ternary compounds and the addition of metal impurities to ChG is described in chapter I. A brief introduction of general properties of ChG has also been given. Various

applications of ChG, motivation and objective of the thesis have also been included in this chapter.

Theoretical background used in the present work is presented in chapter II. This includes topics like structural models for ChG, various methods used in the present work for the calculation of optical parameters and a brief description of Wemple-DiDomenico single oscillator model.

Chapter III describes the experimental techniques used for the preparation of bulk glasses, deposition of thin films, characterization of bulk and thin films by X-ray diffraction, FTIR spectroscopy and optical studies using UV-Vis-NIR spectroscopy. Density measurement of bulk glasses has also been described.

Chapter IV contains experimental results, observations and general discussion of various studies on $Ge_{10}Se_{90-x}Te_x$ system. X-ray diffraction is used to check the nature of bulk as well as thin films. Far infrared transmission through 50 to 650 cm^{-1} of glassy alloys is described to study the bonding arrangements in ChG glasses. Optical parameters of Ge-Se-Te thin films are described using transmission spectrum of thin films. The effect of deposition parameters i.e. thickness of thin films, type of substrate, substrate temperature on the optical parameters of Ge-Se-Te thin films has also been given. The conclusions of the studies undertaken are given accordingly after each section.

Chapter V includes calculation of some physical parameters of $Ge_{10}Se_{90-x}Te_x$ system. The physical parameters calculated are coordination number, density and molar volume, compactness, lone pair of electrons, theoretical optical band gap, average heat of atomization and cohesive energy. The last section includes the conclusion of the study in this chapter.

Chapter VI deals with the studies of optical properties of $(As_2Se_3)_{90}Ge_{10}$ thin films and the effect of metal additives (Bi, Cd, Pb and Sn) on the optical properties of As-Se-Ge system. The conclusions of the studies undertaken are given accordingly after each section.

Chapter VII includes the summary of the results obtained through various studies.

List of Publications

1. **Pankaj Sharma** and S. C. Katyal, *"Far-infrared transmission and bonding arrangement in $Ge_{10}Se_{90-x}Te_x$ semiconducting glassy alloys"* **Journal of Non-Crystalline Solids** (2008) doi: 10.1016/j.jnoncrysol.2008.05.010.

2. **Pankaj Sharma** and S. C. Katyal, *"Effect of Tellurium Addition on the Physical Properties of Germanium Selenide Glassy Semiconductors"* **Physica B: Condensed Matter** (2008) doi: 10.1016/j.physb.2008.06.009.

3. **Pankaj Sharma** and S. C. Katyal, *"Effect of Ge addition on the optical band gap and refractive index of thermally evaporated As_2Se_3 thin films"* **Research Letters in Materials Science,** Vol 2008 (2008) doi:10.1155/2008/826402.

4. **Pankaj Sharma** and S. C. Katyal, *"Optical Study of $Ge_{10}Se_{90-x}Te_x$ Glassy Semiconductors"* **Thin Solid Films**, Vol 515 (2007) 7966.

5. **Pankaj Sharma** and S. C. Katyal, *"Determination of Optical Parameters of $a-(As_2Se_3)_{90}Ge_{10}$ Thin Film"* **Journal of Physics D: Applied Physics** Vol 40 (2007) 2115.

6. **Pankaj Sharma** and S. C. Katyal, *"Thickness Dependence of Optical Parameters for Ge-Se-Te Thin Films"* **Materials Letters**, Vol 61 (2007) 4516.

7. **Pankaj Sharma** and S. C. Katyal *"Calculation of optical constants in $a-Ge_{10}Se_{90-x}Te_x$ (x = 0, 30, 40) thin films"* **Journal of Optoelectronics and Advanced Materials**, Vol. 9 (2007) 2000.

8. **Pankaj Sharma** and S. C. Katyal, *"Theoretical Calculation of Physical Parameters of $Ge_{10}Se_{90-x}Te_x$ Glassy Alloys"* **Journal of Optoelectronics and Advanced Materials**, Vol. 9 (2007) 1994.

9. **Pankaj Sharma** and S. C. Katyal, *"Influence of Replacing Se in $Ge_{10}Se_{90}$ Glassy Alloy by 50 at. % Te on the Optical Parameters"* **Journal of Ovonic Research**, Vol. 2 (2006) 105.

10. **Pankaj Sharma**, V. Sharma, S. C. Katyal, *"Variations of optical constants in $Ge_{10}Se_{60}Te_{30}$ thin film"* **Chalcogenide Letters,** Vol. 3 (2006) 73.

11. **Pankaj Sharma** and S. C. Katyal, *"Effect of tin addition on the optical parameters of thermally evaporated As-Se-Ge thin Films"* **Materials Chemistry and Physics** (2007) **[**Communicated**].**

12. **Pankaj Sharma** and S. C. Katyal, "*Influence of metal impurities on the optical properties of $(As_2Se_3)_{90}Ge_{10}$ thin films*" **Vacuum** (2008) **[Communicated]**.

13. **Pankaj Sharma** and S. C. Katyal, "*Effect of substrate temperature on the optical parameters of thermally evaporated Ge-Se-Te thin films*" **Thin Solid Films** (2008) **[Communicated]**.

14. **Pankaj Sharma** and S. C. Katyal, "*Effect of deposition parameters on the optical energy gap and refractive index of a-Ge-Se-Te thin films*" **Philosophical Magazine** (2008) **[Communicated]**.

Conferences

15. **Pankaj Sharma**, Ishu Sharma and S. C. Katyal, "*Optical band gap and refractive index of vacuum evaporated a-$Ge_{10}Se_{90-x}Te_x$ (x = 0, 20) thin films*" **Recent advances in innovative materials (RAIM, NIT Hamirpur)** (2008) 134.

16. **Pankaj Sharma,** Ishu and S. C. Katyal, "*A Study of Ge Additive on the Optical Parameters of Arsenic Selenide*" **International Conference on Condensed Matter Physics (Univ. of Rajasthan, Jaipur, 25-28 Nov, 2007)** Tp. 56, p-123.

17. **Pankaj Sharma** and S. C. Katyal, "*A conjoins in theoretical and experimental optical band gap of Ge-Se-Te thin films*" **DAE-SSPS** Vol. 52 (2007) 597.

18. **Pankaj Sharma**, V. Sharma, S. C. Katyal, "*Refractive Index of Thin Films using Transmission Spectrum*" in Proceeding of **DAE-SSPS** Vol. 51 (2006) 425.

<u>Contents</u>

List of Figures

films.

30, 40, 50) glassy alloys.

List of Tables

CHAPTER I

Introduction

Solids are considered as materials with viscosities exceeding $10^{14.6}$ Poise while fluids (liquids and gases) have viscosities below this value. Generally, solids are characterized into two categories: crystalline solids and non-crystalline solids or amorphous solids. A crystal is a regular three dimensional design and is a consequence of the regular arrangement of atoms, ions or molecules of which it is built up. When this periodicity extends throughout a single piece of material one calls it a single crystal. A polycrystalline material is composed of tiny crystals. The periodicity of the structure in the poly crystalline materials is interrupted at the so called grain boundaries. The size of grains in which the structure is periodic may vary from macroscopic dimensions to a size much larger as compared to the size of the pattern unit. When the size of grains or crystallites become comparable to the size of the pattern unit one can no longer speak of crystals since essential feature of the crystalline material is the periodicity of the structure; one then speaks of non crystalline, amorphous or vitreous solids. The structure of non crystalline solid is not composed of repetitive three dimensional patterns of structural units. These solids do exhibits some local order either in the form of regular coordination polyhedra or of long chain molecules; they lack the long range order of crystals because their sub units are packed together randomly. A distinctive class of amorphous solids is glasses which are defined as amorphous solids obtained from the melt of a solid.

Amorphous solids, like crystalline solids, can be insulators, semiconductors and in some cases at very low temperature they can even be superconductors. It was Ioffe [1] who first pointed out that the basic electronic properties of a solid are determined from the character of bonds between nearest neighbours rather than by long range order. B. T. Kolomiets [2] while working on glasses observed that these glasses behave similar to intrinsic crystalline semiconductors. The chemical bond approach enabled Mooser and Pearson [3,4] to predict many of the semiconducting properties of the amorphous materials.

Amorphous semiconductors on the basis of difference in chemical bonding can be broadly classified into three major categories [5] as shown below

1. Covalent non-crystalline solids

    A. Tetrahedral semiconductors

        Si, Ge, SiC, InSb, GaAs, GaSb, …………

3

B. Chalcogenide glasses

    (i)   Lone pair semiconductors

            Se, S, Te, As_2Se_3, As_2S_3, ………

    (ii)   Cross-linked network

            Ge-Sb-Se, As-Se-Ge, Si-Ge-As-Te, As-Se-Te, As_2Se_3-As_2Te_3,

            Tl_2Se-As_2Te_3

2. Semiconducting oxide glasses

V_2O_5-P_2O_5 MnO-Al_2O_3-SiO_2

V_2O_5-PbO-Fe_2O_3 TiO-B_2O_3-BaO

…………………   ………………

3. Dielectric films

SiO_x, Al_2O_3, ZrO_2, BN, ………………..

      Among the above classification of non crystalline solids the present work shows interest in chalcogenide glasses.

1.1   Historical development of chalcogenide glasses

1.1.1 Chalcogenide glasses and their history

      Chalcogens are elements occupying group VI-A of periodic table – sulphur (S), selenium (Se) and tellurium (Te). The root chalco comes from a Greek word for copper and chalcogenide elements have traditionally been those which form strong compounds with copper. By extension chalcogenide glasses are named for their association between these chalcogens with electropositive materials and organic radicals. Typically any amorphous material containing an abundance of chalcogen atoms is referred to as a chalcogenide glass.

      It is difficult to assign a date that when the field of chalcogenide glasses has been started. For the vast majority of time the vitreous glassy state was limited to oxygen compounds and their derivatives. Schulz-Sellack [6] was the first to report data on oxygen free glass in 1870. Though vitreous selenium and arsenic selenide and sulphides were synthesized for the first time at the end of 19th century but the scientists were not attracted to these materials. Vitreous Se became of most interest

for scientific community at the beginning of 20th century when Wood [7] and Meier [8] reported first on the subject.

The rising of infrared (IR) optics in the 20th century lead to the need of new IR materials. Classical oxide glasses covered a transparency region from 3 μm to 5 μm while heavy oxide materials helped to extend this region up to 8 μm. the interest for the chalcogens comes from the attempt of scientist to extend the IR transparency region in glasses past 8 μm.

The first work on chalcogenide glasses (ChG) was attributed to Frerichs in the early 50 s on As_2S_3 glass [9,10] and As_2Se_3 by Fraser [11] and Dewulf [12]. Frerichs was also at the instigation of development of Se glasses and binary compounds with sulphur. Another scientist of vitreous ChG around that time was Winter-Klein [13]. The major research on ChG was started by two research groups from Saint-Petersburg (USSR), one group was led by B.T. Kolomiets and N.A. Goryunova from the "A.F. Ioffe Physico-Technical Institute" who were reported to discover the first semiconducting glass [14] based on chalcogen elements while the other group was led by R.L. Myuller. In 1968, S.R. Ovshinsky found memory and switching effects in ChG [15,16]. This led to the development of non-crystalline chalcogenide glasses in various fields such as xerography or computer memories. Around the same time Sir N. F. Mott (Nobel prize winner in Physics in 1977) and E.A. Davis developed the theory on the electronic processes in ChG [17]. After that several review books were published in subsequent years on glasses like "Chemistry of Glasses" by A. Paul in 1982 [18], "The Physics of Amorphous Solids" by R. Zallan in 1983 [19], "Physics of Amorphous Materials" by S.R. Elliott [20]. However the first review book entirely dedicated to chalcogenide materials, "Glassy Semiconductors", was published in 1981 by Z.U. Borisova who had worked with Myuller. In Moldova, A.M. Andriesh published in 1988 a book entitled "Glassy Semiconductors in Photoelectric Systems for Optical recording of Information" on ChG with special emphasis to their applications. In 2000, M.A. Popescu gave a detailed account on the physical and technological aspects of chalcogenide systems in his book "Non-Crystalline Chalcogenides" [21]. The Non-Crystalline Chalcogenides is the most detailed book published to date in the field of amorphous and glassy chalcogenide materials. The book covers the scientific and technological information on chalcogens (sulphur,

selenium and tellurium) and chalcogenide combinations. Detailed descriptions and a large corpus of physico-chemical data on these materials are the outstanding features of this book. The influence of various external factors, especially light, is treated in great detail and includes the latest news in the research of non-crystalline chalcogenides. The basic applications in optoelectronics are also discussed. The book is intended for use as a reference and research handbook

1.1.2 Compounds of chalcogenide glasses

1.1.2.1 Binary compounds

Chalcogens can form alloys together, viz. amorphous S-Se [22], Se-Te [23] and S-Te [24,25] compounds were identified, for different compositions by varying one or the other chalcogen. Many binary compounds can be synthesized by associating one of the chalcogen with another element of the periodic table. Among the most interesting elements, phosphorous (P), antimony (Sb), germanium (Ge), arsenic (As) and tin (Sn) are considered good network formers with chalcogen elements. Binary mixtures of Ge and As with Se are most commonly studied because they have large glass forming regions. Abrikosov et al [26] reported the phase diagram for the As-S and As-Se systems, the existence of As_2S_2 and As_2S_3 compound for the first system and AsSe and As_2Se_3 for the second system. The first phase diagram for Ge-Se system was studied by thermal and x-ray phase analysis [27]. Glass formation in Ge-Se system occurs predominantly in alloys enriched with Se containing 0 to 25 at. % of Ge [28]. Tronc et al [29] obtained glasses in Ge-Se system with compositions Ge_xSe_{1-x} where $0 \leq x \leq 0.4$ (from elemental Se to $GeSe_{1.5}$).

1.1.2.2 Ternary Compounds

In chalcogen system, glass formation region is relatively small [30]. Introduction of As, Ge and few other polyvalent elements into chalcogens contribute to considerable stabilization of their structure. Increasing the number of components tends to increase the glass forming range and ternary glasses have been formed with components from every column of periodic table. There are many ternary chalcogenide systems which form glasses over a wide range such as As-Se-Ge [31-

33], Ge-Se-Te [19,34], As-S-Se [35,36], As-Se-Te [37], As-Se-In [38], Ge-Se-In [39] etc.

1.1.3 Metallic additives in chalcogenide glasses

It was thought for a long time that amorphous semiconductors could not be doped because of the following two reasons (i) any foreign atom introduced into an amorphous matrix would take up its normal chemical valence because of supposed flexibility of the random network which is conducive to satisfy the local coordination and (ii) the density of states in the gap is sufficiently large so that the Fermi level does not shift by the addition of electrons and holes supplied by impurity atom.

The possibility of doping these materials was first demonstrated [40,41] in amorphous hydrogenated Si; for doping with hydrogen, a large impurity concentration was required [42,43]. In these studies the term modifier or additive is used for metal atoms introduced. Comparing to conventional dopants in crystalline semiconductors (in which one is considering dopant material in ppm) the modifier or additives are in much larger amounts ranging from a few atomic percent to sometime as high as 20 to 30 at. %.

On metallic addition interesting effects observed in chalcogenide glasses are (i) chemical modification of several chalcogenide glasses by introduction of large quantity of certain metals (ii) transformation in the type of electronic conductivity from the generally observed p type to n type on the addition of metals as Bi, Pb etc.

In general the addition of metal in multicomponent glasses can affect their spatial, structural, chemical, electronic and optical properties. These effects can be therefore being probed not only by studying the electrical conductivity but by a careful characterization and analysis of other properties as well.

1.2 General Properties of Chalcogenide glasses

1.2.1 Glassy structure

Zachariasen was the first to propose a geometrical model for the ideal glass in 1932 [44]. A definite range order is imposed when each and every atom fulfills the chemical valency requirements according to 8-N rule. The 8-N rule states that in most

stable covalent glass an atom with N valence electrons is coordinated such that it would have a completely filled outer shell of electrons. This geometrical model was later the subject of extensive reviews by Weyl and Marboe [45] and Rawson [46]. In 1954, Morey defined glasses as amorphous solids obtained from the melt [47]. Following this idea, Cohen and Turnbull developed the free volume model of the liquid state which implies that all liquids form an amorphous solid except for the intervention of crystallization [48]. The same authors described extensively how to prevent crystallization, i.e. greater the cooling rate and smaller the sample volume hence slower the crystallization rate, and developed numerous thermodynamic criteria [49] that formulate the problem in terms of experimental conditions and macroscopic parameters (such as viscosity). Thus the geometrical approach described earlier, which correlate the molecular constituents and structure to physical properties, can be considered in the end a complementary description to the kinetic approach.

Phillips [50] established his theory on calculation of sum of tensile and transverse stresses of covalent bonds for one atom to define the number of constraints (N_c). It is established that the maximum mechanical stability in coordinate space is obtained for a binary alloy A_xB_{1-x} with only short range interactions which supposed to led maximum glass forming ability [50,51] when short range order defined by bending and stretching forces is sufficient to exhaust the local degrees of freedom. However this criterion suffers from not taking into account long range interactions, ionicity and size effect.

Many other theories have been developed by researchers over the years such as Dieztel [52], Baydakov and Blinov [53] but none of them showed a universal aspect or can not be applied to multi element glasses. Though a large majority of researchers agree on following that after cooling a liquid below its melting point it will either form a glass or crystallize. During the glass formation viscosity, entropy, volume and internal energy changes continuously except in the vicinity of glass transition temperature (T_g) where these changes are often rapid.

The chalcogenide glass structure has been the object of extensive studies, considering both the bulk and thin film forms. Modeling a structure has proven difficult because of great flexibility in the choice of the molecular units in ChG. A vast study has been performed on binary and ternary chalcogenide glasses with As

and Ge as network formers. Goriunova and Kolomiets [54] pointed out the importance of covalent bonding in ChG as most important property to explain the stability of these glasses. As opposed to metallic bonding, covalent bonding ensures easier preparation of glasses. Thus cross linking initiated by As and Ge atoms should reduce the freedom for disorder since the bonds are covalent.

The emergence of Fourier transform infrared (FTIR) spectroscopy and Raman spectroscopy allows the researchers to identify the types of bond and their arrangements in bulk glasses as well as thin films. Ball et al [55] and Lucovsky [56] has used the FTIR spectroscopy for a wide range of germanium selenide glasses and gave a detailed account of structural arrangements in Ge-Se glasses. Boolchand et al [57] has used the Raman spectroscopy for germanium selenide glasses.

A characteristic to ChG is their electronic structure originating in the lone pair electron of chalcogen. For example, Se has four outer p-electrons of which two are used for covalent bonding and the two remaining electrons form a so called lone pair of electrons. This has been observed that there exists no essential difference in the band structure between crystalline and glassy chalcogenides. The two filled bonding (σ) p-states lie in the valence band and are separated from the empty (σ^*) states of conduction band by the band gap [58]. These lone pair states are associated with the defect model of Kastner, Adler and Fritzsche (Valence alteration pair or VAP) [59] and Mott and Street model (charged dangling bonds) [60].

1.2.2 Thermal properties

In any ChG system, increasing the relative chalcogen atomic mass or its atomic content with respect to other element in the network will diminish average bond energy and thus increases the glass transition temperature. The glass transition temperature in Ge-Se and Ge-Se-Te systems was reported by DeNeufville et al [23]. DeNeufville et al [23] have shown that with the increase of Te content to Ge-Se system glass transition temperature increases while the average bond energy decreases. The difference in the values of glass transition temperature found in the literature comes from various techniques used and the way the data was used and treated. This variation can be found for any type of data especially when it comes to results of thermal analysis. In Ge-Se system, the softening and melting temperature

(T_m) obtained from DSC increases with the increase of Ge content in Ge-Se system [23]. According to Thornburg and Johnson [61], T_m was shown to depend strongly on the heating rate while T_g showed a slight dependency.

1.2.3 Electrical properties

For most amorphous semiconductors, the temperature dependence of the (d.c.) electrical conductivity (σ) can be written for a long range of temperature as

$$\sigma = \sigma_0 \exp(-E_a/kT)$$

where σ_0 is the proportionality constant and E_a is the activation energy. The electrical conductivity of amorphous arsenic selenide as a function of temperature and dielectric constants has been reported by Kitao [62]. The activation energy was calculated to be equal to 1.05 eV and 0.9 eV respectively above and below 200°C, values correlated by Iovu et al [63]. Iovu [63] also measured a conductivity of 3 x 10^{-13} Ω^{-1}cm^{-1}. The electrical properties in impurity doped As-Se-Ge thin films have been reported by Katyal et al [64]. The electrical conductivity of Ge-Se-Te [65] at room temperature varies in the range 10^{-6} – 10^{-15} Ω^{-1}cm^{-1} while at softening temperature the electrical conductivity is 10^{-3} – 10^{-10} Ω^{-1}cm^{-1}. The electrical conductivity of the glasses of As-Ge-Se system ranges from $-\log\sigma_{20^0C} = 12.3$ to $-\log\sigma_{20^0C} = 17.1$ and decreases with increase of Ge content. Introduction of Ge to arsenic selenide thus lower the electrical conductivity. Borisova [65] reported a large set of electro-physical parameters (density, conductivity and activation energy) for As-Se and Ge-Se based glasses.

1.2.4 Optical properties

In ChG optical excitation of band edge electrons involves excitation of the lone pair electrons into the conduction band. Even in alloys, the optical behaviour of the glass is strongly determined by the nature and environment of the lone pair electrons. Sulphides usually are transparent in the high wavelength range of the visible region whereas selenides and tellurides are completely opaque. However they all are highly transmissive in the near IR and far IR regions, specifically near 12 μm, 15 μm and 20 μm for sulphides, selenides and tellurides respectively [66,67].

Due to lack of long range order in ChG, their absorption band is radically changed when comparing the crystalline and amorphous states [68].The optical band gap in As$_2$Se$_3$ was determined to be ~ 1.76 eV [65,66]. Gutenev [71] measured the refractive indices (*n*) of multiple amorphous glasses in the system As$_x$S$_{1-x}$ (0.10 < *x* < 0.44). According to Seddon [72] the refractive indices in the systems As-S and As-Se ranges from 2 to 3. Savage [66] has presented the refractive indices for multiple combinations of S, Se or Te with As, Ge, Sb and Si. The optical properties for thin films of chalcogenide glasses for different compositions were reported [73-77].

1.3   Applications of chalcogenide glasses

The optical properties of the ChG make them the candidate materials for a variety of optical applications. The wide range of compositions available and associated with variation in optical, thermal and mechanical properties enable these glasses to be engineered to suit a particular need. For example, some of the applications will require a high value of optical parameters (absorption edge and refractive index) while other require a low value. These apparently goals can be achieved in the ChG by adjusting the composition to select the appropriate properties of materials at the desired operating wavelength.

1.3.1 Xerography

Xerography, discovered by Carlson in 1938, is historically one of the first applications of chalcogenide materials in the industry. Many compositions are used in xerography, As$_2$Se$_3$ and As$_2$S$_3$ based films being often the materials of choice [78].

1.3.2 Infrared fibre optics

Infrared fibres are of great technological importance for communication, imaging, remote sensing and laser power delivery [79]. The chalcogenide glasses fit many of the material requirements for these varied applications [80]. They are chemically stable in air and can be drawn into long core clad fibres. Recently Sanghera et al [81] have shown that ChG have potential to permit new applications that are unachievable with current infrared materials.

The use of fibre optics to deliver high power laser light has led to significant advances in surgical techniques. Present optical fibres absorb light in the mid and far IR region and thus cannot be used for delivery of light in this region of wavelengths. Power up to 3 W at 10.6 μm has been carried without damaging fibres made of $Te_2Se_{3.9}As_{3.1}I$ [82]. This may be sufficient for some applications. However, further research would lead to compositions with much higher power handling capabilities.

ChG are likely to revolutionize the field of broadband infrared sensing. Broadband sensing is used for temperature measurement, pollution monitoring and infrared source detection [80].

1.3.3 Optical switching

With the proliferation of fibre optic networks comes the need to switch signals between different fibre segments. Traditionally this switching has been done by converting the optical signals into electrical signals and then using conventional microcircuits to route the signals onto the proper fibres. The speed of these electronic switches limits the speed of the entire optical network. The only way to overcome this bottleneck is to develop switches that are completely optical. Lucent technologies recently announced an optical switch that permits a tenfold increase in throughput over conventional switches [83]. High speed optical switching has been demonstrated with As_2S_3 based fibres [84-86]. Demultiplexing signals of 50 Gbit/s were achieved and the system has the potential to exceed 100 Gbit/s operations [86]. Switching can also be achieved with thin film devices. A thin film optical switch must have waveguides and other optical elements to direct the flow of light to the active region of the switch [87]. These waveguides could be formed on chalcogenide glasses either by photodarkening [88] or photodoping to create the proper variation in the index of refraction.

1.3.4 Optical limiting

Current interest in materials for optical limiting is high. The military is interested in protecting sensitive detectors from high power enemy laser fire. High intensity blasts from infrared lasers can destroy the sensitive detectors used for

guidance and military surveillance. One solution to protect against short laser bursts involves placing a nonlinear optical material in front of the detector [89]. Such a material must be transparent to low intensity IR light in the wavelengths of interest, but must react to high intensity threats. Materials with a non linear index of refraction will have a higher or lower index of refraction for the high power pulses. The change in index of refraction varies with the spatial profile of the beam and exposed region behaves as a graded index lens. The transient lens will defocus the laser on the detector plane thereby reducing the intensity of attacking laser to safe levels and protecting the sensor.

In recent years emphasis has been placed on acousto-optical devices [90] and optical media [91] or photonic band gap structures [92]. Other applications of ChG are in IR imaging [93], thermal imaging [94] etc. A detailed review on the applications of the chalcogenide glasses has been published [81].

The real possibilities of ChG have only been gleaned by some of the cited research but much more must be learned about the structure-property relationships in ChG before we will know the true potential for these glasses in mentioned applications.

1.4   Motivation and purpose of this research

The Chalcogenide glasses will enhance or revolutionize many of the products that operate with or on infrared light. Some of the examples of the potential benefits are presented in the above section. Chalcogenide infrared fibres are available today for spectroscopic applications but their applicability is still limited. Most of the other applications will only be realized after much further study of the properties of chalcogenide glasses. All of the applications depend on our ability to engineer glass compositions to meet the specific requirement of the system. The tailoring of chalcogenide glasses for specific properties is possible but we do not know enough about most of the glass systems to choose according to compositions. It is the intent of this research to develop a basic understanding of the optical behavior of chalcogenides. These results may lead directly to applications or more likely lay a foundation for other research into the optical behaviour of chalcogenide glasses.

Chalcogenide glasses are having relatively high atomic mass and weak bond strength resulting low characteristic phonon energies ($\sim$ 50 - 450 cm^{-1}) even relative to fluoride glasses ($\sim$ 550 cm^{-1}) [95]. Thus, chalcogenide glasses are highly transparent in the mid to far infrared and they originally attract technological and commercial interest for use in IR windows and optics. The transparency window of sulphide glasses is 0.5-12 μm, selenide glasses is approximately 0.8-15 μm while that of telluride glasses transparency window extends to 20 μm wavelength range [66,67]. Related to their narrow band gaps and high linear refractive index, chalcogenide glasses exhibit high nonlinearities in the near IR wavelength region [96]. Key challenges for the use of chalcogenides (S, Se and Te) include disadvantages like short lifetime and low sensitivity etc. Due to high glass forming ability of Se, it represents a good host matrix for the investigation of chalcogenide glasses in the bulk and thin film forms [97-100]. Thus, the above problems can be overcome by alloying Se with some impurity atoms (Bi, Sb, Ge, Ga, As etc), which gives higher sensitivity, higher crystallization temperature and smaller ageing effects [101-103]. Here we have chosen Ge as an additive to Se. Since alloying of Se with Ge improves the thermal stability and gives smaller aging effects. The third element added is Te, as this improves and enhances the IR transmission of Ge-Se glasses [66,67]. Further alloying of Te reduces the optical band gap and hence increases the photosensitivity towards longer wavelength [104]. Even to reduce the energy losses due to multiphonon absorption Te is added to these glass systems. Since the multiphonon absorption edges have been shifted to longer wavelength by increasing the amounts of heavier Te atoms and these Te-rich glasses are preferable for a CO_2 laser power transmitting glass fibres [105,106].

The present work is divided into two parts. The first part deals with the systematic study of the structural and optical properties of $Ge_{10}Se_{90-x}Te_x$ (x = 0, 10, 20, 30, 40, 50) thin films. Ge-Se system is the most studied system for its structural, electrical and optical properties. There is enough structural data on the Ge-Se systems but the structural study on the addition of Te to Ge-Se for these particular compositions have not been performed well. So we have studied the effect of Te addition on the structural properties of Ge-Se system using FTIR spectroscopy. On the other hand what happens to the Ge-Se system, on account of its optical properties

when Te is alloyed to it, is considered important as this was observed that adding Te to Ge-Se increases the transmission region [107]. So we have decided to go for the studies of optical properties of the $Ge_{10}Se_{90-x}Te_x$ (x = 0, 10, 20, 30, 40, 50) thin films in details. Also the effect of deposition parameters i.e. thickness of thin films, type of substrate, substrate temperature on the optical properties of Ge-Se-Te thin films has been described. Along with structural and optical properties some of the physical parameters have also been calculated for $Ge_{10}Se_{90-x}Te_x$ glassy alloys which support our experimental results.

The second part deals with the optical study of $(As_2Se_3)_{90}Ge_{10}$ thin films. The effect of metal additives on the optical properties of $[(As_2Se_3)_{90}Ge_{10}]_{95}M_5$, where M = Bi, Sn, Pb and Cd, thin films has also been studied. As-Se-Ge is a much widely studied glass system because of the fact that Ge, As and Se are the elements of same period in groups IV-VI and brings about the covalent character of the interaction between their atoms. This result in a broad glass formation region in As-Se-Ge system [65] among all investigated three component chalcogenide systems. Earlier it was believed that chalcogenide glasses are insensitive to added impurities but in recent research scenario, it has been observed that chalcogenide glasses are sensitive to composition, impurities and deposition parameters like thickness, substrate type and substrate temperature [108-113]. Recent experiments [113,114] reveal that the addition of impurities likes Bi and Pb have produced a remarkable change in the optical and electrical properties of chalcogenide glasses. In As-Se-Ge system the addition of Bi, Cd, Sn and Pb impurities, which have a large electronegativity difference with As, Se and Ge atoms, are supposed to modify the structure of As-Se-Ge system and thus it's electrical and optical properties. The electrical properties of these impurities added As-Se-Ge system have already been reported [64] but not the optical properties. This is conjectured that the addition of metal impurities in $(As_2Se_3)_{90}Ge_{10}$ thin films may change its optical properties remarkably. Thus, a thorough study of optical properties is considered crucial to have better understanding of the system.

References

1.   Ioffe A F 1951 *Bull. Acad. Sci. USSR* **15** 447

2.   Kolomiets B T 1964 *Phys. Stat. Solidi* (*b*) **7** 359, 713

3.   Mooser E, Pearson W B 1956 *Phys. Rev.* **101** 1608

4.   Mooser E, Pearson W B 1960 *Progresses in Semiconductors V* (London : Butterworth)

5.   Fritzsche H 1972 *Annual Review Report of Material Science* **2** 697

6.   Schultz-Sellack C 1870 *Annalen der Physik und Chemie* **139** 182

7.   Wood R W 1902 *Phil. Mag.* **3** 607

8.   Meier W 1910 *Annalen der Physik und Chemie* **31** 1017

9.   Frerichs R 1950 *Phys. Rev.* **78** 643

10.   Frerichs R 1953 *J. Opt. Soc. Am.* **43** 1153

11.   Fraser W A 1953 *J. Opt. Soc. Am.* **43** 823

12.   Dewulf G 1954 *Rev. Opt.* **33** 513

13.   Winter Klein A 1955 *Verres et Refractaires* **9** 147

14.   Goriunova N A, Kolomiets B T 1955 *Zhurnal Tekhnicheskoi Fiziki* **25** 2069

15.   Ovshinsky S R 1968 *Phys. Rev. Lett.* **21** 1450

16.   Ovshinsky S R 1970 *J. Non-Cryst. Solids* **2** 99

17.   Mott N F, Davis E A 1979 *Electronic Processes in the Non-Crystalline Materials* (Oxford : Clarendon Press)

18.   Paul A 1990 *Chemistry of Glasses*, Second Edn (Dordrecht: Kluwer Academic)

19.   Zallan R 1983 *The Physics of Amorphous Solids* (New York: John Wiley)

20.   Elliott S R 1990 *Physics of Amorphous Materials* Second Edn (Longman:New York)

21.   Popescu M 2000 *Non-Crystalline Chalcogenides* (Dordrecht: Kluwer Academic)

22.   Gill W D and Street G B 1973/1974 *J. Non-Cryst. Solids* **13** 120

23.   Sarrach J, de Neufiville J P and Hawoth W L 1976 *J. Non-Cryst. Solids* **22** 245

24.   Hawes L 1963 *Nature* **198** 1267

25.   Li D T, Sharma R C and Chang Y A 1989 *Bulletin Alloy Phase Diagrams* **10** 348

26.   Abrikosov N Kh, Bankina V F, Poretskaya L V, Shelimova L E and Skudnova E V 1969 *Semiconducting II-VI, IV-VI and V-VI Compounds* (New York : Plenum Press)

27.   Chun-Hua L, Pashinkin A S and Novoselova A V 1962 *Dokl. Acad. Nauk SSSR* **146(5)** 1092

28.   Kislitskaya E A, Nosov V B and Kokorina V F 1977 *Fiz. Khim. Stekla* **3(6)** 624

29.   Tronc P, Bensonssan M, Brenac A and Cebenne C 1973 *Phys. Rev. B* **15** 1

30.   Suvorova L N, Borisova Z U and Orlova G M 1974 *Izv. Acad. Nauk SSSR, Neorg. Mater.* **10(3)** 441

31.   Vinogradova G Z, Dembovskii S A and Luzhnaya N P 1968 *Zh. Neorg. Khim.* **13(5)** 1444

32.   Nemilov S V 1964 *Zh. Prikl. Khim.* **37(7)** 1452

33.   Nemilov S V 1964 *Zh. Prikl. Khim.* **37(8)** 1699

34.   Pazin A V, Obraztsov A A and Borisova Z U 1972 *Izv. Acad. Nauk SSSR, Neorg. Mater.* **8(2)** 247

35.   Flaschen S S, Pearson A D and Northover W R 1959 *J. Am. Ceram. Soc.* **42(9)** 450

36.   Flaschen S S, Pearson A D and Northover W R 1960 *J. Am. Ceram. Soc.* **43(5)** 274

37.   Ligero R A, Casas-Ruiz M, Vazquez J and Jimenez-Garay R 1993 *Physics and Chemistry of Glasses* **34(1)** 12

38.   Flaschen S S, Pearson A D and Northover W R 1960 *J. Appl. Phys.* **31(1)** 219

39.   Saffarini G 2002 *Applied Physics A : Materials Science & Processing* **74**(2) 283

40.   Spesr W E and Lecombor P J 1976 *Phil. Mag.* **33** 935

41.   Paul W, Lewis A J, Connell G A N and Moustakas T D 1976 *Solid State Commun.* **20** 969

42.   Araki M and Zaki H 1976 *Solid State Commun.* 18 1603

43.   Ovshinsky S R 1977 *Amorphous and Liquid Semiconductors* Ed. Spear W E (*Proc. 7th International Conf. on Amor. and Liq. Semiconductors, Edinburg*) 519

44. Zachariasen W H 1932 *J. Am Chem. Soc.* **54** 3841

45. Weyl W A, Marboe E C 1962 *The Constitution of Glasses : A Dynamic Interpretation* **1 & 2** (New York : Interscience Pub.)

46. Rawson H 1967 *Inorganic Glass Forming Systems* (New York : Academic Press)

47. Morey G W 1954 *The Properties of Glasses* (New York : Reinhold Pub.)

48. Cohen M H and Turnbull D 1959 *J. Chem. Phys.* **31** 1164

49. Cohen M H and Turnbull D 1960 *Modern Aspects of Vitreous State* **1** (London : Butterworth)

50. Philips J C 1979 *J. Non-Cryst. Solids* **34** 153

51. Thorpe M F 1983 *J. Non-Cryst. Solids* **57** 355

52. Dietzel A 1942 *Z. Electrochem.* **48** 9

53. Baydakov L A and Blinov L N 1987 *Fisika Khim. Stekla* **13** 340

54. Goriunova N A and Kolomiets B T, Shilo V P 1958 *Soviet Phys. Tech. Phys.* **3** 917

55. Ball G J and Chamberlain 1978 *J. Non-Cryst. Solids* **29** 239

56. Lucovsky G, Galeener F L, Keezer R C, Geils R H and Six H A 1974 *Phys. Rev. B* **10** 5134

57. Boolchand P, Bresser W, Zhang M, Wu Y, Wells J and Enzweiler R N 1995 *J. Non-Cryst. Solids* **182** 143.

58. Kastner M 1973 *Phys. Rev. B* **7** 5237

59. Kastner M, Adler D and Fritzsche H 1976 *Phys. Rev. Lett.* **37** 1504

60. Street R A and Mott N F 1975 *Phys. Rev. Lett.* **35** 1293

61. Thornburg D D and Johnson R I 1975 *J. Non-Cryst. Solids* **17** 2

62. Kitao M 1972 *Jap. J. Appl. Phys.* **11** 1472

63. Iovu M, Shutov, Popescu M, Furniss D, Kukkonen L and Seddon A B 1999 *J. Optoelect. and Adv. Commun.* **1** 15

64. Katyal S C, Okano, Bando T and Suzuki M 1987 *J. Non-Cryst. Solids* **97&98** 1195

65. Borisova Z U 1981 *Glassy Semiconductors* (New York : Plenum Press)

66. Savage J A 1985 *Infrared Optical Materials and their Antireflection Coatings* (London : Adam Hilger)

67. Hocdé S, Boussard-Plédel C, Fonteneau G and Lucas J 2001 *Solid State Sciences* **3** 279

68. Tauc J 1974 *Amorphous and Liquid Semiconductors* (New York : Plenum Press)

69. Tanaka K 1980 *J. Non-Cryst. Solids* **35 & 36** 1023

70. Skordeva E 1999 *J. Optoelect. and Adv. Commun.* **1** 43

71. Gutenev M S 1985 *Fiz. Him. Stekla* **11(3)** 311

72. Seddon A B 1995 *J. Non-Cryst. Solids* **184** 44

73. Othman A A, Aly K A and Abousehly A M 2007 *Thin Solid Films* **515** 3507

74. Elliot S R 2005 *Material Science and Technology A Comprehensive Treatment Vol 9* Ed. Chan R.W et al (New York : John Wiley & Sons)

75. Khan S A, Zulfequar M and Husain M 2002 *Physica B* **324** 336

76. Farid A M 2002 *Egypt J. Sol.* **25(1)** 23

77. Wahab L A and Amer H H 2005 *Egypt J. Sol.* **28(2)** 255

78. Mort J 1989 *The Anatomy of Xerography* (London: McFirland & Co.)

79. Miyashita T and Manabe T 1982 *IEEE J. Quantum Electron.* **18(10)** 1432

80. Klocek P, Roth M and Rock R D 1987 *Opt. Eng.* **26(2)** 88

81. Sanghera J S and Aggarwal I D 1999 *J. Non-Cryst. Solids* **256 & 257** 6

82. Blanchetière C, Le Foulgoc K, Ma H L, Zhang X H and Lucas J 1995 *J. Non-Cryst. Solids* **184** 200

83. http://www1.alcatel-lucent.com/gsearch/search.jhtml?_requestid=227431

84. Asobe M, Kanamori T and Kubodera K I 1993 *IEEE J. Quantum Electron.* **29(8)** 2325

85. Asobe M, Ohara T, Yokohama I and Kaino T 1996 *Electron Lett.* **32(15)** 1396

86. Uchiyama K, Morioka T, Saruwatari, Asobe M and Ohara T 1996 *Electron Lett.* **32(17)** 1601

87. Andriesh A M 1985 *J. Non-Cryst. Solids* **77&78** 1219

88. Ramachandran S and Bishop SG 1999 *Appl. Phys. Lett.* **74(1)** 13

89. VanStryland E W, Wu Y Y, Hagan D J, Soileau M J and Mansour K 1988 *J. Opt. Soc. Am. B* **5(a)** 1980

90.   Seddon A B and Laine M J 1997 *Physics and Applications of Non-Crystalline Semiconductors in Optoelectronics* Ed. Andriesh A and Bertolotti M (Dordrecht : Kluwer)

91.   Lucas J, Fonteneau G, Bonnagad, Hua Z X 1987 *New Materials for Optical Waveguides* SPIE **799** 101

92.   Dale G, Langford R M, Ewen P J S and Reeves C M 2000 *J. Non-Cryst. Solids* **266-269** 913

93.   Yang K, Wu P, Wei G and Yu B 1995 *J. Non-Cryst. Solids* **184** 40

94.   Suto H 1997 *Infrared Phys. Technol.* **38** 93

95.   Gauglitz G and Vo-Dinh T 2003 *Handbook of Spectroscopy* (Wiley-VCH Verlag : Weinheim)

96.   Slusher R E, Lenz G, Hodelin J, Sanghera J, Shaw L B and Aggarwal I D 2004 *J. Opt. Soc. Amer. B* **21** 1146

97.   Reddy K V, Bhatnagar A K and Srivastava V 1992 *J. Phys.: Condens. Matter* **4** 5273

98.   Othman A A, Tahon K and Osman M A 2002 *Physica. B* **311** 356

99.   Mott N F and Davis E A 1979 *Electronic Processes in Non-Crystalline Materials* (Oxford : Clarendon)

100.   Othman A A 2006 *Thin Solid Films* **515** 1634

101.   Shimakawa K 1985 *J. Non-Cryst. Solids* **77–78** 1253

102.   Shim J Y, Park S W and Baik H K 1997 *Thin Solid Films* **292** 31

103.   Saitar J M, Ledru J, Hamou A and Saffarini G 1998 *Physica B* **245** 256

104.   Vaezi-Nejad S M and Juhasz C 1988 *J. Mat. Sci.* **23**

105.   Calventus Y, Surinach S and Baro M D 1997 *Mater. Sci. Eng. A* **226-228** 818

106.   Wang Z, Tu C, Li Y and Chen Q 1995 *J. Non-Cryst. Solids* **191** 132

107.   Othman A A, Aly K A and Abousehly A M 2007 *Thin Solid Films* **515** 3507

108.   Tigau N, Ciupina V, Rusu G I, Prodan G, Vasile E 2005 *Rom. Journ. Phys.* **50** 859

109.   Ahmed E, Tomlinson R D, Pilkington R D, Hill A E, Ahmed W, Nasar Ali and Hassan I U 1998 *Thin Solid Films* **335** 54

110.   Parlak M and Ercelebi C 1998 *Thin Solid Films* **322** 334

111.	Pathinettam Padiyan D, Marikani A and Murali K R 2004 *Mater. Chem. Phys.* **88** 250

112.	Bacaksiz E, Basol B M, Altunbas M, Novruzov, Yanmaz E and Nezir S 2007 *Thin Solid Films* **515** 3079

113.	El-Samanoudy M M, 2003 *Thin Solid Films* **423** 201

114.	Pattanaik A K and Srinivasan A 2004 *Semicond. Sci. Technol.* **19** 157

CHAPTER II

Theoretical Background

A short theoretical background has been presented in this chapter. This includes the structural models for chalcogenide glasses; methods to determine optical properties and Wemple – DiDomenico model.

2.1   Structural models for chalcogenide glasses

The atom scale structure of glasses is approached by presenting a method for systematically describing the development of the local order in a binary system $A_{1-x}B_x$ (A = Ge, As; B = S or Se) where A and B are atomic species from column a and b of the periodic table [1]. The network structure of the amorphous solids can be specified in three stages (i) atomic coordination (ii) distribution of bonds between the atoms and (iii) the molecular structure of the network forming groups. It is assumed that all bonds with in the network are satisfied. In melt quenched glasses, the coordination at each atom satisfies the normal chemical valence given by 8-N rule. There are two ways to specify distribution of bonds in a covalent network. The first is purely statistical and is known as "Random Covalent Network Model" (RCNM) [2]. For a binary system $A_{1-x}B_x$, the distribution is completely determined by the two atomic coordinations and the concentration. Considering the atomic coordination for A as m and for B as n and normalizing the alloy composition to one atom, the number of bonds of a particular type is given by

$$N_{AA} = m^2(1-x)^2 \big/ 4N_t \tag{2.1}$$

$$N_{BB} = n^2 x^2 \big/ 4N_t \tag{2.2}$$

$$N_{AB} = mnx(1-x) \big/ 2N_t \tag{2.3}$$

where N_t is total number of bonds and is simply one half of the total coordination i.e.

$$N_t = [m(1-x) + nx] \big/ 2 \tag{2.4}$$

The RCNM includes A-A, A-B, B-B bonds for all compositions except for x = 0 and x = 1. This distribution, therefore, neglects all factors especially the relative bond energies which could promote a non-statistical distribution.

The second model for the bond distribution is called chemically ordered network model (CONM) [3] which emphasizes just on the relative bond energies and thereby favours heteropolar A-B bonds for all concentrations [4]. This model includes a

compound composition, $x_c = m/m+n$ in which there are only A-B bonds. The composition range given by $x_c < x \leq 1$ is called B-rich alloy regime and contains A-B and B-B bonds whereas the range $0 \leq x < x_c$ is called A-rich and has A-B and A-A bonds. The total number of bonds in any composition is still given by equation (2.4), but now the bond distribution must be specified separately for the alloy regimes defined above and for the compound composition x_c.

$$N_{AA} = 0, \quad N_{AB} = m(1-x), \quad N_{BB} = [(m-n)x - m]/2 \quad \text{for} \quad x_c < x \leq 1 \tag{2.5}$$

$$N_{AA} = 0, \quad N_{BB} = 0, \quad N_{AB} = mn/(m+n) \quad \text{for} \quad x = x_c \tag{2.6}$$

$$N_{AA} = [m-(m-n)x]/2, \quad N_{AB} = nx, \quad N_{BB} = 0 \quad \text{for } 0 \leq x < x_c \tag{2.7}$$

Figures 2.1 and 2.2 illustrates the bond distribution for two important classes of alloy systems, $m = 3$, $n = 2$ and $m = 4$, $n = 2$. Ge-Se and As-Se alloys corresponds to 4-2 and 3-2 alloys. Here in the present study we are concerned with chemically ordered compounds in Ge-Se. For 4-2 alloys the cluster is AB_4 and for 3-2 alloys the cluster is AB_3. The three dimensional character of the local molecular cluster depends on the nature of the bonding orbitals of the central atom. Clusters in Ge-Se and As-Se have tetrahedral and pyramidal structures. In the B-rich alloy regime there are only A-B and B-B bonds and the local clusters at the A atom sites are the same clusters that characterize the compound compositions and their number is simply proportional to the number of atoms. If B is two-fold coordinated then the general form of a second molecular cluster is B_n where $n \geq 2$. The local molecular cluster in the A rich alloy regime cannot be specified in a unique way since only some of the more highly coordinated A atoms must have both A and B type immediate neighbours. For 3-2 alloys there are four pyramidal clusters AB_3, AB_2A, ABA_2 and AA_3. For 4-2 alloys there are five tetrahedral clusters AB_4, AB_3A, ----- etc. An alternate way of describing molecular clusters in the A-rich regime is based on the existence of additional compound compositions in which the network forming clusters have both A-A and A-B bonds. Figure 2.3 shows the molecular cluster in Ge-X and As-X (X = S, Se or Te) for X-rich and Ge or As-rich regimes. Infrared and Raman spectra provide additional information on the structure of molecular clusters in glasses. By comparing glassy spectra with crystalline spectra and utilizing quasi-selection rules regarding infrared
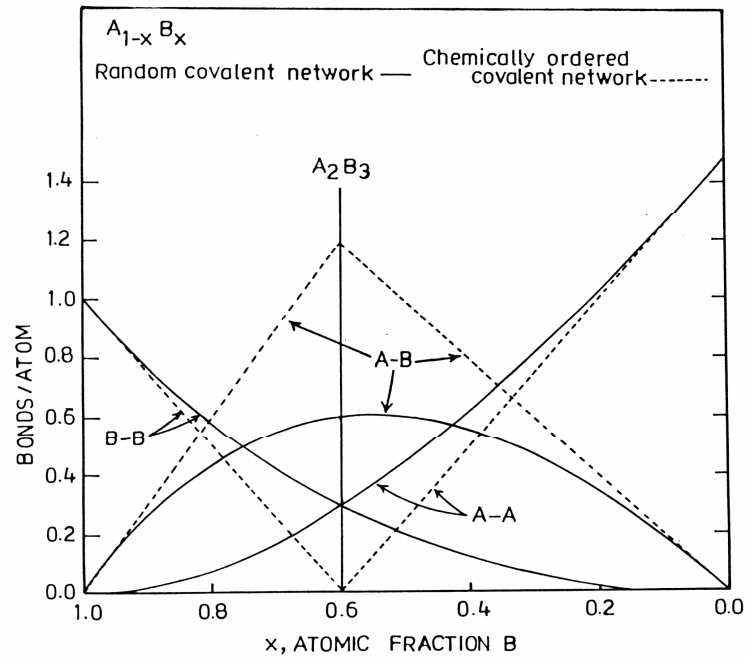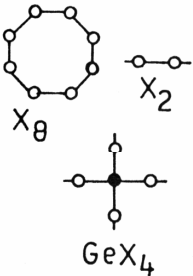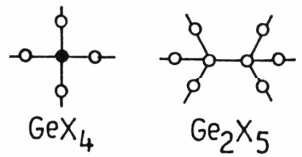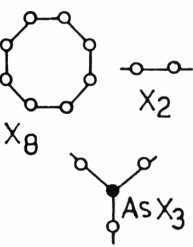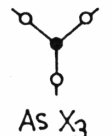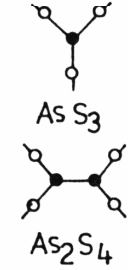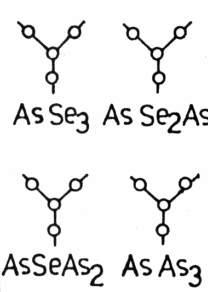
Figure 2.1 Bond counting statistics for 3-2 coordinated alloy $A_{1-x}B_x$. The solid lines are derived from RCN model and dashed lines from CON model.
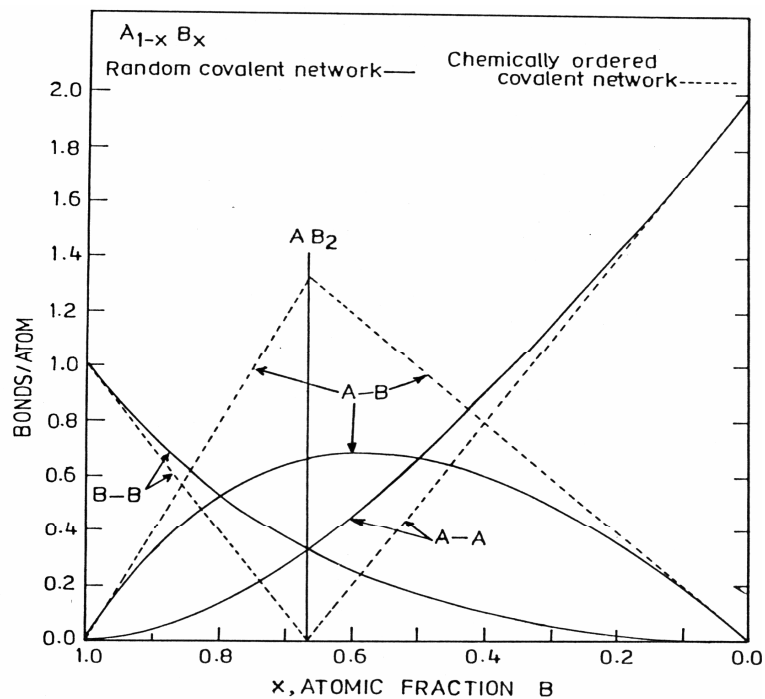
Figure 2.2 Bond counting statistics for 4-2 coordinated alloy $A_{1-x}B_x$. The solid lines are derived from RCN model and dashed lines from CON model.

27

Figure 2.3 A schematic representation of the molecular structures in the alloy system $Ge_{1-x}Ch_x$ and $As_{1-x}Ch_x$ ($Ch = S, Se$).
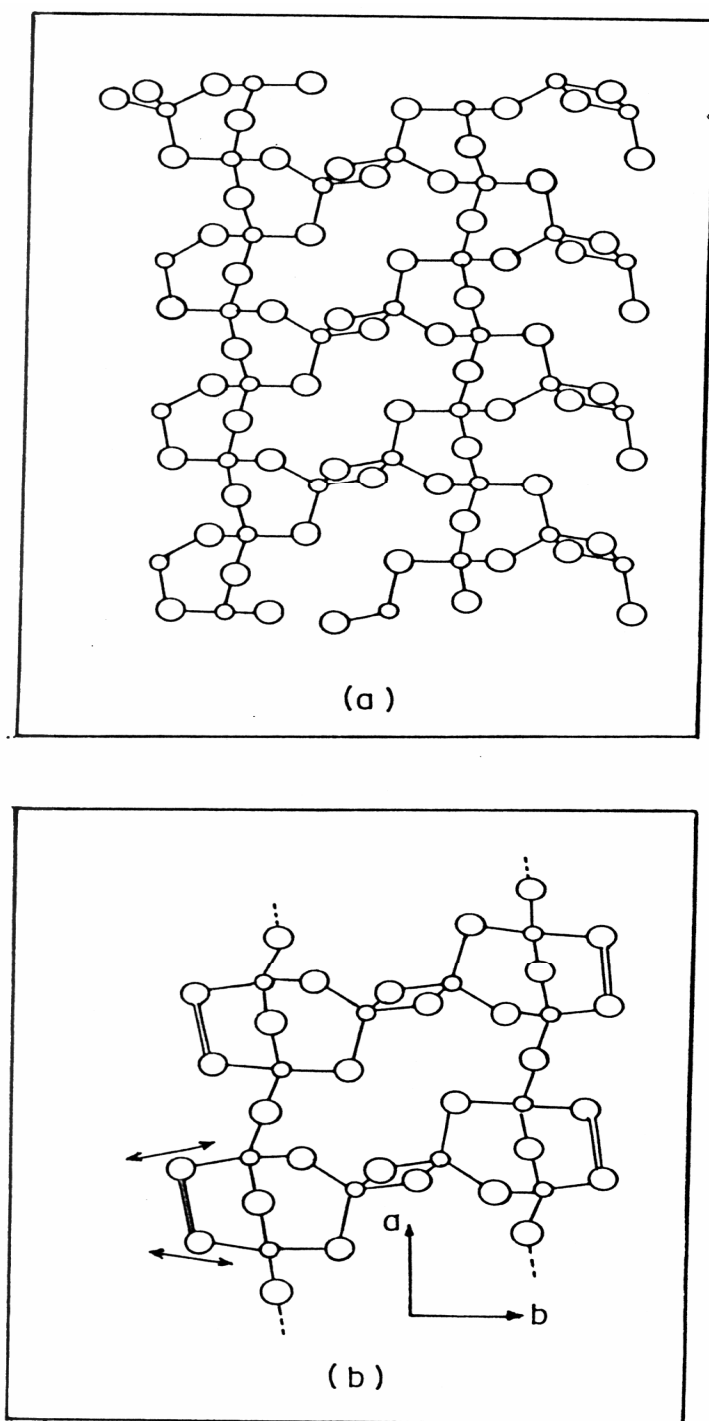
Figure 2.4 Molecular models of: (a) one layer of the high temperature form of $GeSe_2$ and (b) the smallest unit of a particularly polarized cluster in the glass. Ge-atoms are represented by the small balls.

versus Raman activity, one may be able to identify local vibrational modes in the glass which are also present in the crystal. The high temperature crystal structure has been determined [5,6] in both GeX_2 (X = S, Se). It is a layer structure with the basic units consisting of central Ge layers covered by outer chalcogen layers. Again $Ge[S_{1/2}(Se_{1/2})]_4$ tetrahedra are the basic structural units. In the (a,b) plane corner sharing tetrahedra form chains parallel to a-axis. In order for these chains to be cross-linked without very large distortions of bond angles two tetrahedra share edges [7] (a kind of 3-dimensional analogue of diborane, H_2-B-H_2-B-H_2) as shown in figure 2.4(a). Bridenbaugh et al [8] proposed that the basic structural unit in g-Ge(S,Se)$_2$ is a large cluster which is a fragment of the layer crystal structure which is still polymerized along the a-axis but is terminated along the b-axis by Se dimmer as shown in figure 2.4(b).

2.2   Methods to determine optical properties

Optics is the study of the interaction of light with matter. Light is quantized electromagnetic wave, the quantum units of which are photons. Matter is a conglomeration of atoms, which are composed of electrons, protons and neutrons. Photons interact with charged particles in matter. The nature of this interaction between light and matter is expressed in the dielectric response of the material. The complex dielectric response, ε^*, is also called the dielectric constant, an unfortunate misnomer since it is a function of wavelength of light. The entire interaction of light with matter is contained in the dielectric response and the dielectric response can be calculated from the information about the atomic and electronic structure of the material. So if the structure is known the interaction of light can be calculated. Conversely, the interaction of material with light gives information about the structure of that material via the dielectric response. The dielectric response can be calculated from the complex refractive index. The techniques used to calculate the optical parameters like refractive index (n), extinction coefficient (k), absorption coefficient (α), thickness of thin film (d) and optical band gap (E_g^{opt}) are described in this section.

2.2.1 Refractive index and extinction coefficient

The refractive index of a substance is the ratio of the speed of light in vacuum to the speed of light in that substance. Optical glasses suitable for applications in the IR region should have a high transparency in this spectral range. In addition and according to Lloyd, their refractive indices must have high values and as independent of temperature as possible [9]. However such indices thereby require specific anti-reflection coatings to mitigate the corresponding high Fresnel losses that scale with index. In materials, the photons are absorbed and re-emitted by molecules, which slows down the speed of light. This retardation is represented in Maxwell's equations by having the parameters μ, ε and σ depart from there free space values [10]. The refractive index can be written as

$$n = \left(\frac{\varepsilon \mu}{\varepsilon_0 \mu_0} \right)^{1/2} \tag{2.8}$$

From the Maxwell's equations, the complex refractive index related to complex dielectric constant can also be resolved into real and imaginary components as

$$n^* = n - ik \tag{2.9}$$

It is customary to define n as the refractive index and k as the extinction coefficient or absorption index. This index is a function of the wavelength, so the beams with different colours (or frequencies) travel at different speeds.

There are various methods to estimate the optical parameters n and k but here we are concerned only with those which are applicable to thin films only. Since films are not self supporting, a suitable supporting substrate is used for deposition. This results in a system consisting of three dielectrics namely air, thin film and substrate. It is also possible that both the film and substrate may be transparent or partly or opaque to the incident light. Hence the methods will considerably depend on the optical nature of film. The basic principle is however to measure the reflected or transmitted light or both along with that of the incident one. The last may or may not be polarized. The values of n and k of air or vacuum are taken as 1 and 0. The methods to determine n and k [11] are grouped into categories depending on the mode used such as **(i)** both reflection and transmission **(ii)** only reflection **(iii)** only transmission.

(i) Reflection and transmission method

In this method both reflectance and transmittance are used to calculate the optical constants separately. Reflectance (R) and transmittance (T) are measured at the normal incidence. Transmittance is given by the relation

$$T = \frac{16 n_s (n^2 - k^2) \exp(-4\pi k d / \lambda)}{\{(n+1)^2 + k^2\} \{(n_s + n)^2 + k^2\}} \tag{2.10}$$

where n and n_s are the refractive indices of the thin film and substrate respectively, d is the thickness of the thin film. Further T and R are related by the following relation

$$T = (1 - R)^2 \exp(-4\pi k d / \lambda) \tag{2.11}$$

Extinction coefficient can be determined from the variation T with film thickness given by the relation

$$k = -\frac{2.303 * \lambda}{4\pi d} \log T \tag{2.12}$$

(ii) Reflection method

In this case reflectance from an absorbing surface is measured at normal incidence. n and k are estimated roughly with the help of following relation

$$R = \frac{(n-1)^2 + k^2}{(n+1)^2 + k^2} \tag{2.13}$$

If $(n-1)^2 >> k^2$, then n can reasonably be determined from R. However, a second measurement at another angle of incidence is necessary for the evaluation of n and k.

(iii) Transmission method

This method was basically proposed by J. C. Manificier [12] and extended by Swanepoel [13]. This method considers only transmission spectra of thin films for the calculation of optical parameters. Swanepoel's method has advantage due to its non destructive nature and yield the dispersion relation over a large range of wavelength without any prior knowledge of film's thickness. Consider a thin film having thickness d and complex refractive index $n^* = n - ik$, where n is the real part of the refractive index and k is the extinction coefficient. The index of the surrounding air is

$n_a \approx 1$. The glass substrate is several orders of magnitude thicker than the film and has a refractive index $s = 1.51$. All the multiple reflections at the three interfaces, figure 2.5, are taken into account when calculating transmittance T. If the thickness d is uniform and comparable with wavelength of light which goes through the thin film, interference effect give rise to a typical spectrum such as shown in figure 2.6 the as-deposited conditions on microscope glass slide substrate. Beginning at the long wavelength end and moving to shorter wavelength, we can divide the spectrum following Swanepoel method into different regions according to their transmission intensities. In the transparent spectral region of the film $\alpha \approx 0$, the transmission is determined by n and s through multiple reflections. In the region of weak absorption, α is small so the transmission starts to decrease. In the region of medium absorption α is large and hence determines the overall transmission.

In the region of strong absorption, the transmission decreases drastically almost exclusively due to the influence of α. In the transparent region transmission fringe minima T_m can be used to calculate the refractive index of the film which is given by

$$n = [M + (M^2 - s^2)^{1/2}]^{1/2} \tag{2.14}$$

$$\text{where } M = \frac{2s}{T_m} - \frac{(s^2 + 1)}{2} \tag{2.15}$$

If there are insufficient fringes in the transparent region, one may have to resort to using fringes from the region of weak and medium absorption, where $\alpha \neq 0$. Both extremes, T_M and T_m, are used to determine the film's refractive index (n), then M in equation (2.14) is given by

$$M = 2s\frac{T_M - T_m}{T_M T_m} + \frac{(s^2 + 1)}{2} \tag{2.16}$$

This optical characterization method provides values for refractive index of films at particular wavelengths where transmission spectra are tangential to their corresponding top and bottom envelops. A distinct advantage of using the envelopes of the transmission spectrum rather than only the transmission spectrum is that the envelopes are slow-changing functions of wavelength (λ), whereas the spectrum varies rapidly with λ.
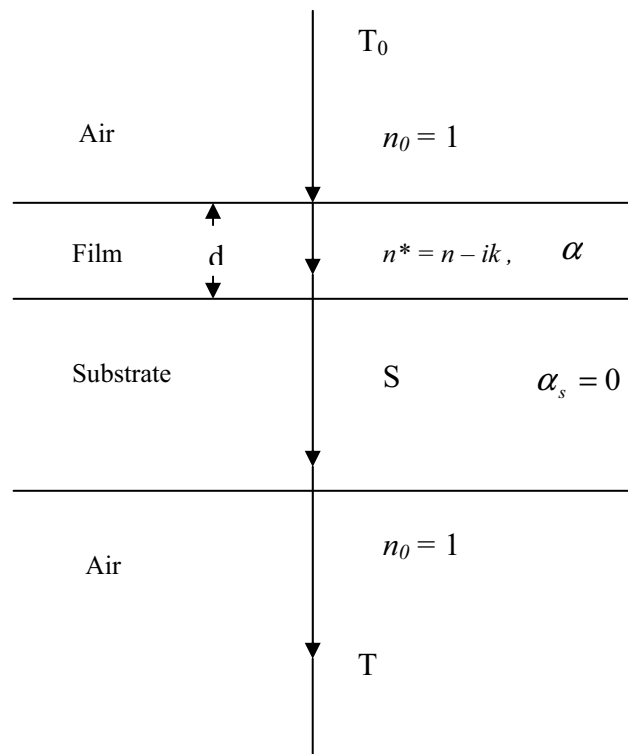
Figure 2.5 System of an absorbing thin film on a thick finite transparent substrate.
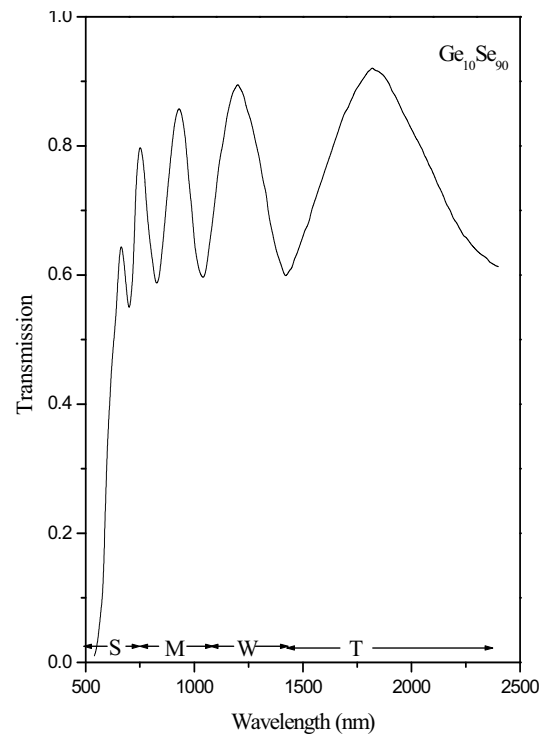
Figure 2.6 A Typical transmission spectrum for $Ge_{10}Se_{90}$ thin film; S = strong absorption, M = medium absorption, W = weak absorption and T = transparent.

34

In the strong absorption region, the transmittance decreases drastically due to the influence of α and the refractive index can be estimated by extrapolating the values of n calculated in the other regions of the spectrum. Then we must evaluate the spectral dependence of the absorbance (x) and finally spectral dependence of absorption coefficient (α). Therefore, we first apply Cauchy's formula to estimate n

$$n = A + \frac{B}{\lambda^2} \tag{2.17}$$

where A and B are material dependent constants. Therefore, the resulting solid line of n in interference region is extrapolated onto the refractive index axis to obtain the value of n in strong absorption region [14]. Then the value of absorbance can be calculated from

$$x = \frac{(n+1)^3(n+s^2)}{16n^2 s} T_0 \tag{2.18}$$

where T_0 represents the transmission in the region of strong absorption. In the region of weak and medium absorption using the transmission maxima, x can be calculated by

$$x = \frac{E_M - [E_M^2 - (n^2-1)^3(n^2-s^4)]^{0.5}}{(n-1)^3(n-s^2)} \tag{2.19}$$

where

$$E_M = \frac{8n^2 s}{T_M} + (n^2-1)(n^2-s^2) \tag{2.20}$$

The extinction coefficient also called absorption index is a measure of the fraction of light lost due to scattering and absorption per unit distance of the participating medium. The extinction coefficient (k) can be calculated using the relation [11]

$$k = \frac{\lambda}{4\pi d} \ln(1/x) \tag{2.21}$$

2.2.2 Thickness of thin film

Thickness of the thin film can be determined from the envelope method proposed by Swanepoel [13]. If n_1 and n_2 are the refractive indices of two adjacent

maxima or minima at wavelengths λ_1 and λ_2, then the thickness d of the film is given by

$$d = \lambda_1\lambda_2 / 2(\lambda_1 n_2 - \lambda_2 n_1) \tag{2.22}$$

2.2.3 Absorption coefficient

An electronic transition between the valence and conduction bands in the crystal starts at the absorption edge which corresponds to the minimum energy difference between the lowest minimum of the conduction band and highest maximum of the valence band. If these extrema lie at the same point of the k-space then the transition is called direct. If this is not, then only the phonon assisted transitions called indirect transitions are possible. In most of the amorphous compound semiconductors the absorption curves appear similar. Optical absorption is characterized in terms of the absorption coefficient (α).

It is crucial to determine the absorption characteristics of glasses and thin films, especially when comes to optical materials in order to evaluate their potential applications. When light is incident on a thin film some of its energy is reflected, some is absorbed and rest is transmitted. The optical absorption of thin films varies with thickness and wavelength and is a function of its physical and chemical structure. The absorption coefficient (α) measures the spatial decrease in intensity of a propagating beam of light due to progressive conversion of the beam into different forms of energy. The values of absorption coefficient from the transmission spectra have been calculated using the equation.

$$\alpha = (1/d)\ln(1/x) \tag{2.23}$$

where d is the thickness of the thin film and x is the absorbance. The absorption coefficient of chalcogenide glasses is known to change rapidly for photon energies close to their band gap and for many glassy and amorphous non-metallic materials, the absorption edge can be divided into three regions [15]

(a) For high absorption coefficient $(\alpha \geq 10^4 \text{ cm}^{-1})$ Tauc's power law states that

$$\alpha h\nu = B(h\nu - E_g^{opt})^n \tag{2.24}$$

where B is the slope of Tauc edge called band tailing parameter that depends on the

width of localized states in the band gap which are attributed to homopolar bonds in chalcogenide glasses. In the above equation *n = 1/2* for a direct allowed transition, *n = 3/2* for a direct forbidden transition, *n = 2* for an indirect allowed transition and *n = 3* for an indirect forbidden transition. E_g^{opt} is the optical band gap.

(b) For intermediate absorption coefficient $(10^1 \, \text{cm}^{-1} < \alpha < 10^4 \, \text{cm}^{-1})$ the absorption coefficient follows the Urbach's exponential relation [16] i.e.

$$\alpha = \alpha_0 \exp(h\nu / E_e), \tag{2.25}$$

where ν is the frequency of the radiation, α_0 is a constant, h is Planck's constant and E_e is an energy which is often interpreted as the width of the tail of localized states in the gap region or Urbach energy. The parameter E_e is thought to provide information about the extent of disorder or randomness in amorphous chalcogenide glasses. Absorption in this region is related to the transition between extended states in one band and localized states in the exponential tail of the other band; hence disorder here refers more towards that of electronic states with in the material as compared to irregularity in atomic arrangement. This relation was first proposed by Urbach [16] to describe the absorption edge in alkali halide crystals at high absorption levels. The relation has been found to hold for many amorphous or glassy materials. Tauc [15] believes that it arises from electronic transitions between localized states in the band edge tails, the density of which is assumed to fall off exponentially with energy. Davis and Mott [17] were uncertain about the precise explanation of the exponential dependence and suggested that the slopes of the observed exponential edges obtained from equation (2.25) are very much same in many semiconductors and the value of E_e for a range of amorphous semiconductors [18] lies between 0.045 and 0.67 eV.

(c) For weak absorption region $(\alpha < 1 \, \text{cm}^{-1})$ the strength and shape of absorption edge were found to depend on the preparation, purity and thermal history of the material.

2.2.4 Optical band gap

Band gap is the energy difference between the lowest minimum of the conduction band and highest maximum of the valence band is called the band or forbidden gap or simply energy gap. When this energy gap is calculated using optical methods then it is called optical band gap. The optical band gap of most of the chalcogenide glasses varies in the range 0.7 to 3.0 eV [19]. By knowing the values of absorption coefficient, optical band gap can be calculated from the relation (2.24). This relationship allows us to estimate the value of optical band gap by plotting $(\alpha h \nu)^{0.5}$ against $h\nu$. The values of E_g^{opt} and B can readily be calculated from the plot of $(\alpha h \nu)^{0.5}$ as a function of $h\nu$. The value of E_g^{opt} can be estimated by the intercept of the extrapolations to zero absorption with the photon energy axis $(\alpha h \nu)^{0.5} \rightarrow 0$. The value of band tailing parameter (B) is of the order of 10^5 - 10^6 as reported in the literature [19].

Theoretically the optical band gap can be calculated for the amorphous alloys from the Shimakawa's relation [20]

$$E_g(AB)(Y) = YE_g(A) + (1-Y)E_g(B) \tag{2.26}$$

where Y is the volume fraction of element A, $E_g(A)$ and $E_g(B)$ are the optical gaps for A and B elements, respectively. The conversion from atomic composition (at.%) or molecular composition (mol %) to volume fraction (Y) is made using atomic or molecular mass and density.

2.2.5 Dielectric constants

The complex dielectric constant is a fundamental intrinsic material property. The real part of it is associated with the term that how much it will slow down the speed of light in the material and imaginary part gives that how a dielectric absorb energy from electric field due to dipole motion. The knowledge of real and imaginary part of dielectric constant provides information about the loss factor which is the ratio of imaginary part of dielectric constant to real part of dielectric constant i.e. larger the imaginary part of dielectric constant or smaller the real part of dielectric constant, larger is the loss factor.

The complex refractive index is given by the relation [11]

$$(n^*)^2 = \varepsilon^* \times \mu^* \tag{2.27}$$

where ε^* is complex dielectric constant (or complex permittivity) and μ^* is complex permeability. For non-magnetic materials $\mu^* = 1$. Then above equation can be written as

$$(n - ik)^2 = \varepsilon_r - i\varepsilon_i \tag{2.28}$$

So the real and imaginary parts of the dielectric constant can be determined using the relations derived from above equation

$$\varepsilon_r = n^2 - k^2 \tag{2.29}$$

and

$$\varepsilon_i = 2nk \tag{2.30}$$

2.2.6 Optical Conductivity

The optical response of a material is most conveniently studied in terms of the optical conductivity. It has dimensions of frequency which is valid only in Gaussian system of units. The optical conductivity (σ) has been determined from the relation [21]

$$\sigma = \alpha n c / 4\pi \tag{2.31}$$

where c is the velocity of light, α is absorption coefficient and n is the refractive index.

2.3 Wemple – DiDomenico model

According to single oscillator model proposed by Wemple-DiDomenico (WDD) model [22], the optical data could be described to an excellent approximation by the following expression

$$n^2(h\nu) = 1 + \frac{E_0 E_d}{E_0^2 - (h\nu)^2} \tag{2.32}$$

where $h\nu$ is photon energy, E_0 is single oscillator energy and E_d is dispersion energy which is a measure of the average strength of interband optical transitions (interband transition energy or also called dispersion energy). Experimental

verification of equation (2.32) can be obtained by plotting $\left(n^2-1\right)^{-1}$ against $(h\nu)^2$. The resulting straight line yields values of parameters E_0 and E_d. Moreover an important achievement of Wemple-DiDomenico model is that it relates the dispersion energy E_d to other physical parameters of the material through a simple empirical relation

$$E_d = \beta N_c Z_a N_e \qquad\qquad (2.33)$$

where N_e is effective number of valence electrons per anion, N_c is effective coordination number of the cation nearest neighbour to the anion, Z_a is the chemical valency of the anion and β is a two valued constant with either an ionic or covalent value (for ionic materials $\beta = 0.26 \pm 0.03$ eV and for covalent materials $\beta = 0.37 \pm 0.04$ eV [23]).

References

1. Connell G A N and Lucovsky G 1978 *J. Non-Cryst. Solids* **31** 123

2. Lucovsky G, Galeener F L, Keezer R C, Geils R H and Six H A 1974 *Phys. Rev. B* **10** 5134

3. Tronc P, Bensoussan M, Brenac A and Sebenne C 1973 *Phys. Rev. B* **8** 5947

4. Bicerno J and Ovshinsky S R 1985 *J. Non-Cryst. Solids* **74** 75

5. Dittmar G and Schafer H 1976 *Acta Crytallorgr. B* **12** 1128

6. Dittmar G and Schafer H 1976 *Acta Crytallorgr. B* **12** 2726

7. Hulliger F 1976 *Structural Chemistry of Layer Type Phase* Ed. F. Levy (Boston: Reidel)

8. Bridenbaugh P M, Espinosa G P, Griffiths J E, Phillips J C and Remeika J P 1979 *Phys. Rev. B* **20** 4140

9. Lloyd J M 1975 *Thermal Imaging Systems* (New York: Plenum Press)

10. Granatstein V L 1991 *Encyclopedia of Physics* Ed. R. G. Lerner and G. L. Trigg 2nd Edition (New York: VCH Publication)

11. Goswami A 2005 *Thin film Fundamental* (New Delhi : New Age International)

12. Manificier J C, Gasiot J and Fillard J P 1976 *J. Phys. E: Sci. Instrum* **9** 1002

13. Swanepoel R 1983 *J. Phys. E : Sci. Instrum* **16** 1214

14. Ambrico M, Smaldone D, Spezzacatenna C, Stagno V, Perna G and Capozzi V 1998 *Semicond. Sci. Technol.* **13** 1446

15. Tauc J 1970 *The optical properties of solids* (Amsterdam: North-Holland)

16. Urbach R 1953 Phys Rev **92** 1324

17. Mott N F, Davis E A 1979 *Electronic Processes in Non-Crystalline Materials* (Oxford : Clarendon Press)

18. Abdelghany A, Elsayed S N, Abou El Ela A H and Mousa N H 1996 *Vacuum* **47** 243

19. Morigaki K 1999 *Physics of Amorphous Semiconductors* (London: Imperial College Press)

20. Andriesh A M and Iovu M S 2003 *Moldavian J. of the Physical Sciences* **2** 3

21. Pankove J I 1975 *Optical Processes in Semiconductors* (New York : Dover)

22. Wemple S H and DiDomenico M 1971 *Phys. Rev. B* **3** 1338

23. Wemple S H 1973 *Phys. Rev. B* **7** 3767

CHAPTER III

Experimental Techniques

This chapter is dedicated to the fabrication and characterization techniques utilized for the bulk glasses and their corresponding thin films, prepared and used in this study. A short theory background is presented in each case along with the reason for using each particular technique.

3.1   Bulk glass fabrication

The most convenient and conventional technique for the bulk glass formation is melt quenching. An essential pre-requisite for glass formation from the melt is that the cooling is sufficiently fast to preclude crystal nucleation and its growth; as thermodynamically crystalline phase is more stable than amorphous phase if allowed to take place. The distinguished feature of the melt quenching process of producing amorphous materials is that the amorphous solid is formed by continuous hardening (i.e. increase in viscosity) of the melt.

Before the development of the chemical vapour deposition and sol-gel processes, melt quenching was the only method by which bulk glasses of acceptable size could be obtained. Even today, glasses produced by melt quenching make up more than 99% of the practical glasses. The advantage of melt quenching technique over other techniques is the large flexibility of variation in compositions. Since quenching of melt does not require stoichiometry among constituents, the preparation of glasses with a wide variety of compositions, consisting of sometimes up to ten kinds of constituents at various ratios from a few to several ten of percent, is possible. The doping or co-doping of active ions such as rare earth or transition metal at a level of few percent or less is also made relatively easily, which is quite important for the production of glasses with special properties.

This technique requires material weighed according to their at. wt. %, quartz ampoule, high temperature furnace with rocking arrangement, ice cold water/liquid nitrogen bath. First materials were weighed according to their at. wt. % followed by sealing of these materials in an evacuated ($\sim 10^{-4}$ Pa) quartz ampoule. The sealed ampoule was then put inside a rocking furnace where the temperature was increased up to a certain temperature depending on the material gradually at a heating rate of 3-4 ^{0}C/min. The temperature – time profile for $Ge_{10}Se_{90-x}Te_x$ (x = 0, 10, 20, 30, 40, 50)
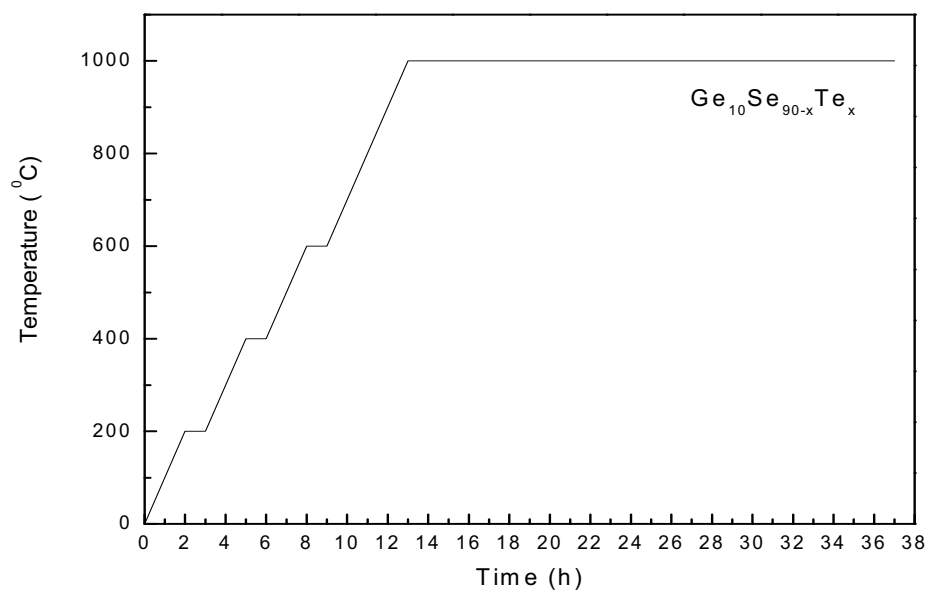
Figure 3.1.1 Temperature time profile for $Ge_{10}Se_{90-x}Te_x$ glassy alloys.
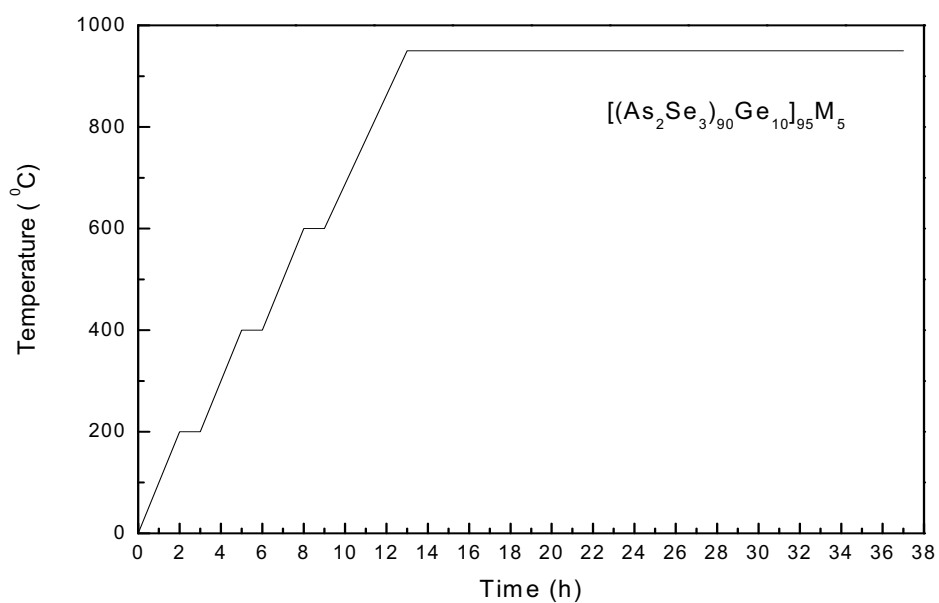
Figure 3.1.2 Temperature time profile for $[(As_2Se_3)_{90}Ge_{10}]_{95}M_5$ glassy alloys.

46

and $[(As_2Se_3)_{90}Ge_{10}]_{95}M_5$ (M = Bi, Cd, Sn and Pb) glassy systems studied are given in figures 3.1 and 3.2.

The ampoule was frequently rocked for 24 h at the highest temperature to make the melt homogeneous. The quenching was done in ice-cold water. The $Ge_{10}Se_{90-x}Te_x$ compositions were quenched at 1000 ^{0}C while $[(As_2Se_3)_{90}Ge_{10}]_{95}M_5$ were quenched at 950 ^{0}C. The bulk glass was taken out by breaking the ampoule.

3.2   Thin film deposition

Thin films can be prepared from a variety of materials such as metals, semiconductors, insulators or dielectrics etc. and for this purpose various preparative techniques have been developed. Techniques involved in general are (i) thermal deposition in vacuum by resistive heating, electron gun or laser gun evaporation, etc. from suitable sources, (ii) sputtering of cathode materials in presence of inert or active gases either at low or medium pressure, (iii) chemical vapour deposition (CVD) by pyrolysis, dissociations, reactions in vapour phase, (iv) Chemical deposition from solutions including electro-deposition, chemical displacement, chemical reaction etc.

In the present work, we have dealt with thermal deposition in vacuum by resistive heating. This is the most commonly used technique adopted for deposition of metals, alloys and also many compounds. The primary requirement for this method is a high vacuum deposition system at a pressure of about 10^{-4} Pa or even less.

Fine powder of the material to be deposited was put into the flash cleaned boat. Flash cleaning was done by passing a heavy current through the boat so as to make it white hot or incandescent for a short period. Then the system was evacuated to a base pressure of 10^{-4} Pa. A shutter was incorporated in between the source and the substrate so that no vapour stream of the material can reach the substrate directly prior to attaining the required deposition conditions. After establishing required source temperature, substrate temperature and vacuum in the chamber, the shutter was removed to start the deposition of film on the cleaned substrate. When the required film thickness was obtained the shutter was brought back to the original position.

Cleaning of the substrate was done in three steps: (i) soap solution cleaning and (ii) cleaning with acetone (vapour cleaning) and (iii) with methanol. Soap solution cleaning basically involves scrubbing the substrate in the soap solution, then

rinsing it thoroughly with distilled water. This procedure was repeated 3 - 4 times for cleaning single substrate. Soap solution cleaning was used to remove any visible oil, grease and dust impurities. Vapour cleaning procedure was used to remove the organic impurities, which may be present on the surface of substrate. Acetone was used for the removal of organic impurities. For the removal of inorganic impurities methanol was used. After all this cleaning the substrates are subjected to dry in an oven at a temperature approximately 110^0C and then put into deposition chamber.

Thin films were kept in the deposition chamber in the dark for 24 h to attain thermodynamic equilibrium as stressed by Abkowitz *et al* [1]. The vacuum evaporation process was carried out in a coating system (HINDHIVAC model 12A4D India). The rate of evaporation of deposited thin films and thickness of the films deposited has been measured by thickness monitor (Model DTM-101).

3.3   X-ray diffraction

X-ray diffraction (XRD) was discovered by Max Von Laue in1912 and immediately applied to structure determination in 1913 by W. L. Bragg and W. H. Bragg. XRD is presently the most widely used technique to detect the crystalline phase in glasses. X-ray energies range from 200 eV to 1 MeV in the electromagnetic spectrum, in between ultraviolet radiation and γ-rays. XRD is a combined effect of scattering and interference [2]. Scattering is a process of absorption and reemission of an electromagnetic radiation. If the scattered waves are in phase they interfere constructively and form diffracted beams with specific directions. The well known Bragg's law associates the wavelength (λ) of x-rays to the spacing between atomic planes and can be expressed as $\lambda = 2d_{hkl}\sin\theta_{hkl}$, where d_{hkl} is the interplanar spacing, θ_{hkl} is the angle between the atomic plane and the incident and diffracted waves.

The powder method was used to check the nature (i.e. amorphous or polycrystalline or crystalline) of the bulk samples. The bulk samples were crushed to fine powder with a pestle and mortar and then this powder was used for taking XRD pattern. Philips PW 1710 X-ray diffractometer (Cu-Kα radiation, λ = 1.540598 $\overset{0}{A}$, 40 KV and 25 mĄ was used to take the XRD patterns of the samples. Data acquisition

was made in the 2θ range from 10° to 100^{0}. Step size was set to 0.05^{0} was employed. Thin films of the fabricated bulk samples deposited on the microscopic glass slides were also characterized to check the nature of the films.

3.4   Transmission spectroscopy

No material is fully transparent in all optical frequencies and hence there is always some absorption in some region of the spectra. When light is incident on a thin film some of its energy is reflected, some is absorbed and rest is transmitted. Thin films are studied more accurately by acquiring transmission instead of absorption as is the case for bulk glasses. The transmission spectra of the thin films in the spectral range 200 – 2400 nm were obtained using a double beam ultraviolet - visible - near infrared spectrophotometer (Hitachi-330 and Perkin Elmer Lambda-750). The spectrophotometer was set with a slit width of 1 nm. Therefore it was unnecessary to make slit width corrections because of a small slit width value in comparison with different line widths [3]. Typical interference fringes were obtained and the signal was used to calculate the refractive index dispersion curves using Swanepoel's technique as mentioned in chapter 2. This technique additionally allows the calculation of thickness of deposited thin films, optical absorbance and absorption coefficient.

3.5   Fourier-Transform infrared spectroscopy

Fourier - Transform infrared (FT-IR) spectroscopy combines the advantages of IR spectroscopy and Fourier -Transform to allow the identification of functional groups and the detection of the presence of impurities. When a molecule absorbs specific frequencies of IR radiation, vibration or rotations of the functional groups are created and an absorbance spectrum regrouping the absorbed frequencies can be observed. This spectrum is specific to each molecule which allows an experimenter to know with precision the functional groups forming the sample. In addition the radiation absorbed is proportional to the concentration of each compound. This electronic process is combined with Fourier transform, named after Jean-Baptiste Joseph Fourier, which converts time based signals into frequency domain. The IR

beam used in FT-IR is split into two components in an interferometer, one component traveling to a mirror placed at a distance and other one to a moving mirror, thus creating constructive and destructive interference [4]. The resulting interference pattern is a time based function that is translated as a function of frequency after Fourier transform.

Far-infrared transmission measurements were obtained in the spectral range 50-650 cm^{-1} at room temperature using Perkin Elmer 1600 FT-IR Spectrometer. The resolution during the measurements was set at 2 cm^{-1}. Measurements were made using the polyethylene pellet method. About 10 mg of finely grounded powder sample was mixed with 500 mg of polyethylene powder and pellet of 2.0 cm diameter was prepared under a pressure of 13 ton/mm^2. To take account of the polyethylene absorption, the spectrum of polyethylene was used as reference spectrum. The sample spectrum was divided by the reference spectrum to nullify the polyethylene absorptions.

3.6   Density measurements

Density refers to the mass contained with in a unit volume under specified conditions and is measured in kg/m^3. Density of bulk samples was measured by Archimedes (buoyancy) method. Archimedes' principle state that the apparent weight of an object immersed in a liquid decreases by an amount equal to the weight of the volume of the liquid that it displaces. The apparatus consists of a beaker filled with double distilled water as a reference liquid. A thermometer was placed in the liquid to measure the temperature. The method is first to calculate the weight of sample in air. Then the sample is placed on the sinker part and plunge it into the beaker in such a way that the sample is covered with at least 10 mm of liquid. After making sure that no bubbles are trapped in between the sample and the sinker the weight of the sample is measured in the liquid. The density of double distilled water (ρ_{water}) is obtained from a calibrated table knowing its temperature. Thus the density of the sample is calculated using the formula

$$\rho = \left[\frac{w_1}{w_1 - w_2} \right] \rho_{water}$$

where w_1 and w_2 are the weight of the sample in air and the weight of the sample in the reference liquid (double distilled water) respectively. Each sample was weighed five times and average density was recorded.

Acknowledgement

I would like to thank SAIF/RSIC, Chandigarh for getting XRD patterns for bulk as well as thin films and transmission spectra of thin films. I would also like to thank Prof. S. M. Sondhi, IIT Roorkee (India) for help in getting Far-IR spectra.

References

1. Abkowitz M, Foley G M T, Markovics J M and Palumbo A C 1984 *Optical Effects in amorphous Semiconductors* (*AIP Conf. Proc.* vol 120) ed P C Taylor and S G Bishop (New York: American Institute for Physics) pp 117–124

2. Suryanarayana C and Norton M G 1998 *X-Ray Diffraction – A Practical Approach* (New York: Plenum Press)

3. Marquez E, Ramirez-Malo J, Villares P, Jimenez-Garay R, Ewen, P J S and Owen A E 1992 *J. Phys. D: Appl. Phys.* **25** 535

4. Goodman J W 1996 *Introduction to Fourier Optics* (New York: McGraw-Hill)

CHAPTER IV[*]

Structural and Optical
Properties of Ge-Se-Te System

[*] • **Pankaj Sharma** and S. C. Katyal, **"*Far-infrared transmission and bonding arrangement in Ge$_{10}$Se$_{90-x}$Te$_x$ semiconducting glassy alloys*"** **Journal of Non-Crystalline Solids,** (2008) doi: 10.1016/j.jnoncrysol.2008.05.010

• **Pankaj Sharma** and S. C. Katyal, "*Optical Study of Ge$_{10}$Se$_{90-x}$Te$_x$ Glassy Semiconductors*" **Thin Solid Films**, Vol. 515 (2007) 7966.

• **Pankaj Sharma** and S. C. Katyal, "*Thickness Dependence of Optical Parameters for Ge-Se-Te Thin Films*" **Materials Letters**, Vol. 61 (2007) 4516.

• **Pankaj Sharma** and S. C. Katyal "*Calculation of optical constants in a-Ge$_{10}$Se$_{90-x}$Te$_x$ (x = 0, 30, 40) thin films*" **Journal of Optoelectronics and Advanced Materials**, Vol. 9 (2007) 2000.

In this chapter we have discussed the preparation and characterization of the Ge-Se-Te system and their bonding arrangement from far-infrared transmission study. Optical properties viz. refractive index, absorption coefficient, optical energy gap have been reported using ultraviolet-visible-near infrared spectroscopy. A detailed account on the effect of deposition parameter has also been discussed on the optical properties for Ge-Se-Te thin films.

4.1   Ge-Se-Te System

The Ge-Se-Te system is of special interest in view of the fact that it forms glasses over a wide domain of compositions. The glass forming region in the ternary Ge-Se-Te system extends to complete replacement of Se by Te, with the rest being Ge. Ge-Se-Te system is an important system as the addition of Te to Ge-Se system creates a configurational and compositional disorder with respect to binary system. Therefore, it is a suitable system for the investigation of its structural and optical properties. The glassy alloys of the system $Ge_{10}Se_{90-x}Te_x$ $(0 < x < 50)$ were prepared by conventional melt quenching technique (chapter 3). The high purity (99.999%) elemental constituents were weighed and mixed in seal evacuated (at $\sim 10^{-4}$ Pa) quartz ampoules. The ampoules were kept inside a furnace where the temperature was increased up to 1000 ^{0}C at a heating rate of 2-3 ^{0}C/min. The ampoules were frequently rocked for 24 hours at the highest temperature to make the melt homogeneous. The melt in the quartz ampoule was then quenched into ice-cold water.

Thin films of the glassy alloys of $Ge_{10}Se_{90-x}Te_x$ ($x = 0, 10, 20, 30, 40, 50$) were prepared on glass substrates by vacuum evaporation technique at a base pressure $\sim 10^{-4}$ Pa. The bulk samples as well as their thin films were characterized by X-ray diffraction (XRD) technique. Figure 4.1.1 shows the XRD patterns for bulk samples while figure 4.1.2 shows XRD patterns for their thin films. The lack of any sharp peak indicates the amorphous nature of bulk glasses as well as their thin films.
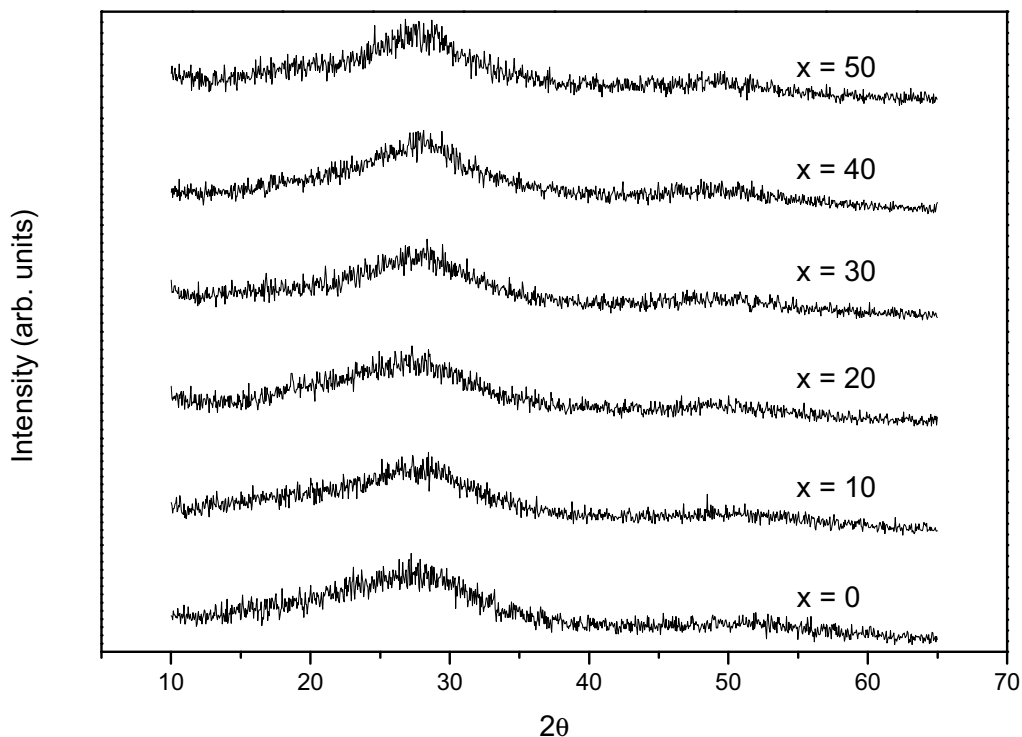
Figure 4.1.1 XRD patterns for $Ge_{10}Se_{90-x}Te_x$ bulk glasses.
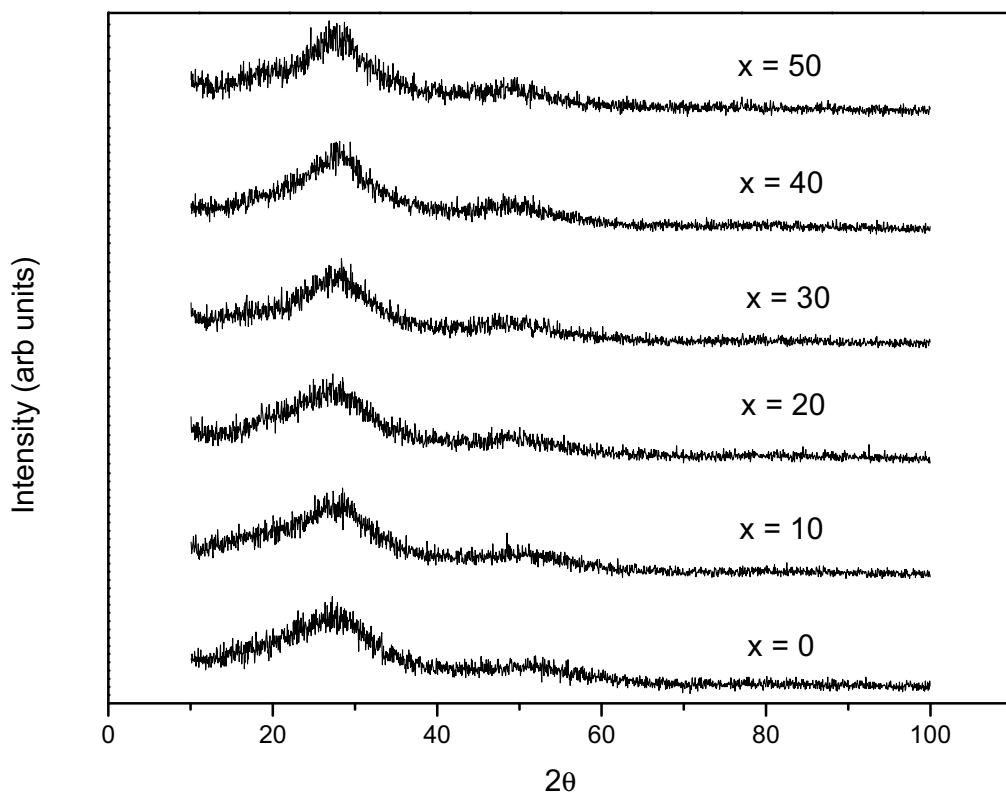
Figure 4.1.2 XRD patterns for $Ge_{10}Se_{90-x}Te_x$ thin films.

4.2   Far-infrared transmission

4.2.1 Introduction

An understanding of the structure of an amorphous material is essential to understand its physical properties. Determining the structure of glasses is difficult for two main reasons. First, unlike for the crystal, there is no direct probe such as X-ray diffraction that can determine the structure of a glass uniquely. This is due to the absence of long range order in the glasses. Second, the glass may be in one of many possible metastable states. These metastable states consist of different atomic configurations which may differ only slightly from one another and result in physical properties very similar to one another. The particular state in which a glass resides is dependent on its history of preparation. That is, the glass forming ability is influenced by the quenching rate, the amount of the sample prepared and the temperature from which the melt of sample is quenched. Infrared (IR) absorption of solids can provide useful information about the lattice vibrational density and structure of solids. In order that the mode of vibration can absorb, a mechanism for coupling the vibration motion to electromagnetic radiation must exist. The basic mechanism is that the motion produces an oscillatory dipole moment which can be driven by oscillating electric field of radiation. Raman scattering in solids is associated with the change of polarizability corresponding to the vibrational modes. The vibrations that contribute to IR absorption can be quantitatively separated into different types of modes characterized by three frequency regimes; low frequency acoustic modes, intermediate frequency bond bending modes and high frequency bond stretching modes. The bond stretching mode generally yield the most direct structural information since their frequencies are determined primarily by nearest neighbour interactions and thus relative IR activity by local molecular symmetry.

Infrared and Raman measurements have been made as a useful means of obtaining information about the structure of chalcogenide glasses [1-9]. In this case this is essentially important to investigate vibrational spectra in the fundamental band region. Several authors [10-13] have measured the IR and Raman spectra of pure glassy Se in order to understand the structure. Structural investigations have also been made for binary chalcogenide glasses as *S-Se*, *Se-Te*, *As-Se* and *Ge-Se* alloys by

measuring the IR and Raman spectra [10-17]. These studies reveal that the pure glassy *Se* consists of Se_8 puckered rings and Se_n spiral chains [10,11,13,14] and in *S-Se* and *Se-Te* glasses $S_{8-x}Se_x$ and $Se_{8-x}Te_x$ mixed rings were formed [14,16]. On the other hand it was considered in *As-Se* and *Ge-Se* glasses that $AsSe_3$ pyramidal molecules [14,16] and $GeSe_4$ tetrahedral molecules [14,15,17] were formed as a local configuration.

The *Ge-Se* system provides a wide range of concentrations for which it is possible to obtain bulk amorphous compounds. The *Ge-Se* system has been widely probed using IR and Raman spectroscopy [1,2,15,18-24]. Alloys of glassy Ge_xSe_{1-x} system with *Ge* concentration range *0 < x < 0.5* are supposedly composed of *Se* chain, $Ge(Se_{1/2})_4$ tetrahedral, $Ge_2(Se_{1/2})_6$ ethane like and $Ge(Se_{1/2})_2$ structural units in proportions varying to comply with the actual *x*-values. Substitution of tellurium (*Te*) into *Ge-Se* system makes the system of interest. The system $Ge_{10}Se_{90-x}Te_x$ *(0 < x < 50)* has been studied here with emphasis on the effect of *Te*. The system is of quite interest as this was shown that addition of *Te* into *Ge-Se* increases the transparency range of the glasses [25-27]. Thus addition of *Te* to *Ge-Se* provides an ideal system for optical study in far-IR region. To have a better understanding of the optical properties one should have the knowledge of its structural constituents. This makes the authors to have a detailed structural study of the $Ge_{10}Se_{90-x}Te_x$ *(0 < x < 50)* system in the far-IR region.

4.2.2 Experimental details

Far-infrared transmission measurements were obtained in the spectral range 50-650 cm^{-1} at room temperature using Thermo Nicolet Nexus 670 FT-IR Spectrometer. The resolution during the measurements was set at 2 cm^{-1}. Measurements were made using the polyethylene pellet method. To take account of the polyethylene absorption, the spectrum of polyethylene was used as reference spectrum. The sample spectrum was divided by the reference spectrum to nullify the polyethylene absorptions.

4.2.3 Results and discussion

The IR spectra of $Ge_{10}Se_{90-x}Te_x$ where $x = 0, 10, 20$ and $x = 30, 40, 50$ glassy alloys are shown in figures 4.2.1 and 4.2.2 respectively. The IR spectra of Ge-based chalcogenide glasses have been largely interpreted in terms of isolated molecular units. Two different models have been proposed for the structure of Ge-Se glasses.

In the first model [15] called chain crossing model (CCM) the four fold tetrahedrally coordinated Ge-atoms act as chain crossing points in Se chain structure. In second model [28] known as random covalent network model (RCNM), the tetrahedrally coordinated Ge-atoms bond to other Ge-atoms as readily as to the two fold Se-atoms. In the chemical bond approach, to explain the structure of chalcogenide glasses Bicerno and Ovshinsky [29] proposed that atoms of one type combine more favourably with atoms of different type and the bonds are formed in the sequence of decreasing bond energy until all available valencies of the atoms are filled. Keeping this view in mind the energies of various possible bonds in $Ge_{10}Se_{90-x}Te_x$ system have been calculated on the basis of relation [30]

$$D(A-B) = [D(A-A) + D(B-B)]/2 + 23(\chi_A - \chi_B)^2 \tag{1}$$

where χ_A and χ_B are the electronegativities of the atoms A and B and $D(A$-$A)$ and $D(B$-$B)$ are the bond energies of A-A and B-B bonds respectively. The relative probabilities of formation of different bonds have also been calculated using the probability function $\exp(D/K_BT)$ at room temperature as well as 1000 ^{0}C at which the samples were prepared. The results are shown in table 4.2.1.

When Ge is introduced into Se, it is four fold tetrahedral coordinated [31]. $GeSe_4$ tetrahedral molecules have four fundamental modes (v_1, v_2, v_3, v_4) [32]. Although only the v_3 and v_4 modes are infrared active in $GeSe_4$ molecules, it is expected that all the fundamental modes appear in infrared absorption spectra because of breakdown of selection rules in glassy materials. Considering first the $Ge_{10}Se_{90}$ bulk glass the main absorption bands appears at $\sim$ 84 cm^{-1}, 102 cm^{-1}, 150 cm^{-1}, 175 cm^{-1}, 220 cm^{-1} and 280 cm^{-1} along with three shoulders at $\sim$ 127 cm^{-1}, 137 cm^{-1} and 193 cm^{-1}. The existence of these absorption bands is in good agreement with the earlier reported results by Ball and Chamberlain [18]. The band at 84 cm^{-1} has been

assigned to Se_8 [E_2 mode] [18] while the sharp absorption band at 102 cm^{-1} has been assigned to A_2 mode of trigonal Se which is strongly infrared active. Ohsaka [14] has also reported infrared active fundamental band in spectra of Se containing Te at 102 cm^{-1} and assigned it to A_2 mode of trigonal Se. The shoulders at 127 cm^{-1} and 137cm^{-1} have been assigned to Se polymeric chains. Absorption peaks at 150 cm^{-1} and 175 cm^{-1} have been observed and assigned to $GeSe_2$ mode [18] which is active in Raman mode. Ball et al [18] has reported $GeSe_4$ (v_1) mode at 197 cm^{-1} for $Ge_{15}Se_{85}$ glassy alloy so a shoulder at 193 cm^{-1} may be assigned to v_1 mode of $GeSe_4$ tetrahedra. A comparatively weak band at 220 cm^{-1} has been assigned to $GeSe_2$ mode. Fukunaga et al [33] also found a weak band at 220 cm^{-1} for $GeSe_2$ and attributed it to the vibrations of Ge-Ge bonds. Ksendzov et al [34] have reported that glasses have increasing ability to relax and optimize bent Se-Se-Se bonds because the large chemically ordered clusters become floppy [35]. So they assigned band at 280 cm^{-1} to vibrations of nearly isolated F_2 mode of $Ge(Se_{1/2})_4$ tetrahedra which are connected with Se chains outside the clusters [33] because of lack of symmetry and relaxation of selection rules. In our spectra a band at 280 cm^{-1} may thus be assigned to an isolated F_2 mode of $Ge(Se_{1/2})_4$ tetrahedra.

When Te is substituted for Se in $Ge_{10}Se_{90-x}Te_x$, the absorption band at 84 cm^{-1} starts to split into bands at ~ 79 cm^{-1} and 89 cm^{-1}. The absorption band at 79 cm^{-1} has been assigned to v_2 (E) mode of $GeTe_2$ structural unit [36] and absorption peak at 89 cm^{-1} has been assigned to E_1 mode due to Se_8 rings. A strong vibrational band at 102 cm^{-1} remains at its same position for $x = 10$ while for other higher Te concentrations i.e. $x = 20$, 30, 40, 50 this absorption band is observed to shift towards higher wavelength and is found at 100 cm^{-1}. The absorption band at 150 cm^{-1} for $x = 0$ [$GeSe_2$ mode] is found missing for $x = 10$ at.% of Te but appears sharply for $x \geq 20$ at.% of Te content. Andrikopoulos et al [37] have assigned this vibrational mode to symmetric stretching vibration of Te-Te bond. In present case i.e. for Ge-Se-Te system this strong vibrational mode at 150 cm^{-1} is assigned to symmetric stretching of Te-Te bonds. The presence of Te-Te bonds at higher frequency is due to the fact that stretching modes occurs at higher frequencies. A weak absorption band at 163 cm^{-1} is observed in all the compositions containing Te content. This weak band has been attributed to v_1 (A_1) vibrational mode for $GeTe_2$. Phillips [36] has also reported v_1 (A_1)
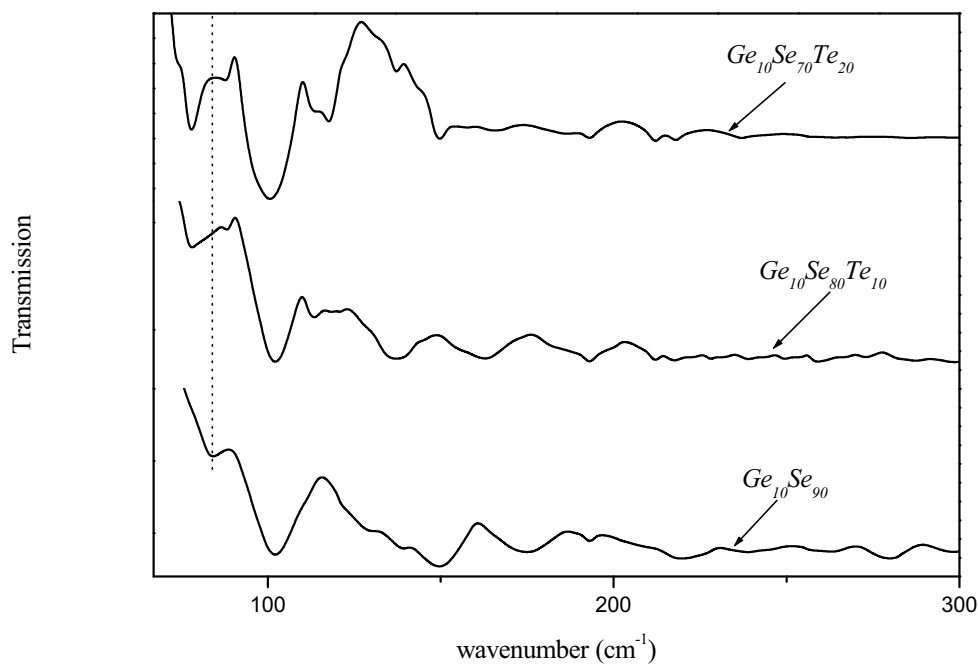
Figure 4.2.1 Far-IR transmission spectra of $Ge_{10}Se_{90-x}Te_x$ ($x = 0, 10, 20$) glassy alloys. The ordinate scale for different x-values is shifted for clarity.
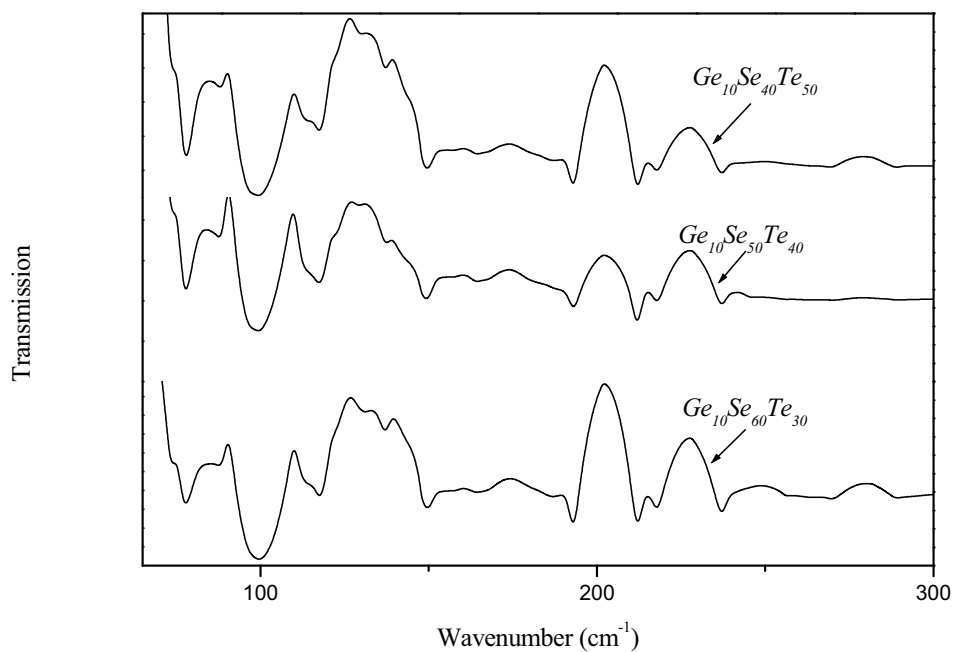
Figure 4.2.2 Far-IR transmission spectra of $Ge_{10}Se_{90-x}Te_x$ ($x = 30, 40, 50$) glassy alloys. The ordinate scale for different x-values is shifted for clarity.

61

Table 4.2.1 Bond energy and the relative probabilities of various bonds in $Ge_{10}Se_{90-x}Te_x$ ($x = 0$, 10, 20, 30, 40, 50) glassy alloys. The probability of the *Ge-Se* bond has been taken as unity.

Bond	Bond energy (kcal/mol)	Relative probability at the following Temperatures	
		27 ^{0}C	1000 ^{0}C
Ge-Se	49.1	1	1
Se-Se	44.0	1.93×10^{-4}	1.33×10^{-1}
Se-Te	40.6	6.50×10^{-7}	3.47×10^{-2}
Ge-Ge	37.6	4.36×10^{-9}	1.06×10^{-2}
Ge-Te	37.4	3.05×10^{-9}	9.81×10^{-3}
Te-Te	33.0	1.91×10^{-12}	1.72×10^{-3}

vibrational mode for $GeTe_2$ at 167 cm^{-1} in Ge-Te glassy alloys. The absorption bands of 175 cm^{-1} [$GeSe_2$ Raman Mode], 220 cm^{-1} [$GeSe_2$] and 280 cm^{-1} [F_2 mode of $Ge(Se_{1/2})_4$] which appears for $x = 0$ have not been observed when Te is substituted for Se in $Ge_{10}Se_{90-x}Te_x$ glassy alloy while 127 cm^{-1}, 137 cm^{-1} [Se polymeric chain] and 193 cm^{-1} [v_1 mode of $GeSe_4$] remains at their positions though their intensity changes for some of the compositions.

On the addition of Te to Ge-Se system a well resolved doublet at 113 cm^{-1} and 117 cm^{-1} has been observed and two distinguishable absorption peaks are observed at 211 cm^{-1} and 217 cm^{-1} in all the compositions ($x = 10, 20, 30, 40, 50$). The intensity of these peaks increase with the increase of Te content. The doublet of 113 cm^{-1} and 117 cm^{-1} has been associated with v_1 (A_1) vibrational frequency of GeTe$_4$ tetrahedron [37]. The absorption band at 211 cm^{-1} has been assigned to the vibrations of Se-Te bonds. Wang et al [38] also have reported the vibrations of Se-Te bonds at 210 cm^{-1} in $Ge_2Se_5Te_3$ glassy alloy. Further Ohsaka [14] has reported the frequency of IR band in Se-Te alloy at 205 cm^{-1} which does not vary with the Te content. Consequently he did not assign this band to $Se_{n-x}Te_x$ chains but to $Se_{8-x}Te_x$ mixed rings and is estimated to be due to Se_5Te_3 mixed rings. The absorption band at 217 cm^{-1} observed for Te added Ge-Se system has been assigned to the vibrations of Se-Te bonds. Schottmiller et al [16] also showed that the Raman band at 216 cm^{-1} found in Se-Te alloys was attributed to $Se_{8-x}Te_x$ rings probably Se_6Te_2 rings. Absorption peak at 237 cm^{-1} which does not show its appearance in compositions with $x = 0, 10, 20$ at.% starts showing its existence for $x \geq 30$ at.% of Te content. Phillips [36] has also reported an absorption band at 230 cm^{-1} in Ge-Te glass and attributed it to v_3 (F_2) vibrational mode for $GeTe_2$. In our case, the band at 237 cm^{-1} appears as Te replaces Se for $x \geq 30$ at.% and this may be assigned to v_3 (F_2) vibrational mode for $GeTe_2$.

In order to understand the IR absorption spectra obtained above for $Ge_{10}Se_{90-x}Te_x$ where $x = 0, 10, 20, 30, 40, 50$ glasses the absorption spectra of these glasses have been compared with the IR studies of pure Se [10], binary Ge-Se [18], Ge-Te [37], Se-Te [14] and ternary Ge-Se-Te glasses [38]. As seen for $Ge_{10}Se_{90}$ glassy alloy the absorption bands appears at 84 cm^{-1}, 102 cm^{-1}, 150 cm^{-1}, 175 cm^{-1}, 220 cm^{-1} and 280 cm^{-1} along with three shoulders at ~ 127 cm^{-1}, 137 cm^{-1} and 193 cm^{-1}. On the

addition of *Te* to *Ge-Se* system the absorption peak for E_2 mode of Se_8 at 84 cm^{-1} splits into two bands at 79 cm^{-1} and 89 cm^{-1} leading to the formation of $GeTe_2$ and Se_8 structural units respectively. The other new absorption bands which appears at 113 cm^{-1}, 117 cm^{-1}, 163 cm^{-1}, 211 cm^{-1} and 217 cm^{-1} shows the existence of tetrahedra of $GeTe_4$ at 113 cm^{-1} and117 cm^{-1} doublet, $GeTe_2$ unit at 163 cm^{-1} while vibrations of *Se-Te* bonds in $Se_{8-x}Te_x$ mixed rings at 211 cm^{-1} and 217 cm^{-1}. Moreover it is found that the absorption band at 150 cm^{-1} for $x = 0$ composition disappears for $x = 10$ at.% whereas it again appears at 150 cm^{-1} for $x \geq 20$ at.% showing the symmetric stretching vibrations of *Te-Te* bonds. Further for $x \geq 30$ at.% the band at 237 cm^{-1} appears due to $GeTe_2$ molecular unit.

With the increase of *Te* content it has been observed that some of the *Ge-Se* and *Se-Se* bonds disappear leading to the formation of *Se-Te* and *Ge-Te* bonds. Further the existence of *Te-Te* bonds has also been observed at 150 cm^{-1}. *Ge-Se* and *Se-Se* bonds remain in the $Ge_{10}Se_{90-x}Te_x$ glassy alloy even on the addition of *Te* may be explained in terms of their higher relative probability of formation (table 4.2.1). The formation of *Se-Te* and *Ge-Te* bonds may be explained on the basis of supremacy of heteropolar on homopolar bonds [29]. The existence of *Ge-Ge* bonds has not been observed as the compositions under study were chalcogen rich. The absorption peaks at 150 cm^{-1} (for $x \geq 20$ at. %) confirms the formation of *Te-Te* bonds. However these appear for higher *Te* content compositions. The least formation of *Te-Te* bonds may be attributed to their lower relative probability of formation. The formation of *Te-Te* bonds may also be explained on the basis of chemical bond approach (CBA) method [29]. Among chalcogens (*Se* and *Te*) *Te* acts as 3-fold coordinated. Thus for $x > 20$ at. % , *Te* become excessive and remain unsatisfied producing *Te-Te* homopolar bonds and appears at 150 cm^{-1} due to symmetric stretching of *Te-Te* bonds.

4.2.4 Conclusion

The addition of *Te* to $Ge_{10}Se_{90}$ shows that the far-IR transmission spectra shift a little towards the lower wavenumber side. The addition of *Te* in $Ge_{10}Se_{90}$ has shown the appearance of $GeTe_2$ and $GeTe_4$ molecular units and vibrations of *Se-Te* bond in $Se_{8-x}Te_x$ mixed rings. The results were explained in terms of the vibrations of the

isolated molecular units. This has been observed that some of the *Ge-Se* and *Se-Se* bonds disappear leading to the formation of *Se-Te* and *Ge-Te* bonds. The existence of *Ge-Ge* bonds has not been observed as the compositions under study were chalcogen rich. The absorption peaks at 150 cm^{-1} (for $x \geq 20$ at. %) confirms the formation of *Te-Te* bonds. However these appear for higher *Te* content compositions. The least formation of *Te-Te* bonds may be attributed to their lower relative probability of formation and also to excess of *Te-Te* bonds according to CBA. These results are supported by observation that optical band gap decrease with the addition of *Te* to *Ge$_{10}$Se$_{90-x}$Te$_x$* system (section 4.3.3).

4.3 Optical properties

4.3.1 Introduction

Chalcogenide glasses recognized as promising materials for infrared optical elements, infrared optical fibres, xerography, switching and memory devices, photolithography and in the fabrication of inexpensive solar cells and more recently for reversible phase change optical records [39-52]. The influence of impurities on electrical, optical and the structural properties of chalcogenide glasses are of important concern with respect to their application. This influence can be widely different for different impurities. Many approaches were proposed to explain the compositional dependence of various physical properties of chalcogenide networks [39,53-56].

The chemical composition and energy band structure change on introducing the Ge atoms into the Se matrix. The variation of the Ge-Se structure is reflected in different properties such as the glass forming regions, glass transition temperature, photoluminescence, IR and Raman spectra and the optical properties [57-59]. Optical properties of IV-VI compounds have been studied by various researchers [60,61]. The optical band gap and the localized states width were found to depend on the composition.

The optical band gap and refractive index are the most significant parameters in amorphous semiconducting thin films. The optical behaviour of material is utilized to determine its optical constants. Films are ideal specimen for absorbance and

transmittance type measurements. Therefore, accurate measurements of the optical constants are extremely important. The optical properties of amorphous semiconductors have been extensively studied [60,61] on Ge-Se system because of their wide range of applications and strong dependence on composition.

In $Ge_{10}Se_{90}$ system the average coordination number $<r>$ is 2.2 *i.e.* the system is in floppy mode. Alloying of $Ge_{10}Se_{90}$ with a fourth element of group VI (Te) is very important from the basic as well as application point of view because for $Ge_{10}Se_{90-x}Te_x$ (*x = 0, 10, 20, 30, 40, 50*) compositions $<r>$ varies from 2.2 to 2.7 *i.e.* the system varies from floppy mode to rigid mode with a change in mode at 2.4 [54,56]. In the present work, therefore, the effect of Te additive on the optical properties of such a technically important system $Ge_{10}Se_{90}$ has been studied. The optical parameters refractive index (*n*), extinction coefficient (*k*), absorption coefficient (α) and optical band gap (E_g^{opt}) of the amorphous thin films of $Ge_{10}Se_{90-x}Te_x$ (*x = 0, 10, 20, 30, 40, 50*) have been calculated by analyzing their transmission spectra. The dielectric constant and optical conductivity has also been calculated using the other optical parameters.

4.3.2 Experimental details

The normal incidence transmission spectra in the transmission range 200-2400 nm for $Ge_{10}Se_{90-x}Te_x$ (*x=0, 10, 20, 30, 40, 50*) thin films (thickness 800 nm) were obtained by a double beam ultraviolet-visible-near infrared spectrophotometer [Hitachi-330]. The spectrophotometer was set with a slit width of 1 nm. The normal incidence transmission spectra were also obtained by a double beam ultraviolet-visible-near infrared spectrophotometer [Perkin Elmer Lambda-750]. In UV region no transmission has been observed. The results obtained from both the instruments are in good agreement.

4.3.3 Results

Figures 4.3.1, 4.3.2 and 4.3.3 show transmission spectra for $Ge_{10}Se_{90-x}Te_x$ (*x=0, 10, 20, 30, 40, 50*) thin films. The fringes in the spectra are due to interference
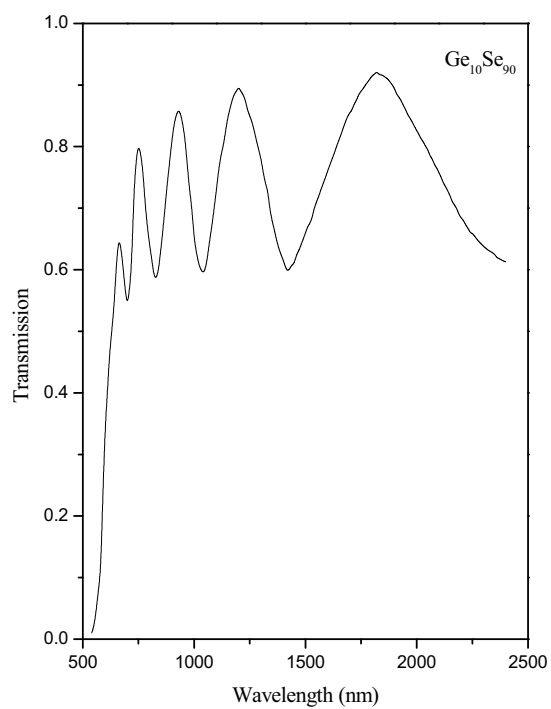
Figure 4.3.1 Transmission spectrum for $Ge_{10}Se_{90}$ thin film.
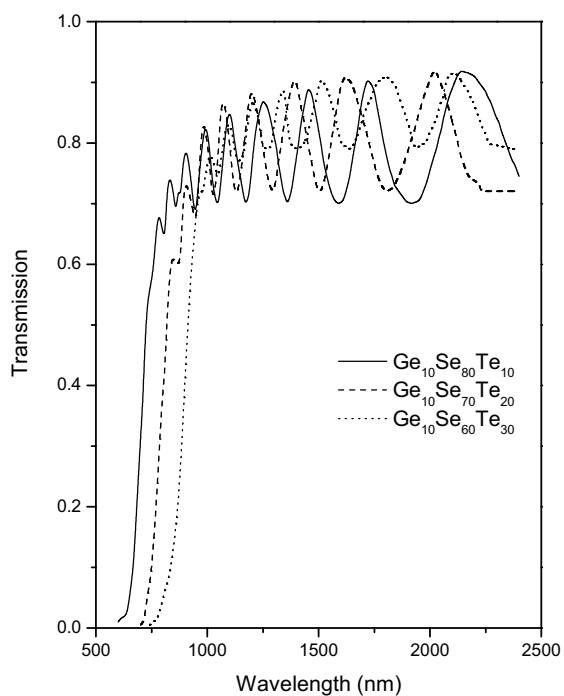
Figure 4.3.2 Transmission spectra of $Ge_{10}Se_{90-x}Te_x$ ($x = 10, 20, 30$) thin films.
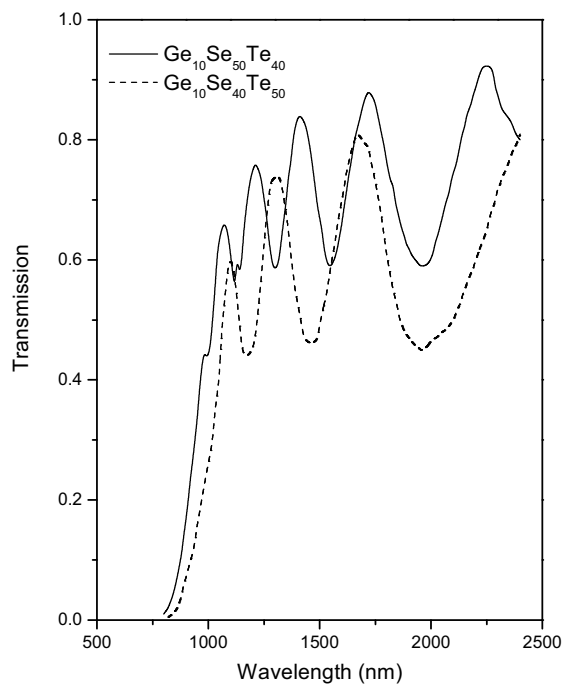
Figure 4.3.3 Transmission spectra of $Ge_{10}Se_{90-x}Te_x$ ($x = 40, 50$) thin films.
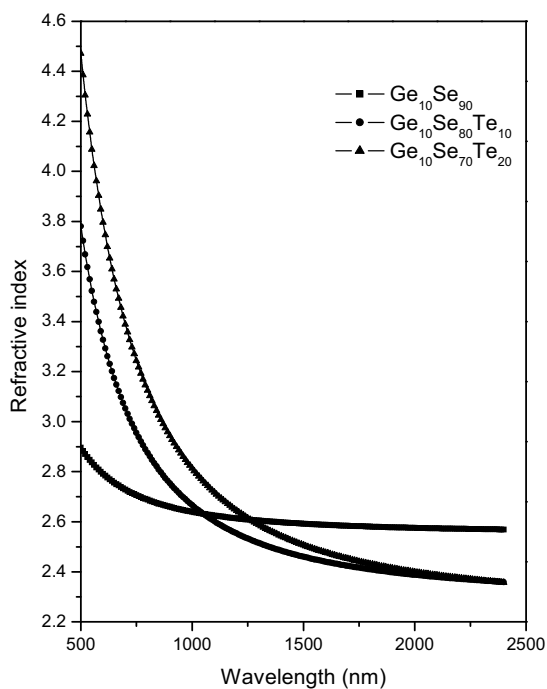
Figure 4.3.4 Variation of refractive index with wavelength for $Ge_{10}Se_{90-x}Te_x$ ($x = 0, 10, 20$) thin films.
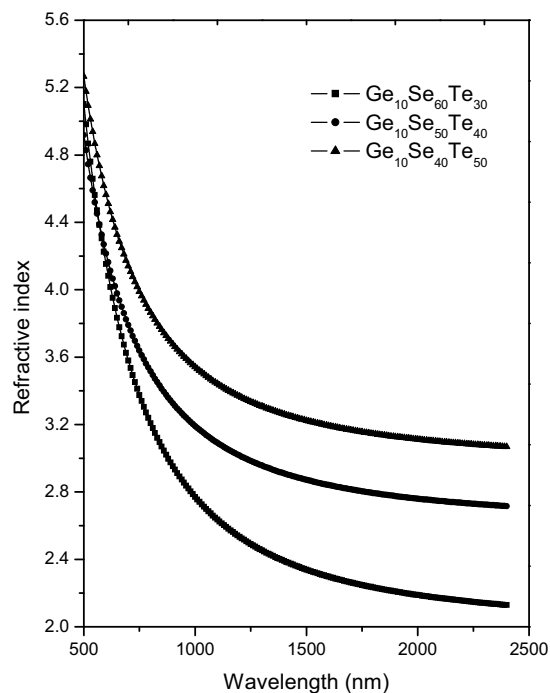
Figure 4.3.5 Variation of refractive index with wavelength for $Ge_{10}Se_{90-x}Te_x$ ($x = 30, 40, 50$) thin films.
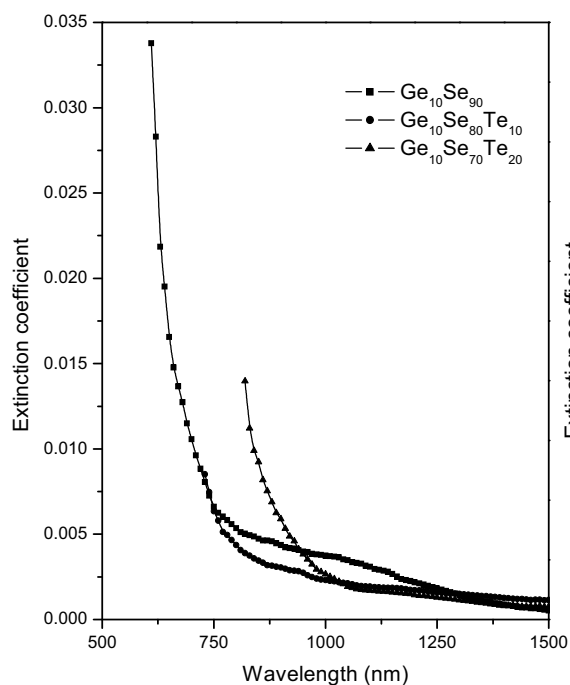
Figure 4.3.6 Variation of extinction coefficient with wavelength for $Ge_{10}Se_{90-x}Te_x$ ($x = 0, 10, 20$) thin films.
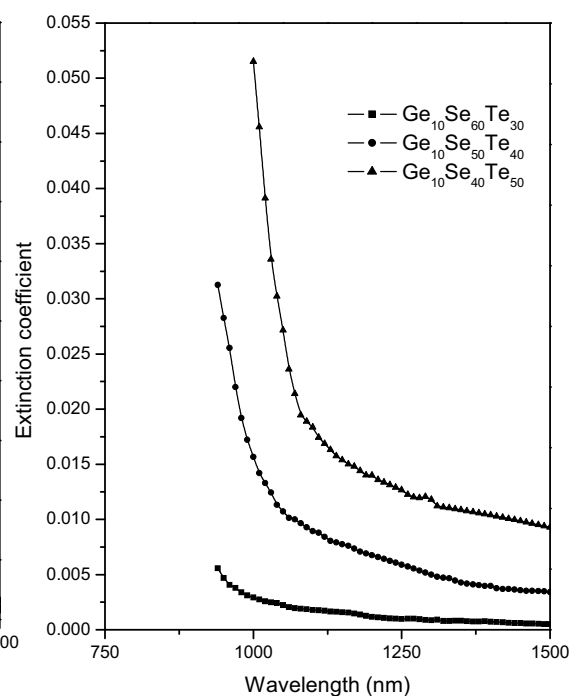
Figure 4.3.7 Variation of extinction coefficient with wavelength for $Ge_{10}Se_{90-x}Te_x$ ($x = 30, 40, 50$) thin films.

at various wavelengths. The maxima and minima of these fringes are used to calculate the various optical parameters. This is found that maxima and the minima of the fringes shift towards higher wavelength region with the increase of Te content in $Ge_{10}Se_{90-x}Te_x$. This may be due to the influence of the absorption coefficient (α) and scattering of light by defects.

Refractive index (n) and extinction coefficient (k) have been calculated using the technique proposed by Swanepoel (chapter 2). The spectral distribution of refractive index is shown in figures 4.3.4 and 4.3.5 and extinction coefficient is shown in figures 4.3.6 and 4.3.7 respectively. The values of refractive index at 800 nm are given in table 4.3.1.

The values of thickness of the thin films under investigation have been calculated using equation (2.22) and are given in table 4.3.1. The difference in thickness measured from thickness monitor and calculated from equation (2.22) lies with in ± 45 nm for all investigated thin films.

The high frequency properties of thin films could be treated as single oscillator. According to the single-effective oscillator model proposed by Wemple and DiDomenico [62] the optical data could be described to an excellent approximation by the following relation

$$n^2 - 1 = \frac{E_d E_0}{E_0^2 - (h\nu)^2}$$

where $h\nu$ is the photon energy, n is refractive index, E_0 is the oscillator strength also called average energy gap, E_d is the dispersion energy. The latter quantity measures the average strength of the interband optical transitions. Plotting $(n^2 - 1)^{-1}$ against $(h\nu)^2$ allows us to determine the oscillator parameters by fitting a straight line to the points. Figure 4.3.8 shows the plot of $(n^2 - 1)^{-1}$ versus $(h\nu)^2$. The values of E_0 and E_d can be directly determined from the slope $(E_0 E_d)^{-1}$ and the intercept on the vertical axis (E_0 / E_d) respectively. The values of static refractive indices (n_0) for thin films under investigation are calculated by extrapolating the Wemple-DiDomenico dispersion equation to $h\nu \rightarrow 0$ and are given in table 4.3.1. The high
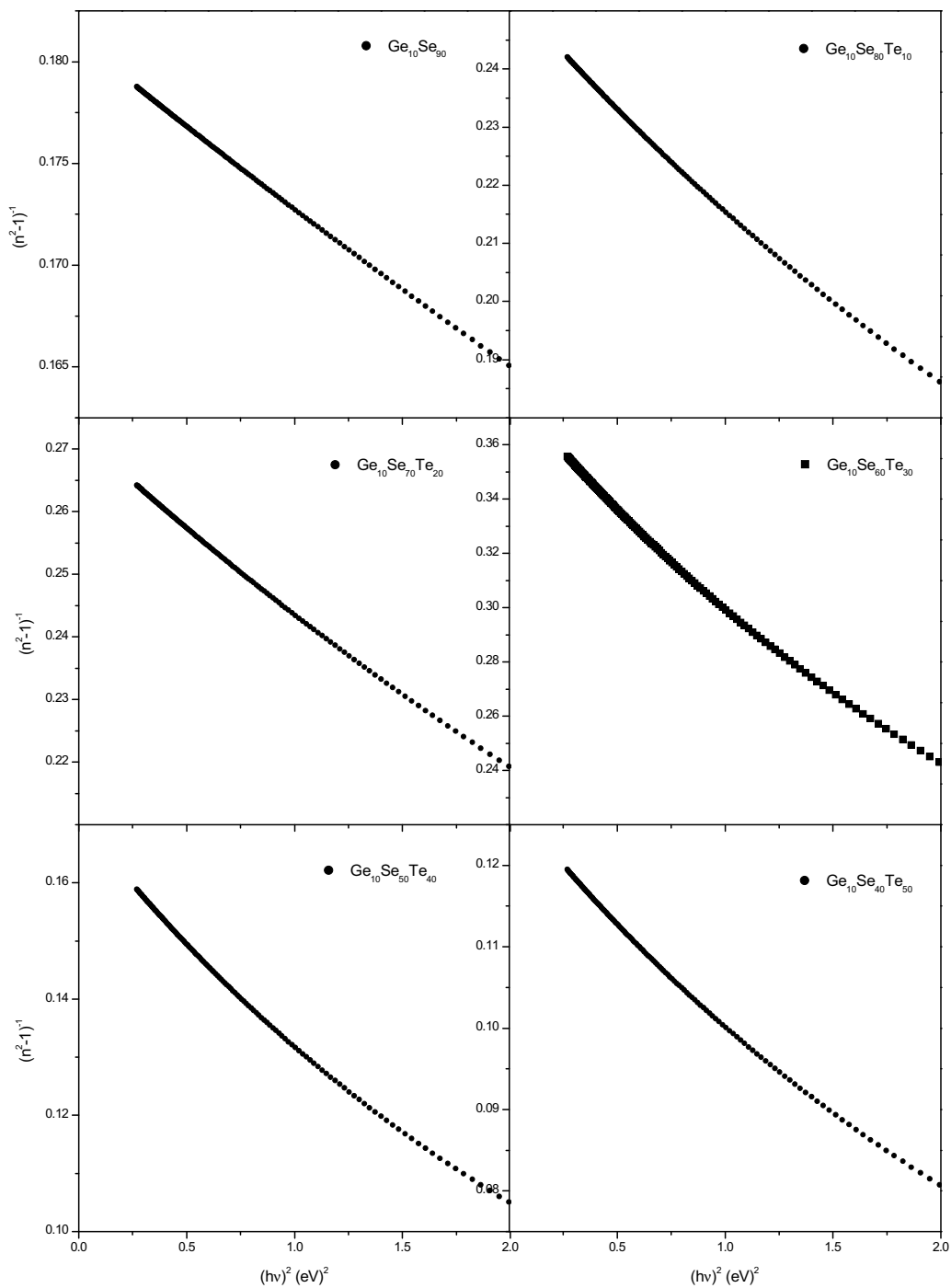
Figure 4.3.8 Plot of refractive index factor $(n^2-1)^{-1}$ vs. $(h\nu)^2$ for $Ge_{10}Se_{90-x}Te_x$ ($x = 0, 10, 20, 30, 40, 50$) thin films.
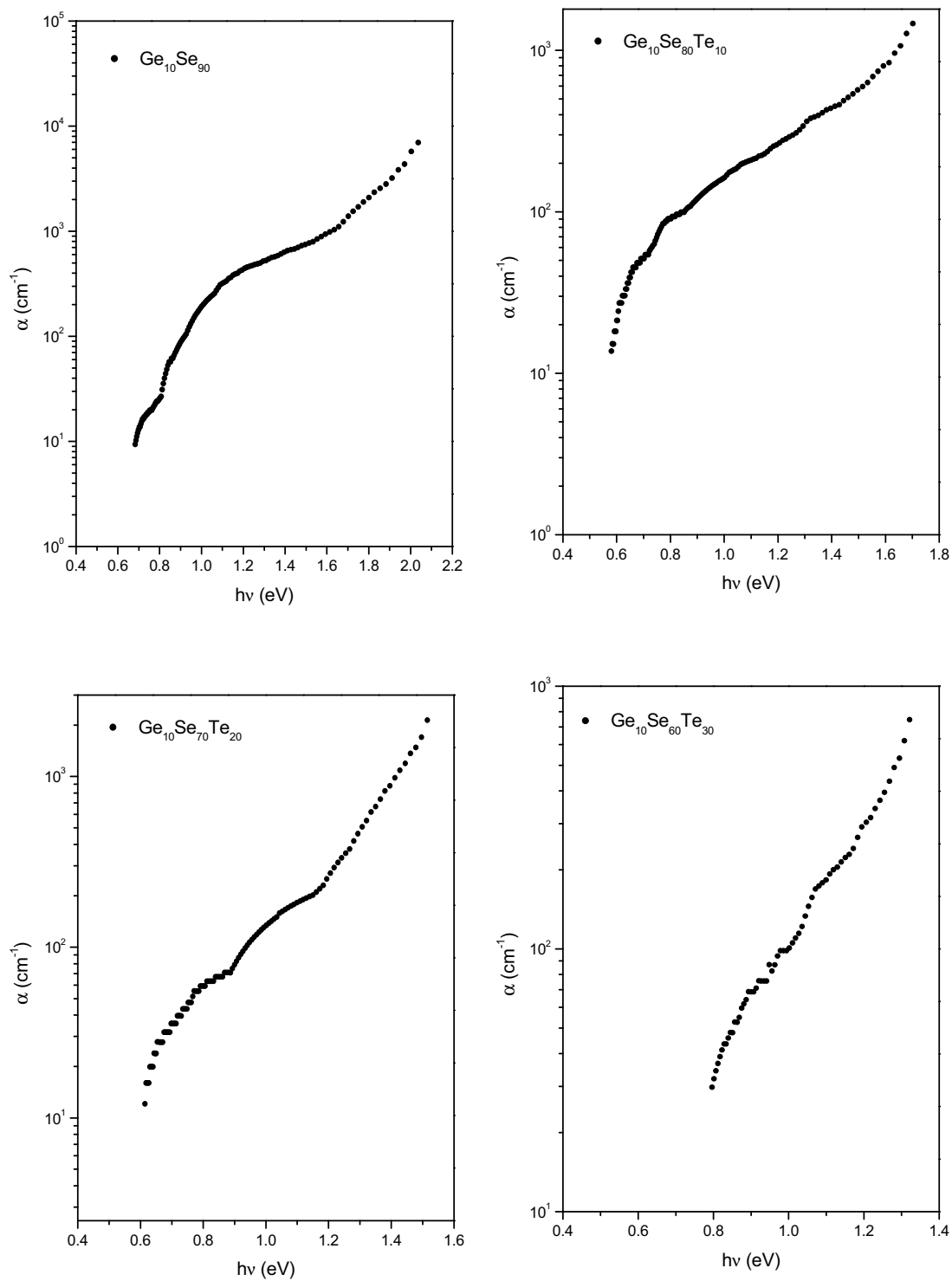
Figure 4.3.9 Plot of absorption coefficient (α) vs. hν for $Ge_{10}Se_{90-x}Te_x$ ($x = 0$, *10, 20, 30*) thin films.
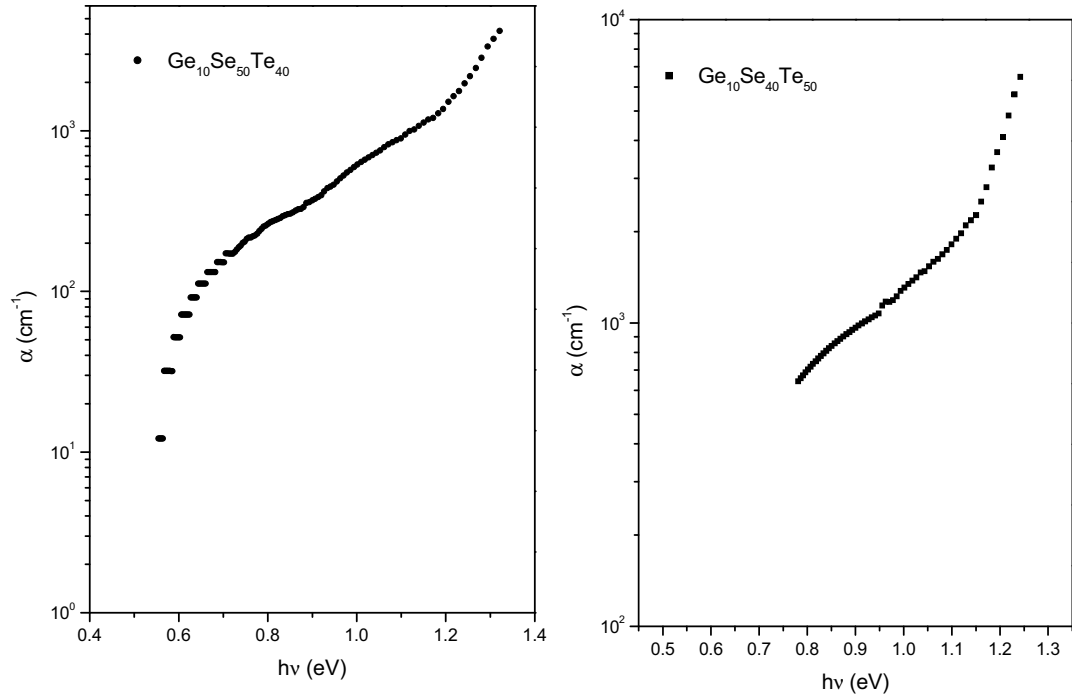
Figure 4.3.10 Plot of absorption coefficient (α) vs. hν for $Ge_{10}Se_{90-x}Te_x$ (*x = 40, 50*) thin films.
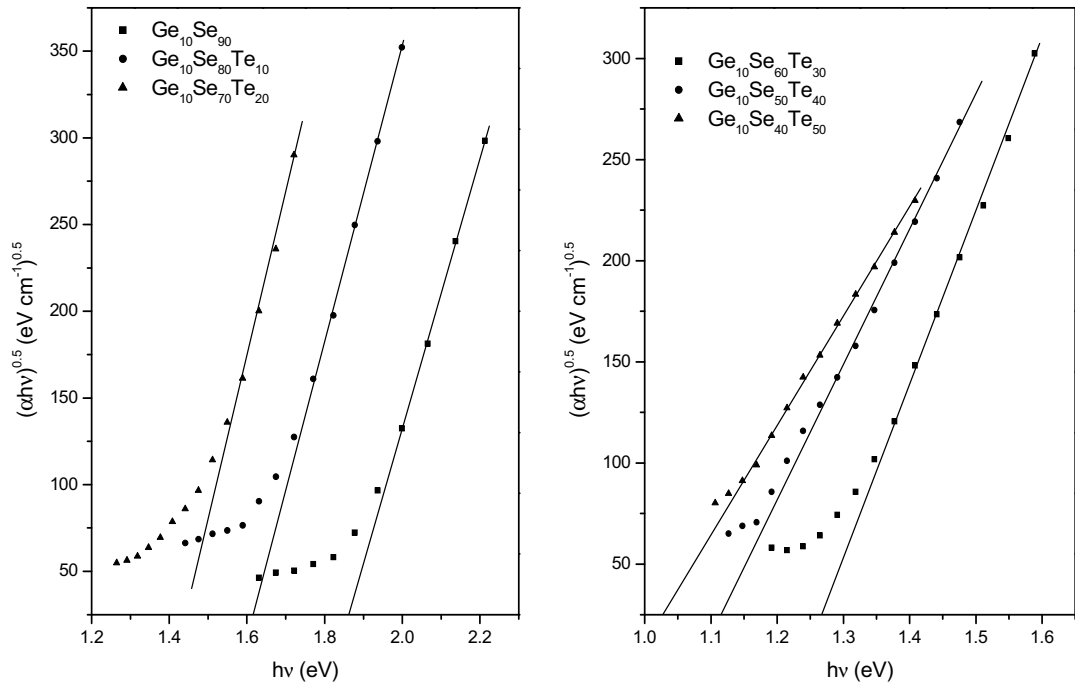
Figure 4.3.11 Plot of $(\alpha h\nu)^{0.5}$ vs. hν for $Ge_{10}Se_{90-x}Te_x$ (*x = 0, 10, 20, 30, 40, 50*) thin films.

73

frequency dielectric constants [64] $\varepsilon_\infty = (n_0)^2$ for $Ge_{10}Se_{90-x}Te_x$ thin films are also given in table 4.3.1. Moreover an important achievement of Wemple-DiDomenico model is that it relates the dispersion energy E_d to other physical parameters of the material through a simple empirical relation $E_d = \beta N_c Z_a N_e$ where N_e is effective number of valence electrons per anion, N_c is effective coordination number of the cation nearest neighbour to the anion, Z_a is the chemical valency of the anion and β is a two valued constant with either an ionic or covalent value (for ionic materials $\beta = 0.26 \pm 0.03$ eV and for covalent materials $\beta = 0.37 \pm 0.04$ eV).

Figures 4.3.9 and 4.3.10 show the variation of absorption coefficient (α) with energy for the $Ge_{10}Se_{90-x}Te_x$ thin films. The absorption coefficient is measured in high and intermediate absorption regions, not in the weak absorption region. The values of α are calculated using equation (2.23). The absorption coefficient has been observed to decrease with the decrease in energy or increase in wavelength for all the thin films.

Figure 4.3.11 shows the plot of $(\alpha h\nu)^{1/2}$ vs. $h\nu$ for calculation of optical band gap (E_g^{opt}). The optical gap is determined by taking the intercept of the extrapolations to zero absorption with the photon energy axis $\{(\alpha h\nu)^{1/2} \rightarrow 0\}$ [65]. It is clear from the figure 4.3.11 that the optical gap decreases with increasing Te content. Figures 4.3.12 and 4.3.13 show the plots of real (ε_r) and imaginary (ε_i) parts of dielectric constants against photon energy respectively. The values ε_r and ε_i are calculated by using n and k values in the relations $\varepsilon_r = n^2 - k^2$ and $\varepsilon_i = 2nk$ [66]. The optical conductivity (σ) has been determined from the relation $\sigma = \alpha nc/4\pi$ [67]. Figure 4.3.14 shows the variation of σ vs. $h\nu$.

4.3.4 Discussion

Addition of Te in Ge-Se shifts the transmission towards higher wavelength side (figures 4.3.1, 4.3.2 and 4.3.3). This may be due to the influence of absorption coefficient and scattering of light by heavier Te atoms replacing the Se atoms as size of atoms play a crucial role in the scattering of light.
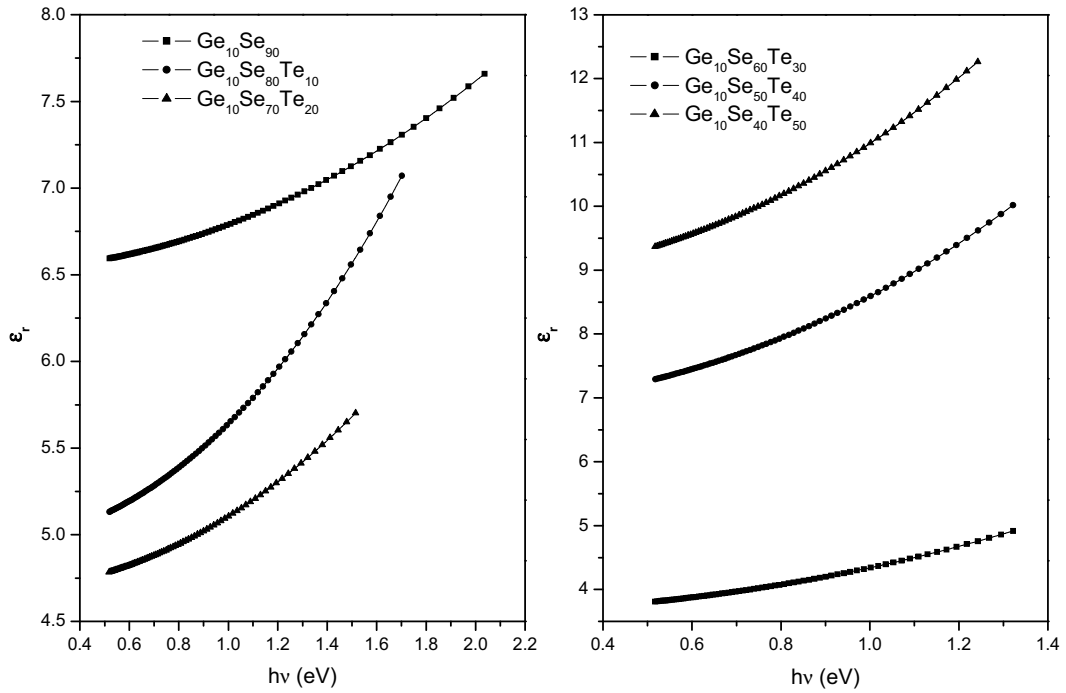
Figure 4.3.12 Plot of real part of dielectric constant (ε_r) vs. hν for $Ge_{10}Se_{90-x}Te_x$ ($x = 0, 10, 20, 30\ 40, 50$) thin films.
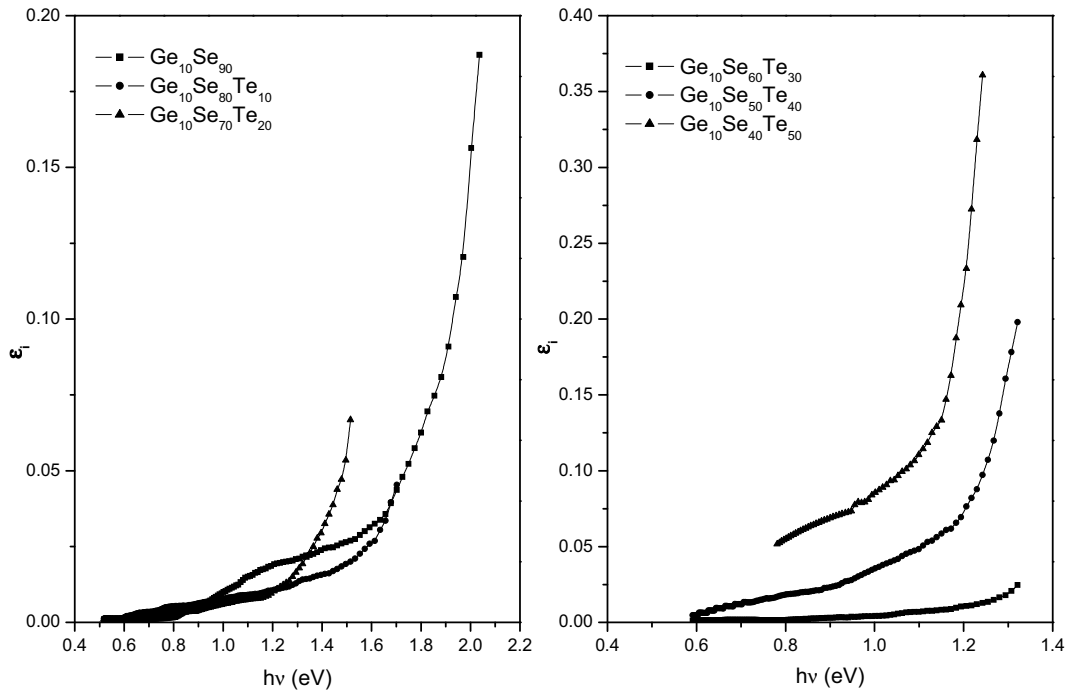
Figure 4.3.13 Plot of imaginary part of dielectric constant (ε_i) vs. hν for $Ge_{10}Se_{90-x}Te_x$ ($x = 0, 10, 20, 30\ 40, 50$) thin films.
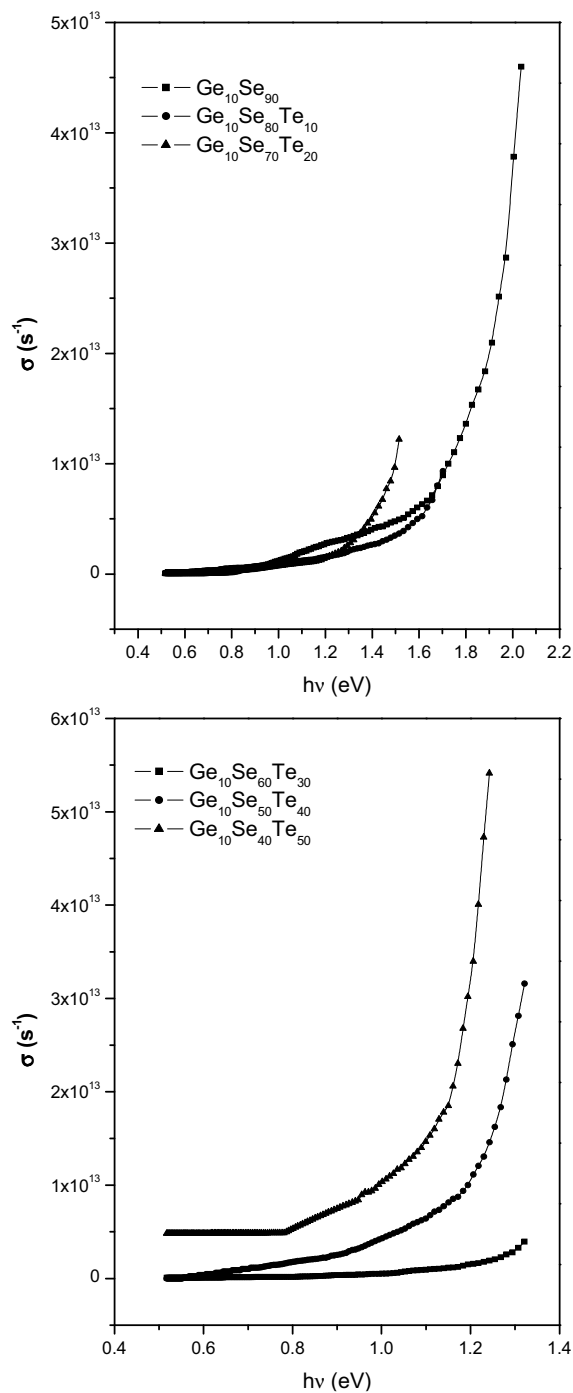
Figure 4.3.14 Plot of optical conductivity (σ) vs. hν for $Ge_{10}Se_{90-x}Te_x$ ($x = 0, 10, 20, 30, 40, 50$) thin films.

Table 4.3.1 Values of thickness (d), refractive index (n at 800 nm), optical band gap (E_g^{opt}), oscillator strength (E_0), dispersion energy (E_d), static refractive index (n_0) and high frequency dielectric constant (ε_∞) for $Ge_{10}Se_{90-x}Te_x$ (x = 0, 10, 20, 30, 40, 50) thin films

x	d (nm)	n	E_g^{opt} (eV)	E_0	E_d	n_0	ε_∞
0	798	2.69	1.87 ± 0.01	4.89	27.76	2.58	6.66
10	836	2.88	1.62 ± 0.01	3.43	22.13	2.73	7.45
20	829	3.12	1.46 ± 0.01	3.12	20.79	2.81	7.90
30	749	3.21	1.27 ± 0.01	2.72	20.42	2.94	864
40	813	3.52	1.12 ± 0.01	2.39	20.19	3.09	9.55
50	782	3.86	1.03 ± 0.01	2.20	20.17	3.19	10.18

Figures 4.3.4 and 4.3.5 show the variation of refractive index with wavelength. It is found that with the increase of wavelength there is a continuous decrease in refractive index showing the normal dispersion behaviour of the material. The refractive index is found to increase with the increase of Te content. This increase is large for the higher Te contents. This may be due to the change in stoichiometry [68] and internal strain [69] of the glassy alloy with large incorporation of the Te content. The addition of Te into Ge-Se system causes increase in the disorder which in turn may lead to increase of refractive index. Dispersion of refractive index has been studied in terms of Wemple-DiDomenico single oscillator model. This model leads to the calculation of oscillator strength (E_0) which, according to Tanaka [70], is related to optical band gap by the relation $E_0 \approx 2 \times E_g^{opt}$. The values of oscillator strength observed in our case are in concordance with the Tanaka's relation showing the justification of our results.

Figures 4.3.9 and 4.3.10 show that the absorption coefficient lies in the range 10^3 - 10^4 cm^{-1}. The absorption around the absorption edge has been often found to increase suddenly rather than gradually as in the case of oxide glasses. Optical band gap has been determined using the Tauc's extrapolation method. It is clear from Figure 4.3.11 that the optical gap decreases with increasing Te content. This can be correlated with the character of the chemical order of chalcogenide amorphous semiconductors. According to the model described by Kastner [71], the dominant contribution for states near the valence band edge in materials having chalcogen atoms as major constituents, comes from chalcogen atoms, especially from their lone-pair p-orbital. The lone-pair electrons in these atoms adjacent to electropositive atoms will have higher energies than those close to electronegative atoms. Therefore, the addition of electropositive elements to the alloy may raise the energy of some lone-pair states sufficiently to broaden further the band inside the forbidden gap. The electronegativities of Ge, Se and Te are 2.01, 2.55 and 2.1 respectively. According to these values, it is noticed that Te is less electronegative than Se, so the substitution of Te for Se may raise the energy of some lone-pair states and hence broaden the valence band. This will give rise to additional absorption over a wider range of energy leading to band tailing and hence shrinking of the band gap. The optical gap decreases from

1.87 to 1.03 eV for x = 0 to x = 50 Te content as shown in table 4.3.1. The addition of Te in the glass structure causes deeper band tails extended in the gap and thereby leading to a decrease in the value of optical band gap. The decrease in optical band gap with increasing Te content may also be related to the increase in number of Ge-Te (37.4 kcal/bond), Se-Te (40.6 kcal/bond) and Te-Te (33.0 kcal/bond) bonds and decrease of Se-Se (44.0 kcal/bond) and Ge-Se (49.1 kcal/bond) bonds. The strength of Ge-Te, Se-Te and Te-Te bonds is lower as compare to Ge-Se and Se-Se bonds so the optical absorption edge shifts towards higher values of wavelength with the addition of Te. Tellurium enters into the tetrahedral structure of GeSe$_2$ forming units containing all the three elements (Ge, Se, Te) thus leading to the modification of the glassy network. Further, the optical band gap is strongly dependent on the fractional concentration of Te atoms. This may be due to the tendency of Te atoms to form chemical disordering and to create localized states in the forbidden gap [72] leading to lower the optical band gap.

In chalcogenide glassy semiconductors, there are a large number of charged defect states, which are due to dangling bonds or valence alteration. The addition of Te to Ge-Se system induces structural changes in the host network because in chalcogenide glasses among divalent atoms, Te acts as three fold coordinated leading to acceptors or holes and thus supplying holes in the valence band. The increase of Te content leads to the formation of composition with higher degree of disorder and hence higher densities of localized states. The change in the optical properties for $Ge_{10}Se_{90-x}Te_x$ compositions may be explained by assuming that Te atoms act as an impurity center in the mobility gap. For binary Ge-Se alloy E_F is approximately pinned at the center of mobility gap where the charged defect centers have equal concentration. Thus the distribution and density of localized states are modified and even some new trap states may be created in the mobility gap leading to changes in the optical gap.

The other parameters i.e. dielectric constants and optical conductivity have been determined by making use of the refractive index (n), extinction coefficient (k) and absorption coefficient (α). Figures 4.3.12 and 4.3.13 show the variation of real and imaginary parts of dielectric constants and found to increase with the photon energy. Figure 4.3.14 shows the plot of optical conductivity and it also increases with

photon energy. Since dielectric constants and optical conductivity depends on n, k and α, thus their variation can be explained similarly to n, k and α.

4.3.5 Conclusion

Different parameters related to optical properties were calculated for the thin films of $Ge_{10}Se_{90-x}Te_x$ glassy alloy. Transmission spectra show that with the addition of Te content there is red shift in the transmission. Refractive index has been found to decrease with the increase of wavelength. The refractive index increases sharply for higher content of Te addition. Absorption coefficient lies in the range $10^{-3} - 10^{-4}$ cm^{-1}. Optical band gap has been calculated from Tauc's extrapolation method and found to decrease with the increase of Te content. The optical band gap changes from 1.87 eV to 1.03 eV for x = 0 to x = 50 respectively in $Ge_{10}Se_{90-x}Te_x$ thin films. The decrease of optical band gap has been explained on the basis of decrease of bond energy of the system and electronegativity concept.

4.4 Effect of deposition parameters on the optical properties

Thin films deposited under different conditions produce different results, whether it is the case of method of thin film deposition or the parameters considered while deposition. In this section we have considered three important parameters on which the properties of films may depend. These parameters contain variation of thickness of films, type of substrates used and the substrate temperature at which films are deposited. The optical properties, viz. refractive index and optical band gap, of films deposited under these three conditions were investigated in this section.

4.4.1 Effect of thickness

The thickness dependent study has been performed for the optical properties of $Ge_{10}Se_{90-x}Te_x$ (x = 0, 10, 20, 30, 40, 50) thin films. Thin films of three different thicknesses have been deposited on microscopic glass substrates for all the six samples of Ge-Se-Te glassy alloys. Thickness of the thin films was measured while deposition using thickness monitor (DTM-101) attached with coating unit (HINDHIVAC 12A4D). The temperature of substrate was kept at 303 K.

The transmission spectra of all the thin films have been obtained using UV-Vis-NIR spectrophotometer (Perkin Elmer Lambda-750) in the spectral range 200-1500 nm. In UV region no transmission has been observed. Figures 4.4.1 and 4.4.2 show the transmission spectra for 500 nm and 1100 nm thick films. Figures 4.3.1, 4.3.2 and 4.3.3 show transmission spectra for 800 nm thick films. Refractive index (n) has been determined from the envelope method proposed by Swanepoel using transmission data only (chapter 2). Optical band gap (E_g^{opt}) has been determined from the Tauc's extrapolation method (chapter 2). The accuracy in the values of thickness measured and calculated using equation (2.22) was with in ± 45 nm.

The variation of refractive index with wavelength for 500 nm and 1100 nm thick films is shown in figure 4.4.3. Figures 4.3.4 and 4.3.5 show the variation of refractive index for d = 800 nm. Table 4.4.1 shows the refractive indices calculated at 800 nm wavelength for 500 nm, 800 nm and 1100 nm thick films.

This has been observed from table that there is almost no variation of refractive index with the change in thickness of the films from 500 nm to 1100 nm. The standard deviation in the results is almost 0.018 on the average for all compositions. So there is no change with in experimental error on the refractive index in the thickness range from 500 nm to 1100 nm. Concerning the variation of refractive index with composition, it increases with increasing Te ratio for all the thicknesses, which may be attributed to the compactness of the material and/or material aggregation leading to increase in disorder, as discussed earlier.

Figures 4.3.11 and 4.4.4 show the plots of $(\alpha h \nu)^{0.5}$ versus $h \nu$ for the optical band gap estimation. The corresponding values of optical band gap for all composition for different d values are listed in Table 4.4.1. This has been observed that the thicker films are accompanied with the larger optical band gap. This can be explained in terms of insufficient number of atoms deposited on the amorphous film, resulting in the existence of unsaturated bonds, which are responsible for the formation of some defects in the film. These, in turn, produce localized states in the band gap resulting in lowering of band gap. Thus thicker films are characterized by a homogeneous network, which minimizes the number of defects and the localized states, thereby increasing the optical band gap.

Table 4.4.1 Value of refractive index at 800 nm and optical band gap of $Ge_{10}Se_{90-x}Te_x$ (x = 0, 10, 20, 30, 40, 50) thin films for d = 500 nm, 800 nm and 1100 nm.

Sample	Refractive Index (at 800 nm wavelength)			Optical Band Gap (eV) ± 0.01 eV		
	500 nm	800 nm	1100 nm	500 nm	800 nm	1100 nm
0	2.67	2.69	2.68	1.78	1.87	1.80
10	2.85	2.88	2.90	1.42	1.62	1.48
20	3.10	3.12	3.08	1.28	1.46	1.58
30	3.25	3.21	3.24	1.11	1.27	1.40
40	3.49	3.52	3.50	1.02	1.12	1.26
50	3.84	3.86	3.85	0.91	1.03	1.09
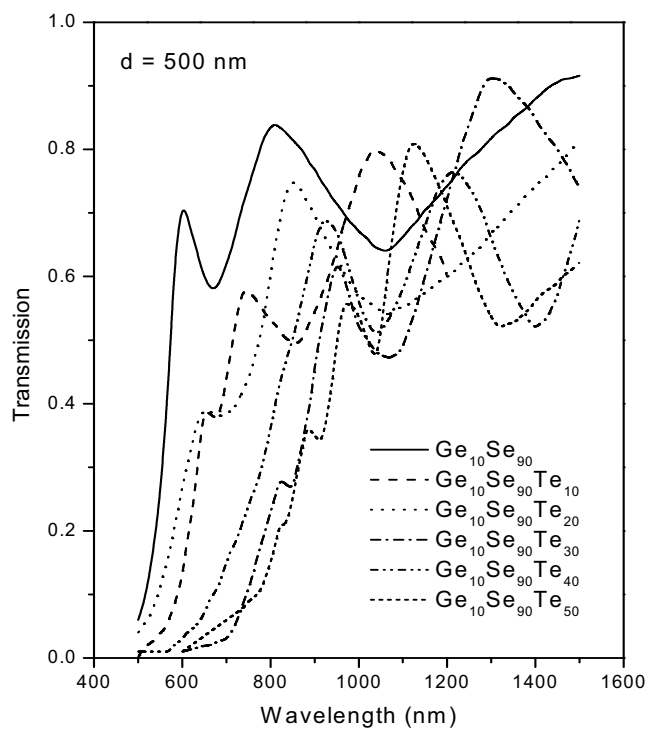
Figure 4.4.1 Transmission spectra for 500 nm thick $Ge_{10}Se_{90-x}Te_x$ films.
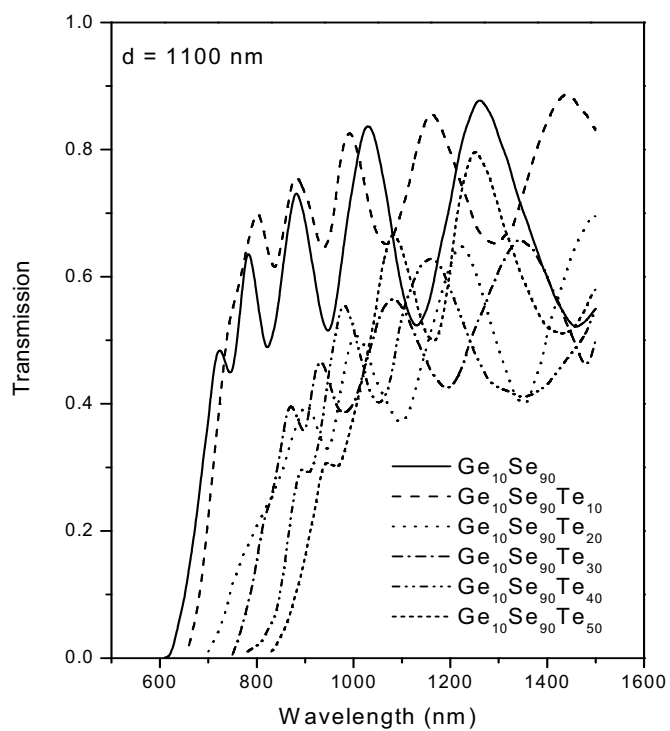
Figure 4.4.2 Transmission spectra for 1100 nm thick $Ge_{10}Se_{90-x}Te_x$ films.
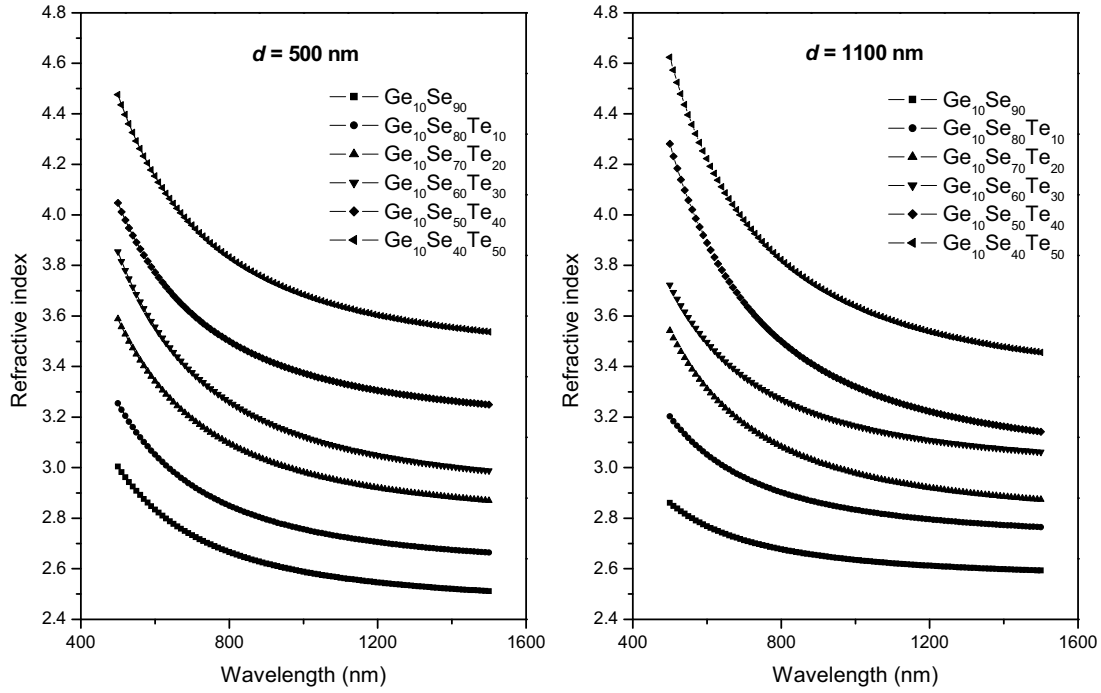
Figure 4.4.3 Variation of refractive index with wavelength for different thickness values (d = 500 nm and 1100 nm).
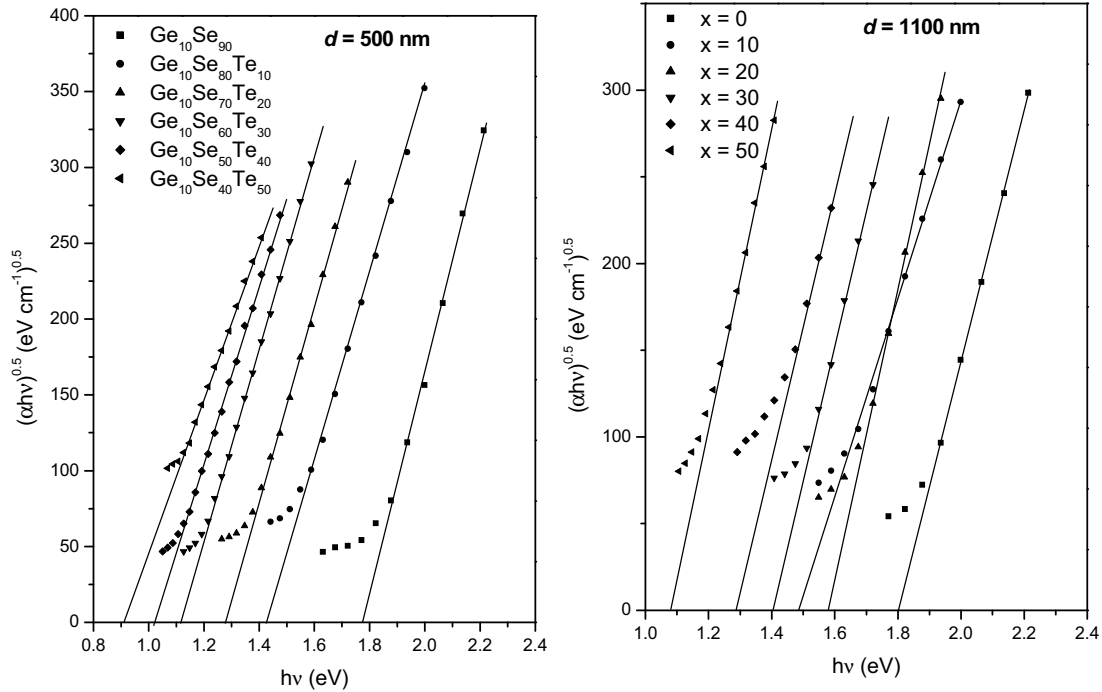
Figure 4.4.4 Plots of $(\alpha h\nu)^{0.5}$ versus $h\nu$ for different thickness values (d = 500 nm and 1100 nm).

4.4.2 Effect of substrate type

To study the effect of substrate material on the optical properties of thin films, three types of substrates have been used, (i) microscopic glass, (ii) quartz and (iii) mica. Films of $Ge_{10}Se_{90-x}Te_x$ (x = 0, 10, 20, 30, 40, 50) glassy alloys were deposited on these three substrates keeping thickness at 800 nm. The normal incidence transmission spectra of films were obtained in the spectral range 200-2400 nm. In UV region no transmission has been observed. The spectrophotometer was set with a suitable slit width of one nm in the measured spectral range. Figures 4.4.5 and 4.4.6 show the transmission spectra for Ge-Se-Te films deposited on quartz and mica substrates respectively. Figures 4.3.1, 4.3.2 and 4.3.3 show transmission spectra for films deposited on microscopic glass. The refractive index (n) has been determined by the envelope method proposed by Swanepoel using transmission data only. The values of refractive indices used for three substrates are; s (microscopic glass) = 1.51, s (quartz) = 1.46, s (mica) = 1.56. The optical band gap (E_g^{opt}) has been determined from the Tauc's extrapolation method (chapter 2).

The spectral dependence of refractive index for the three substrates used is shown in figure 4.4.7. The values of refractive index at 800 nm are given in table 4.4.2. This is clear from the table that refractive index has maximum value for mica substrate while for quartz substrate it has minimum values. The trend for refractive index values is as $n_{mica} > n_{microscopic\ glass} > n_{quartz}$. The higher values of refractive index for mica may be attributed to the increase of disorderness and the internal strain in the films [69]. The effect of the substrate becomes less significant with the increase in film thickness [73]. In terms of composition, refractive index increases (for all types of substrates) with the increase of Te content. This may be explained on the basis of polarizability. Larger the atomic radius of the atom larger will be its polarizability and consequently according to Lorentz- Lorenz relation of refractive index and polarizability [74] larger will be the refractive index.

Figures 4.3.11, 4.4.8 and 4.4.9 show the plots of $(\alpha h \nu)^{0.5}$ versus $h\nu$ for the optical band gap estimation corresponding to microscopic glass, quartz and mica substrates respectively. The values of optical band gap for all composition under investigations are also listed in table 4.4.2.
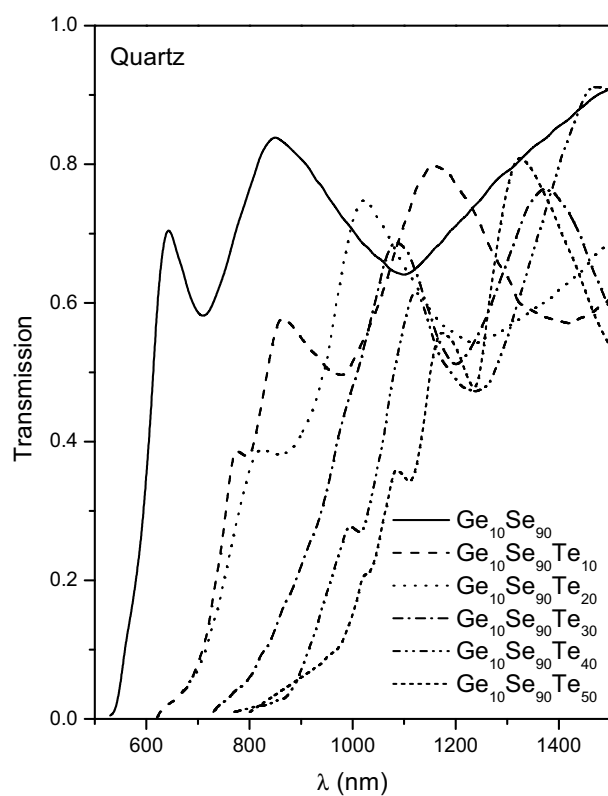
Figure 4.4.5 Transmission spectra for $Ge_{10}Se_{90-x}Te_x$ films deposited on quartz.
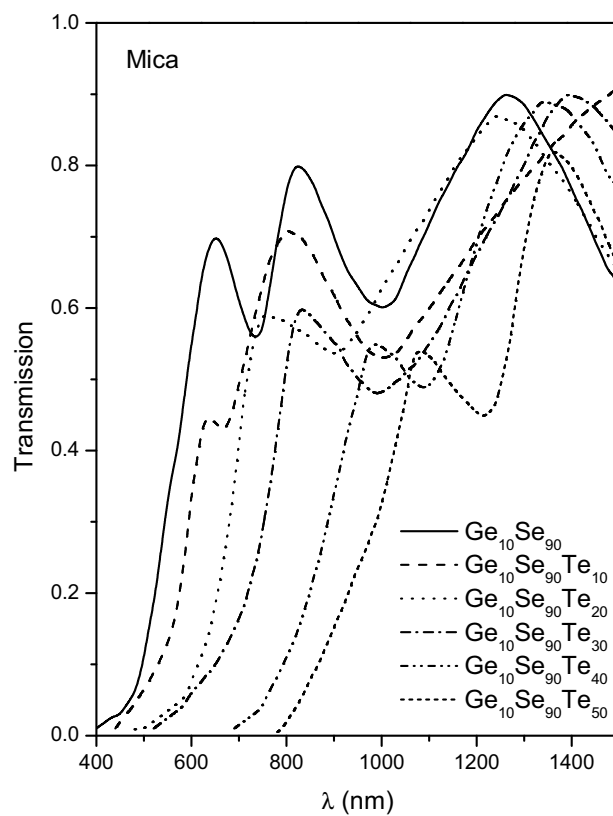
Figure 4.4.6 Transmission spectra for $Ge_{10}Se_{90-x}Te_x$ films deposited on mica.
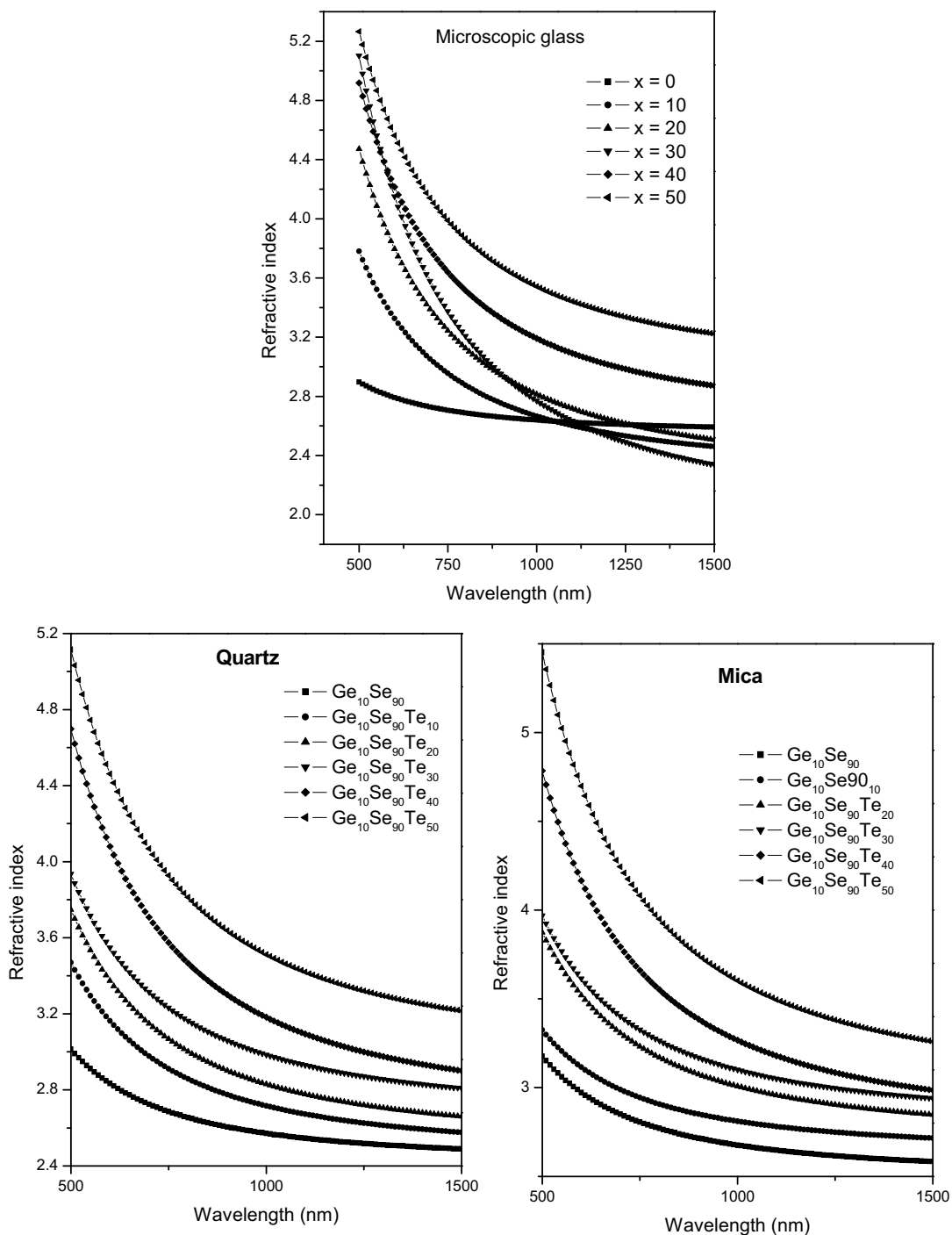
Figure 4.4.7 Variation of refractive index for different substrates used for deposition of $Ge_{10}Se_{90-x}Te_x$ (x = 0, 10, 20, 30, 40, 50) thin films.
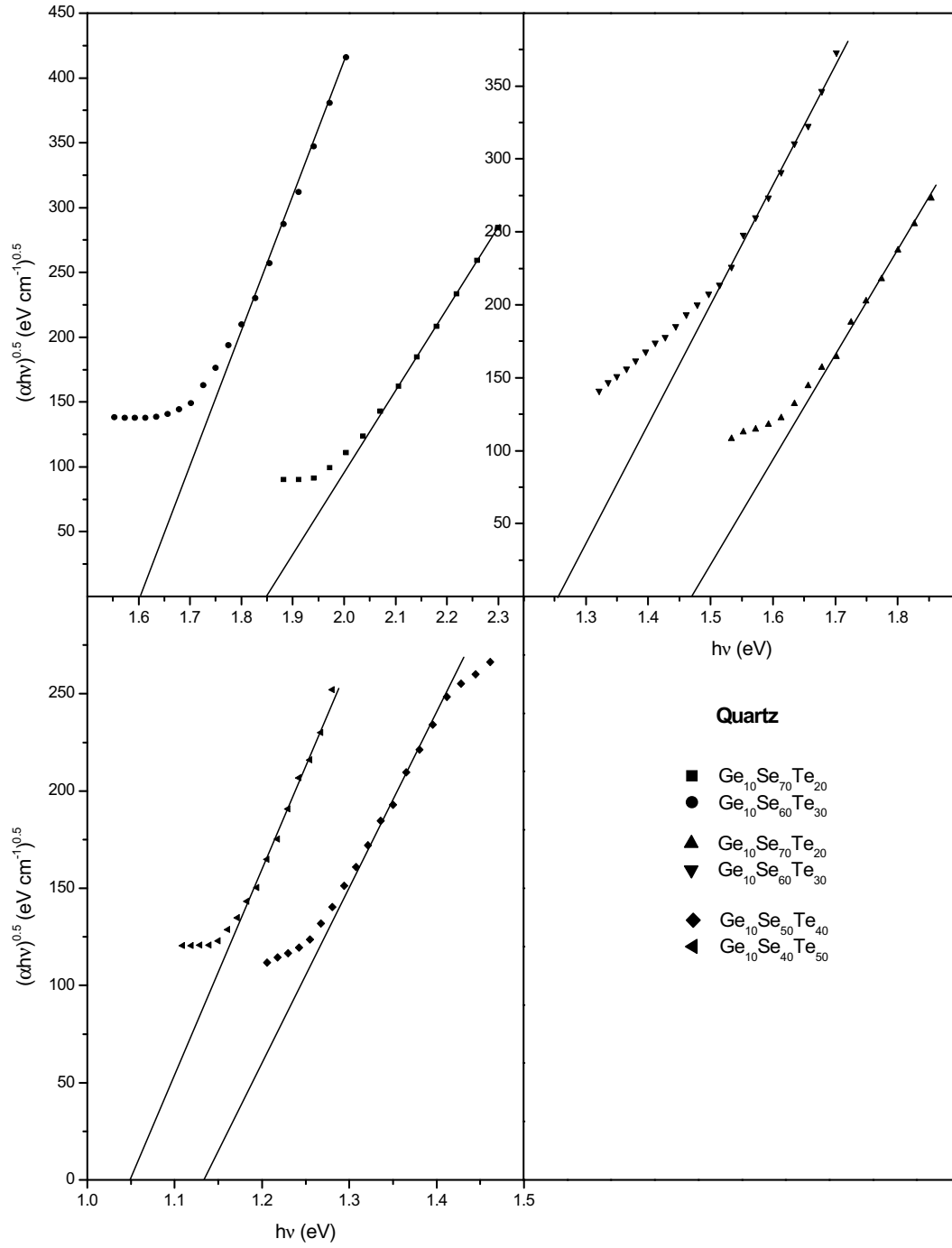
Figure 4.4.8 Plots of $(\alpha h\nu)^{0.5}$ versus $h\nu$ for $Ge_{10}Se_{90-x}Te_x$ (x = 0, 10, 20, 30, 40, 50) thin films deposited on quartz substrates.
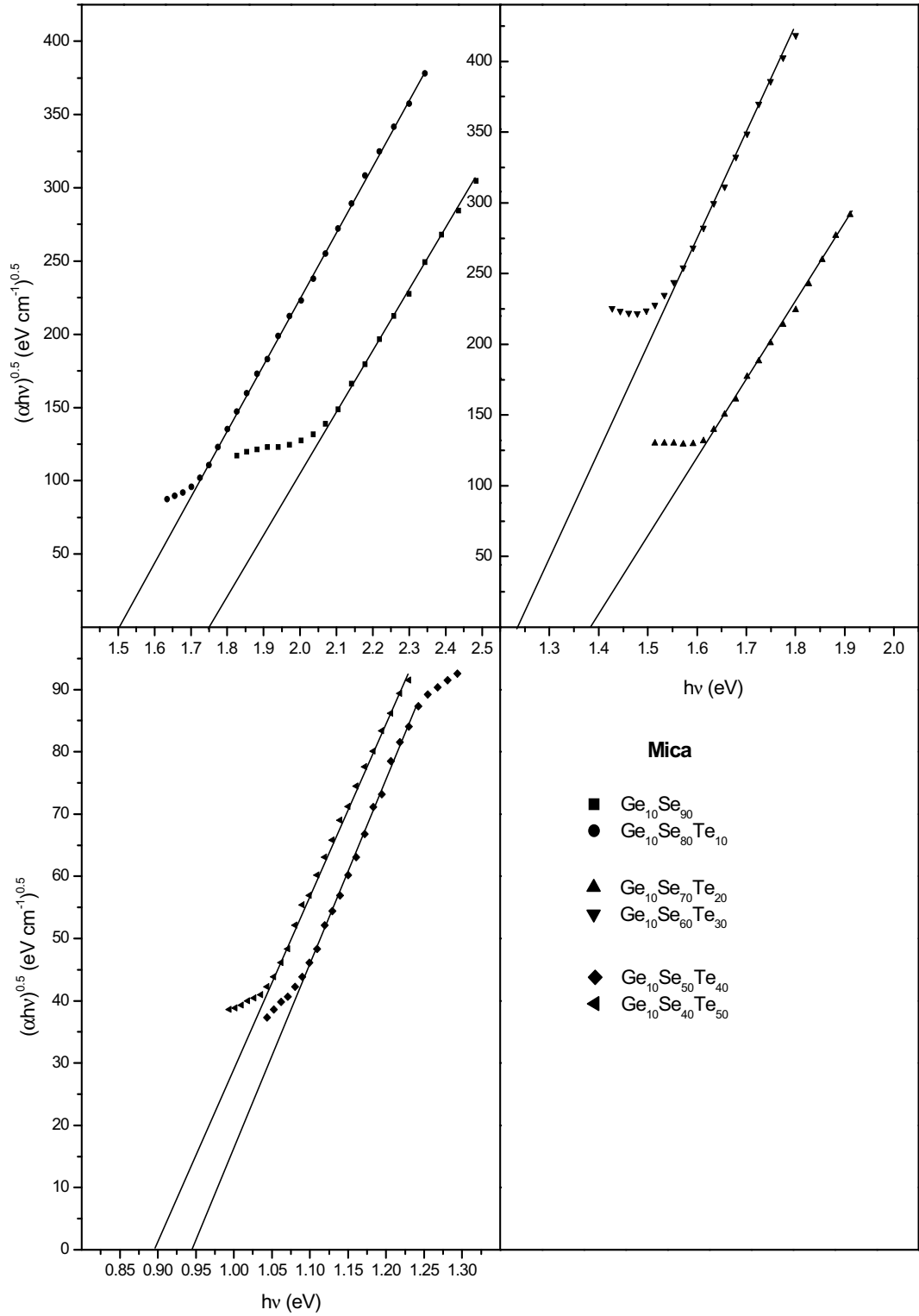
Figure 4.4.9 Plots of $(\alpha h\nu)^{0.5}$ versus $h\nu$ for $Ge_{10}Se_{90-x}Te_x$ (x = 0, 10, 20, 30, 40, 50) thin films deposited on mica substrates.

Table 4.4.2 Value of refractive index at 800 nm and optical band gap of $Ge_{10}Se_{90-x}Te_x$ (x = 0, 10, 20, 30, 40, 50) thin films deposited on different substrates.

x	Refractive Index (at 800 nm)			Optical Band Gap (eV) ± 0.01 eV		
	Microscopic glass	Quartz	Mica	Microscopic glass	Quartz	Mica
0	2.69	2.65	2.77	1.87	1.85	1.75
10	2.88	2.85	2.91	1.62	1.61	1.50
20	3.12	3.00	3.16	1.46	1.47	1.38
30	3.21	3.16	3.26	1.27	1.26	1.23
40	3.52	3.46	3.55	1.12	1.13	0.94
50	3.86	3.81	3.94	1.03	1.05	0.89

The films deposited on mica substrates have lower optical energy gap compared to films deposited on glass and quartz substrates. The low values of E_g^{opt} of films grown on mica may be attributed to that there might be some dangling bonds on the mica which may further contribute to the defects at substrate film interface. These defects may lead to decrease in E_g^{opt}. In such systems the degree of chemical order has a considerable effect on the band-gap. The chemical order and structured features depend in principle on the composition and deposition parameters, such as substrate type. The effect of the substrate becomes less significant with the increase in film thickness. These results are in good agreement with the results reported for Ge-Se-Bi-S system [73].

4.4.3 Effect of substrate temperature

The effect of substrate temperature on the optical properties, optical band gap and refractive index, of thermally deposited $Ge_{10}Se_{90-x}Te_x$ (x = 0, 10, 20, 30, 40, 50) thin films have been reported using transmission data. Thin films of the glassy alloys were prepared on glass substrates by vacuum evaporation technique at three different substrate temperatures 303 K, 363 K and 423 K. Thickness of the films has been kept at 800 nm. XRD patterns of $Ge_{10}Se_{90-x}Te_x$ (x = 0, 10, 20, 30, 40, 50) thin films deposited at 303 K reveals the amorphous nature of the films as they do not show any spectacular peak (figure 4.1.2) while those deposited at 363 K (figure 4.4.10) and 423 K (figure 4.4.11) show the polycrystalline nature of films. The normal incidence transmission spectra in the spectral range 200-1500 nm of $Ge_{10}Se_{90-x}Te_x$ (x = 0, 10, 20, 30, 40, 50) thin films were obtained by a double beam ultraviolet-visible-near infrared spectrophotometer [Perkin Elmer Lambda-750]. All transmission spectra were obtained at room temperature (300 K). Transmission spectra of films deposited at 363 K and 423 K have shown in figures 4.4.12 and 4.4.13 respectively. Figures 4.3.1, 4.3.2 and 4.3.3 show transmission spectra for films deposited at 303 K.

Refractive index (*n*) has been determined from the envelope method and optical band gap (E_g^{opt}) from Tauc extrapolation method for all the films deposited at three different substrate temperatures. The spectral dependence of refractive index has been shown in figure 4.4.14. The values of refractive index at 800 nm are given in
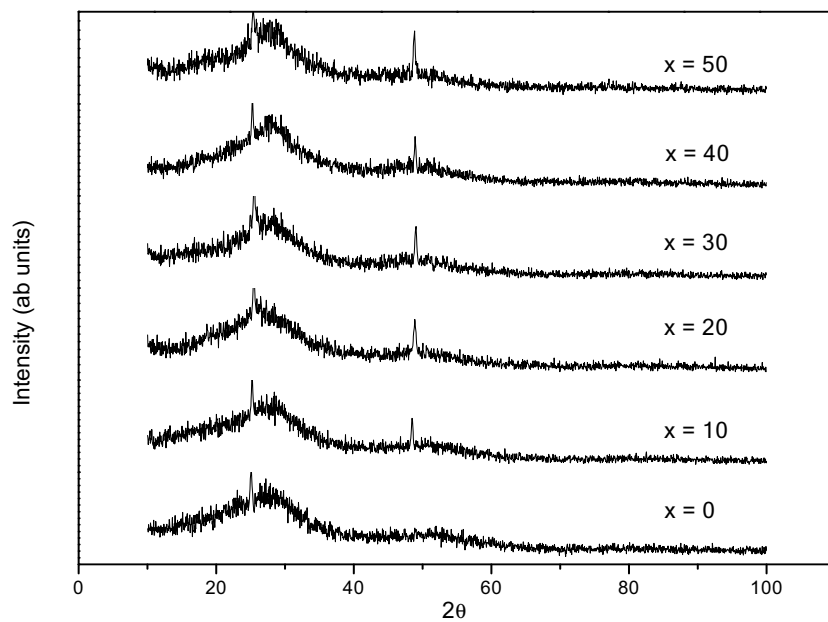
Figure 4.4.10 XRD pattern of $Ge_{10}Se_{90-x}Te_x$ films deposited at substrate temperature of 363 K.
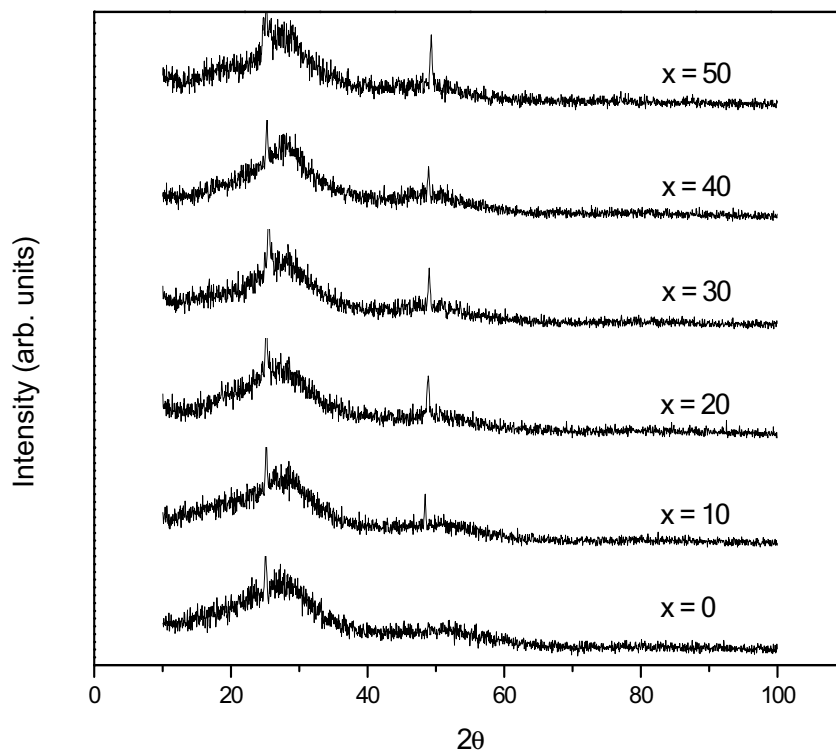
Figure 4.4.11 XRD pattern of $Ge_{10}Se_{90-x}Te_x$ films deposited at substrate temperature of 423 K.

Table 4.4.3 Value of refractive index at 800 nm and optical band gap of $Ge_{10}Se_{90-x}Te_x$ (x = 0, 10, 20, 30, 40, 50) thin films deposited for different substrate temperatures.

| x	Substrate Temperatures					
	303 K		363 K		423 K	
	E_g^{opt} (eV)	n	E_g^{opt} (eV)	n	E_g^{opt} (eV)	n
0	1.87	2.69	1.82	2.70	1.75	2.71
10	1.62	2.88	1.59	2.91	1.51	2.95
20	1.46	3.12	1.40	3.12	1.33	3.10
30	1.27	3.21	1.21	3.22	1.17	3.21
40	1.12	3.52	1.09	3.53	1.04	3.55
50	1.03	3.86	0.99	3.88	0.93	3.87
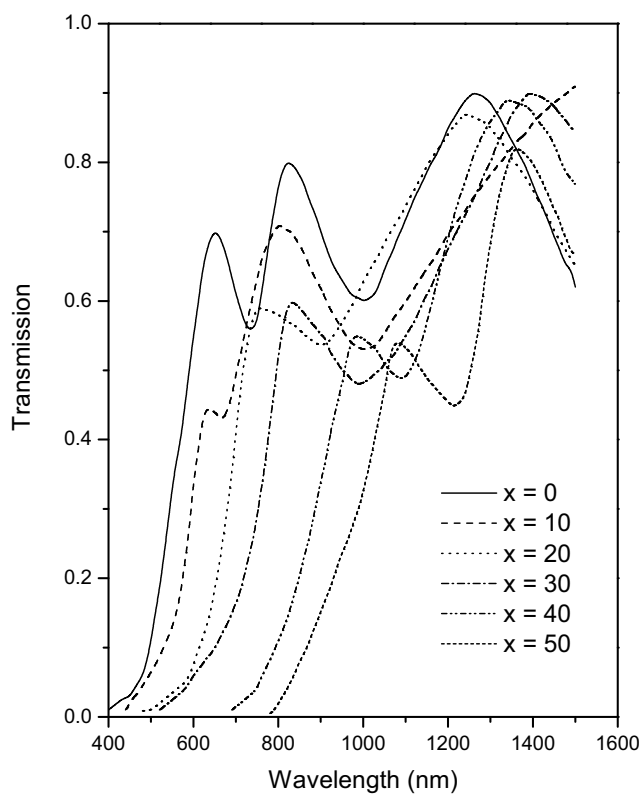
**Figure 4.4.12** Transmission spectra of $Ge_{10}Se_{90-x}Te_x$ films deposited at 363 K.
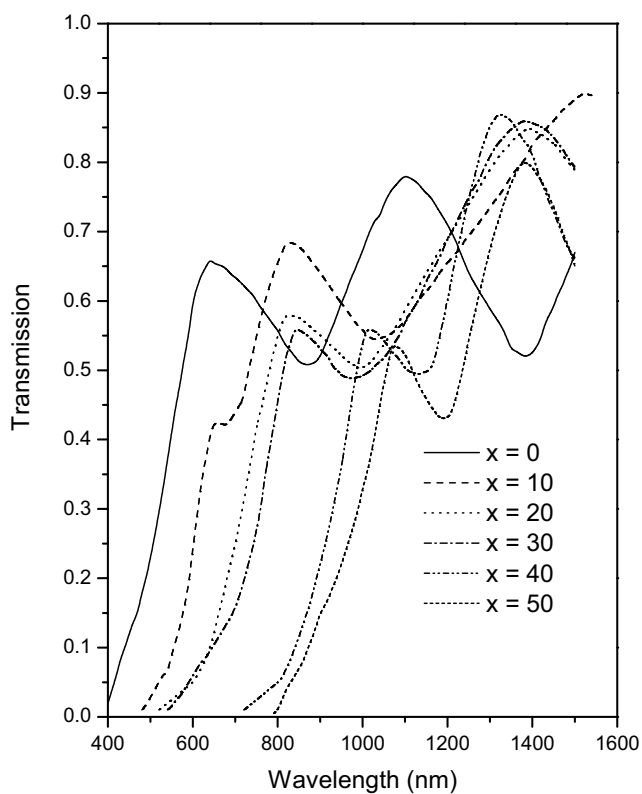
Figure 4.4.13 Transmission spectra of $Ge_{10}Se_{90-x}Te_x$ films deposited at 423 K.
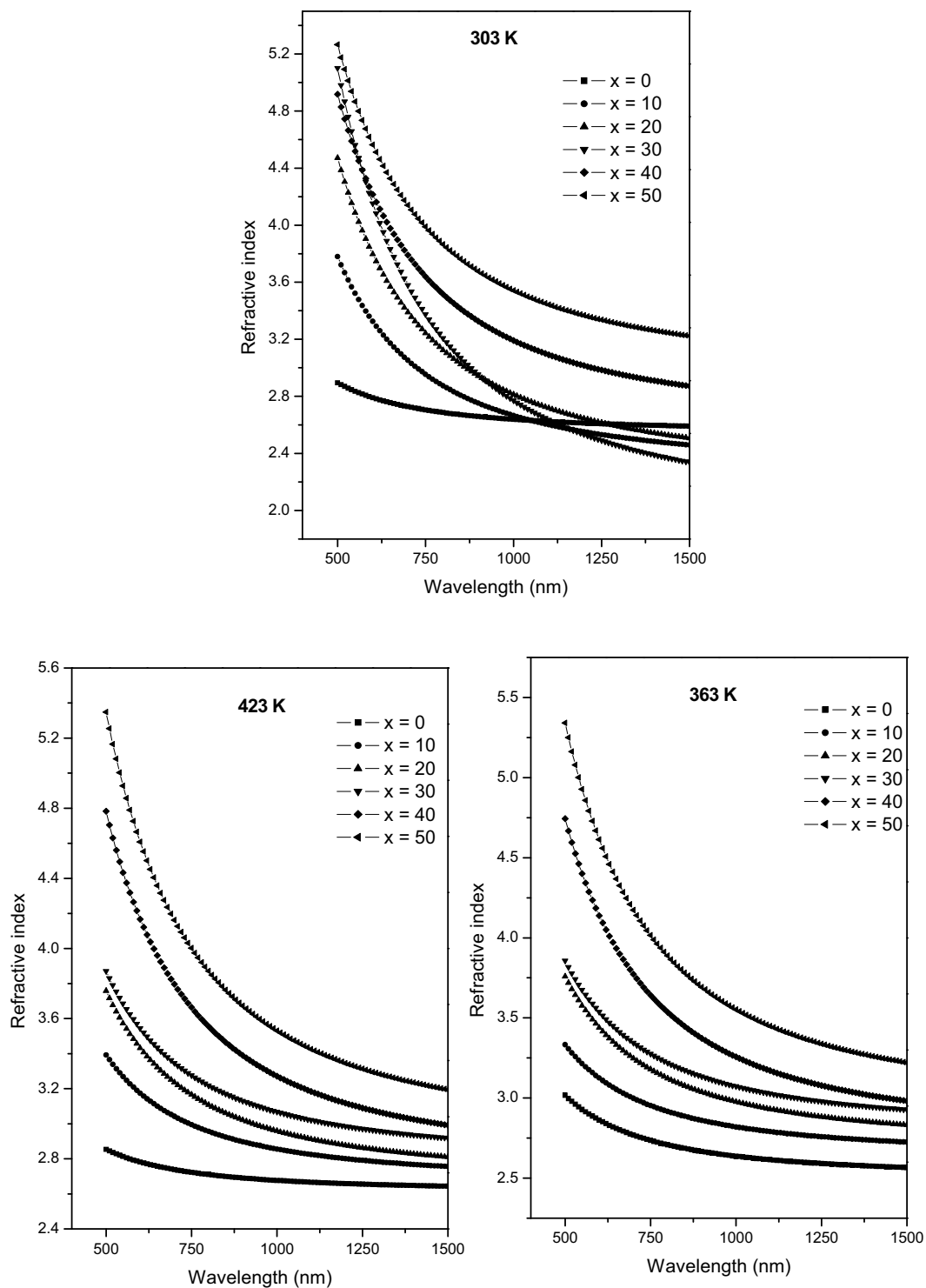
Figure 4.4.14 Variation of refractive index for different substrate temperatures of deposition for $Ge_{10}Se_{90-x}Te_x$ (x = 0, 10, 20, 30, 40, 50) thin films.
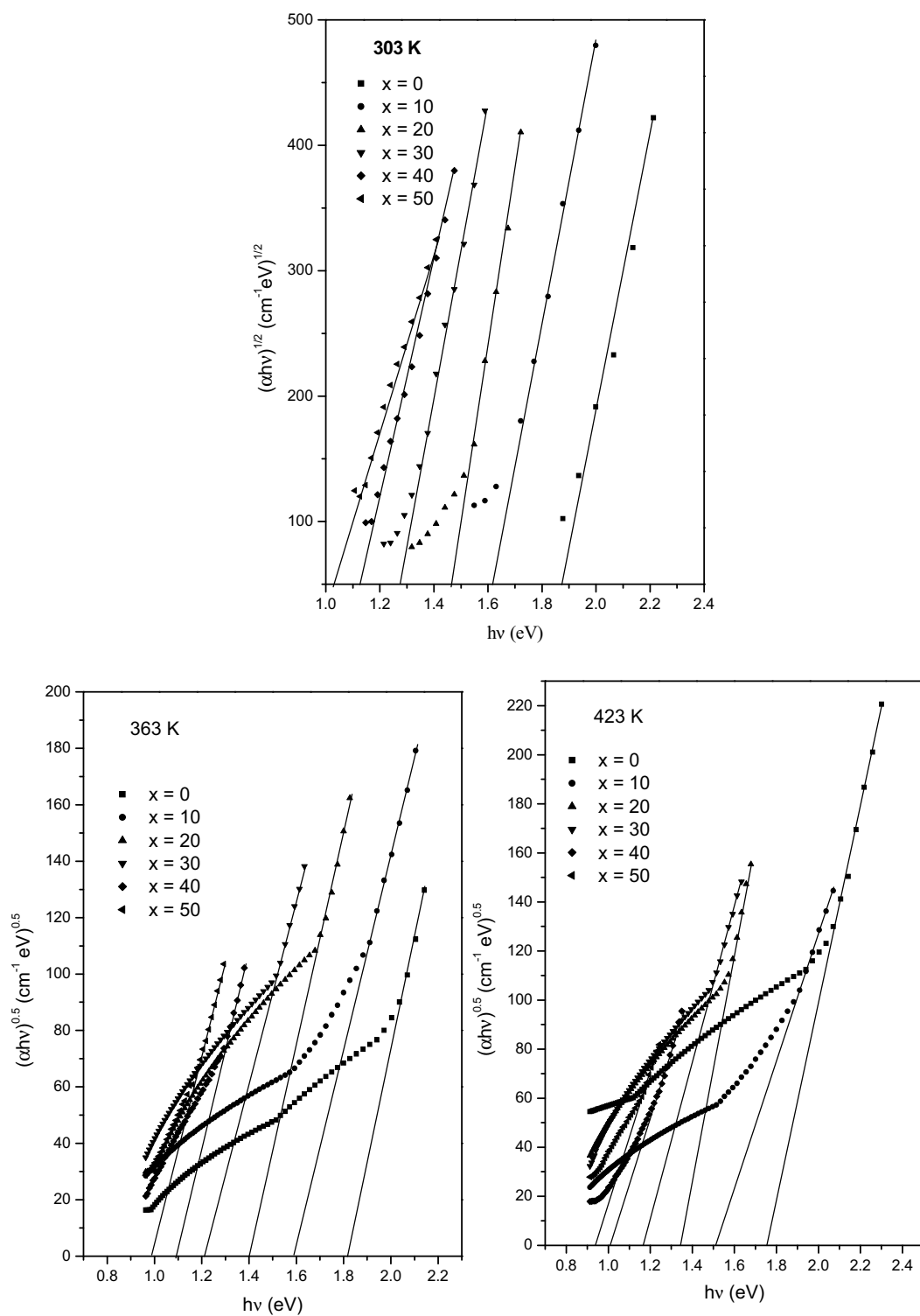
Figure 4.4.15 Plots of $(\alpha h\nu)^{0.5}$ versus $h\nu$ for different substrate temperatures of deposition for $Ge_{10}Se_{90-x}Te_x$ (x = 0, 10, 20, 30, 40, 50) thin films.

table 4.4.3 for comparison sake. It is seen from the table that there is almost no change in the refractive index with the increase of substrate temperature. According to Lorentz-Lorenz relation [75], refractive index depends on polarizability which further depends on the covalent radius (Ge = 122 pm, Se =117 pm, Te = 137 pm [20]) of atom. So the refractive index shows its dependence on the composition of films (table 4.4.3). It does not show any dependence on the substrate temperature. The optical band gap (E_g^{opt}) has been estimated using the Tauc relation [65], $\alpha h \nu = B(h\nu - E_g^{opt})^n$ where B is the slope of Tauc edge called band tailing parameter that depends on the width of localized states in the band gap which are attributed to homopolar bonds in chalcogenide glasses. In the above equation $n = 1/2$ for a direct allowed transition, $n = 3/2$ for a direct forbidden transition, $n = 2$ for an indirect allowed transition and $n = 3$ for an indirect forbidden transition. This relationship allows us to estimate the value of optical band gap. For substrate temperatures 303 K, 363 K and 423 K the plots of $(\alpha h \nu)^{0.5}$ versus $h\nu$ are shown in figure 4.4.15.

The values of the optical band gap for the thin films under investigation corresponding to different substrate temperatures are given in table 4.4.3. The optical gap has been found to decrease with the increase of substrate temperature for all the thin films. This reveals the increase in crystallinity of compositions [77]. Substrate temperature higher than room temperature may have enough vibrational energy to break some of the weaker bonds, thus introducing some translational degrees of freedom to the system. Consequently, increase in crystallinity via nucleation and growth becomes possible [78]. The area occupied by the crystallites increases, where some of them may be interconnected and some may be isolated, due to which there may be a decrease in optical gap. The decrease in energy gap and the increase in the width of localized state tails with the increase in substrate temperature can be interpreted by assuming it to be the product of surface dangling bonds around the crystallites during the process of crystallization. The obtained values of optical gap are in good agreement with that reported previously [79-81]. This is also observed that the optical gap decreases with the increase of Te content for all substrate temperatures. The shrinking of optical gap with increasing Te content can be correlated with increase in covalent character of glass network. Since Ge-Te bonds (~

97

99% covalent) are more covalent than Ge-Se (~90 % covalent) so optical gap decreases with the increase in Te contents. A detailed discussion on the decrease of optical gap with Te content is given in section 4.3.4.

4.4.4 Conclusion

Optical properties of $Ge_{10}Se_{90-x}Te_x$ (x = 0, 10, 20, 30, 40, 50) thin films have been studied for different deposition conditions, i.e. thickness, type of substrate and substrate temperature. The concluding points are summarized below:

➢ With the increase of thickness (500 nm - 1100 nm) the optical band gap has been found to increase while no significant change has been observed for refractive index with in experimental errors.

➢ For different substrate used in deposition of thin films the refractive index follows the order as $n_{mica} > n_{microscopic\ glass} > n_{quartz}$. The optical band gap for mica substrate is the smallest whereas no significant change has been observed for microscopic glass and quartz substrate.

➢ With the increase of substrate temperature (i.e. from 303 K – 423 K) refractive index remains unchanged while optical band gap decreases.

References

1. Fayek S A 2005 *Infrared Physics & Technology* **46** 193

2. Tikhomirov V K, Furniss D, Seddon A B, Savage J A, Mason P D, Orchard D A and Lewis K L 2004 *Infrared Physics & Technology* **45** 115

3. Petkov P and Petkova T 2000 *Semicond. Sci. Technol.* **15** 331

4. Maged A F, Montasser K I and Amer H H 1998 *Materials Chemistry and Physics* **56** 184

5. Trodahl H J 1982 *Solid State Communications* **44** *319*

6. Lukic S R, Petrovi D M, Skuban S J, Radonji L and Cveji Z 2003 *J. Optoelectron and Adv. Mater.* **5** 1223

7. Nagels P, Tichy L, Sleeckx E and Callaerts R 1998 *J. Non-Cryst. Solids* **227-230** 705

8. Tichy L, Ticha H, Nagels P and Callaerts R 1998 *J. Non-Cryst. Solids* **240** 177

9. Dwivedi P K, Tripathi S K, Pradhan A, Kulkarni V N and Agarwal S C 2000 *J. Non-Cryst. Solids* **266-269** 924

10. Lucovsky G 1969 *Physics of Selenium and Tellurium* ed. W C Cooper (Oxford : Pergamon) 255

11. Lucovsky G, Mooradian A, Taylor W, Wright G B and Keezer R C 1967 *Solid State Commun.* **5** 113

12. Caldwell R S and Fan H Y 1959 *Phys. Rev.* **114** 664

13. Mooradian A and Wright G B 1969 *Physics of Selenium and Tellurium* ed. Cooper W C (Oxford : Pergamon) 269

14. Ohsaka T 1975 *J. Non-Cryst. Solids* **17** 121

15. Tronc P, Bensoussan M, Brenac A and Sebenne C 1973 *Phys. Rev. B* **8** 5947

16. Schottmiller J, Tabak M, Lucovsky G and Ward A 1970 *J. Non-Cryst. Solids* **4** 80

17. Shirafuji J, Ohshima Y and Inuishi Y 1974 *J. Phys. Soc. Japan* **36** 915

18. Ball G J and Chamberlain J M 1978 *J. Non-Cryst. Solids* **29** 239

19. Izvekov V P, Koos M and Somogyi I K 1983 *J. Non-Cryst. Solids* **59-60** 1011

20. Kumagi N, Shirafuji J and Inuishi Y 1977 *J. Phys. Soc. Japan* **42** 1262

21. Nemanich R J, Connell G A N, Hayes T M and Street R A 1978 *Phys. Rev. B* **18** 6900

22. Sayers D E, Lytle F W and Stern E A 1972 *J. Non-Cryst. Solids* **8-10** 401

23. Lucovsky G, Nemanich R J and Galeener F L 1977 *Proc. 7th Int. Conf. on Amor. and Liq. Semiconductors* (Edinburgh) ed W E Spear (University of Edinburgh, Edinburgh, Scotland, 1977) 130

24. Katyal S C and Verma R C 1993 *J. Phys.: Condens. Matter* **5** 3469

25. Sharma P and Katyal S C 2007 *Thin Solid Films* **515** 7966

26. Othman A A, Aly K A and Abousehly AM 2007 *Thin Solid Films* **515** 3507

27. Savage J A 1985 *Infrared Optical Materials and their Antireflection Coatings* (London : Hilger)

28. Lucovsky G, Galeener F L, Keezer R C, Geils R H and Six H A 1974 *Phys. Rev. B* **10** 5134

29. Bicerno J and Ovshinsky S R 1985 *J. Non-Cryst. Solids* **74** 75

30. Sarrach J, de Neufiville J P and Hawoth W L 1976 *J. Non-Cryst. Solids* **22** 245

31. Thorpe M F and Phillips J C 2002 *Phase Transitions and Self-Organization in Electronic and Molecular Networks* (New York : Kluwer Academic)

32. Herzberg G 1945 *Molecular Spectra and Molecular Structure vol 2 Infrared and Raman Spectra of Polyatomic Molecules* (Princeton : Van Nostrand) 306

33. Fukunaga T, Tanaka Y and Murase K 1982 *Solid State Commun.* **42** 513

34. Ksendov A, Pollak F H, Espinosa G P and Phillips J C 1987 *Phys. Rev. B* **35** 2740

35. Phillips J C and Thorpe M F 1985 *Solid State Commun.* **53** 699

36. Phillips J C 1981 *J. Non-Cryst. Solids* **43** 37

37. Andrikopoulos K S, Yannopoulos S N, Voyiatzis G A, Kolobov A V, Ribes M and Tominaga J 2006 *J. Phys.: Condens. Matter* **18** 965

38. Wang Z, Tu C, Li Y and Chen Q 1995 *J. Non-Cryst. Solids* **191** 132

39. Tanaka K 1989 *Phys. Rev. B* **39** 1270

40. Seddon A B 1995 *J. Non-Cryst. Solids* **184** 44

41. Marquez E, Villars P and Jimenez R G 1988 *J. Mater. Res.* **3** 314

42. Hilton A R, Hayes D and Rechtin M 1975 *J. Non-Cryst. Solids* **17** 319

43. Dessaur J H and Clarke H E 1965 *Xerography and Related Processes* (London: Focal Press)

44. Ovshinsky S R 1968 *Phys. Rev. Lett.* **21** 1450

45. Carlson D E and Wronski C R 1976 *Appl. Phys. Lett.* **28** 671

46. Mott N F 1967 *Adv. Phys.* **16** 49

47. Mott N F 1976 *Philos. Mag.* **34** 285

48. Vasko A 1978 *Appl. Opt.* **17** 675

49. Sanghara J S and Agarwal I D 1999 *J. Non-Cryst. Solids* **256 & 257** 6

50. Schwartz K 1993 *The Physics of Optical Recording* (Berlin: Springer-Verlag)

51. Bradley A 1989 *Optical Storage for Computers Technology and Applications* (New York Ellis: Horwood Limited)

52. Bardangna J and Keneman S A 1977 *Holographic recording Media* ed. H. M. Smith (Berlin: Springer-Verlag)

53. Lucovsky G, Galeener F L, Geils R H and Keezer R C 1977 *The Structure of Non-Crystalline Materials* ed. P. H. Gaskell (New York: Taylor and Francis)

54. Phillips J C 1979 *J. Non-Cryst. Solids* **34** 153

55. Thorpe M F 1983 *J. Non-Cryst. Solids* **57** 355

56. Phillips J C and Thorpe M F 1985 *Solid State Commun.* **53** 699

57. Wada Y, Wang Y, Matsuda O, Inoue K and K. Murase 1976 *J. Non-Cryst.Solids* **198-200** 732

58. Feltz A, Aust H and Blayer A 1983 *J. Non-Cryst. Solids* **55** 179

59. Asokan S, Parthasarathy G and Gopal E S R 1988 *Phil. Mag. B* **57(1)** 49

60. Sharma P, Vashistha M and Jain I P 2005 *J. Opt. Adv. Mater.* **7** 2647

61. Thakur A, Sharma V, Saini G S S, Goyal N and Tripathi S K 2005 *J. Opt. Adv. Mater.* **7** 2077

62. Wemple S H and DiDomenico M 1971 *Phys. Rev. B* **3** 1338

63. Wemple S H 1973 Phys. Rev. B. **7** 3767

64. Tigau N, Ciupina V, Rusu G I, Prodan G, Vasile E 2005 *Rom. Journ. Phys.* **50** 859

65. Tauc J and Menth A 1972 *J. Non-Cryst. Solids* **8** 569

66. Goswami A 2005 *Thin film Fundamental* (New Delhi : New Age International) p.413

67. Pankove J I 1975 *Optical Processes in Semiconductors* (New York : Dover) p.91

68. Yamaguchi K, Nakayama N, Matsumoto H and Kegami S I 1977 *Jpn. J. Appl. Phys.* **16** 1203

69. Ashour A, El-Kdry N and Mahmoud S A 1995 *Thin Solid Films* **269** 117

70. Tanaka K 1980 *Thin Solid Films* **66** 271

71. Kastner M, Adler D and Fritzsche H 1976 *Phys. Rev. Lett.* **37** 1504

72. Mott N F and Davis E A 1979 *Electronic Processes in Non-Crystalline Materials* (Oxford: Clarendon Press)

73. El-Samanoudy M M 2003 *Thin Solid Films* **423** 201

74. Marquez E, Gonzalez-Leal J M, Bernal-Oliva A M, Jimenez-Garay R, Wagner T   2007 *J. Non-Cryst. Solids* doi:10.1016/j.jnoncrysol.2007.06.087

75. Elliott S R 2000 *The Physics and Chemistry of Solids* (Chichester: Wiley)

76. Soltan A S, Abu El-Oyoun M, Abu-Sehly A A and Abdel-Latief A Y 2003 *Mater. Chem. Phys.* **82** 101

77. Amutha R, Subbarayan A and Sathyamoorthy R 2006 *Cryst. Res. Technol.* **41** 1174

78. Tigau N, Ciupina V, Rusu G I, Prodan G and Vasile E 2005 *Rom. Journ. Phys.* **50** 859

79. Salem A M and Selim M S 2001 *J. Phys. D: Appl. Phys.* **34** 12

80. Sankapal B R, Mane R S and Lokhande C D 1999 *J. Mat. Sci. Lett.* **18** 1453

81. El Zawawi I K, Abdel-Moez A, Terra F S and Mounir M 1998 *Thin Solid Films* **324** 300

CHAPTER V[*]

Compositional Dependence of Physical Parameters in Ge-Se-Te System

[*] • **Pankaj Sharma** and S. C. Katyal, "*Effect of Tellurium Addition on the Physical Properties of Germanium Selenide Glassy Semiconductors*" **Physica B: Condensed Matter** (2008) doi: 10.1016/j.physb.2008.06.009.

• **Pankaj Sharma** and S. C. Katyal, "*Theoretical Calculation of Physical Parameters of $Ge_{10}Se_{90-x}Te_x$ Glassy Alloys*" **Journal of Optoelectronics and Advanced Materials**, Vol. 9 (2007) 1994.

In this chapter we have determined some physical parameters viz. coordination number, density, molar volume, compactness, lone pair electrons, theoretical band gap, average heat of atomization, cohesive energy and electronegativity of Ge-Se-Te system.

5.1   Introduction

Recently, variation of physicochemical, mechanical and optical properties of multicomponent chalcogenide glasses and thin films caused by changes in the average coordination number (m), has been the subject of intensive research [1-3]. The model of bond arrangement [4,5] and topological models such as the constraints model [6,7] and the structural transition model [8], have been used in the interpretation of the compositional dependence of these properties. Distinct features such as an extremum or a kink caused by chemical ordering are observed in the compositional dependence at the stoichiometric or tie-line compositions (also known as chemical thresholds of the system [9]). The topological model based on the constraints theory is also employed to explain the peculiarities in property-compositional dependence of covalently bonded chalcogenide glasses. In this model the properties are discussed in terms of the average coordination number, m, which is not influenced by the nature of the atoms [8]. At $m =$ 2.4 the glass network has a mechanical or floppy-to-rigid percolation threshold. At this m the network structure changes from an elastically floppy type to a rigid type [7]. Taking into account not only the short range constraints, but also the constraints of the medium range order (MRO), Tanaka [8] has predicted another structural phase transition. It is the transition from two dimensional (2D) layer-like structures to 3D cross-linked network. This transition is observed at $m \approx 2.67$ and may be regarded as a topological one. The above mentioned thresholds have been observed in several chalcogenide systems such as glasses [8] and thin films [3].

5.2   Coordination number

Nearest neighbour coordination number (m) in the ternary system $Ge_{10}Se_{90-x}Te_x$ (x = 0, 10, 20, 30, 40, 50) is suitable for testing the validity of topological concepts

[6,7] because of its large glass forming domain. The average coordination number in $Ge_{10}Se_{90-x}Te_x$ system has been calculated using the relation

$$m = \frac{\alpha N_{Ge} + \beta N_{Se} + \gamma N_{Te}}{\alpha + \beta + \gamma} \tag{5.1}$$

where α, β and γ are the at.% of Ge, Se and Te respectively and N_{Ge} = 4, N_{Se} = 2 and N_{Te} = 3 are their respective coordination numbers. The calculated coordination number (m) values lie in range $2.2 \leq m \leq 2.7$ and are given in table 5.1.

The calculated values of m, listed in Table 5.1, indicate that m increases with increase of Te content. In compositions with Te content i.e. x = 0 and 10; the value of m is less than 2.4. According to Phillips [6] these compositions have a floppy or spongy glass network and are assumed to be undercoordinated, while in compositions with Te content x = 20, 30, 40 and 50; $m \geq 2.4$. These have a rigid glass network and hence more closely packed structure and are assumed to be over coordinated. This conclusion is confirmed if correlated with the increases of density with Te content.

5.3   Density and molar volume

Density of bulk samples was measured by Archimedes (buoyancy) method. The apparatus consists of a beaker filled with double distilled water as a reference liquid. A thermometer was placed in the liquid to measure the temperature. The method is first to calculate the weight of the sample in air. Then the sample is placed on the sinker part and is plunged into the beaker in such a way that the sample is covered with at least 10 mm of liquid. After making sure that no bubbles are trapped in between the sample and the sinker the weight of the sample is measured in the liquid. The density of double distilled water (ρ_{water}) is obtained from a calibrated table knowing its temperature. Thus the density of the sample is calculated using the formula

$$\rho = \left[\frac{w_1}{w_1 - w_2} \right] \rho_{water} \tag{5.2}$$

where w_1 and w_2 are the weight of the sample in air and the weight of the sample in the reference liquid (double distilled water) respectively. Each sample was weighed five times and average density was recorded. The average recorded densities for

Table 5.1 Values of average coordination number (m), density (ρ), molar volume (V_m) and compactness (δ) for $Ge_{10}Se_{90-x}Te_x$ (x = 0, 10, 20, 30, 40, 50) glassy alloys.

Composition	m	ρ	V_m	δ
$Ge_{10}Se_{90}$	2.2	4.473	17.96	-0.10278
$Ge_{10}Se_{80}Te_{10}$	2.3	4.593	18.35	-0.09998
$Ge_{10}Se_{70}Te_{20}$	2.4	4.678	18.79	-0.09918
$Ge_{10}Se_{60}Te_{30}$	2.5	4.863	19.11	-0.09301
$Ge_{10}Se_{50}Te_{40}$	2.6	5.028	19.45	-0.08799
$Ge_{10}Se_{40}Te_{50}$	2.7	5.179	19.82	-0.08461

different compositions are given in table 5.1. This is found that the density of the system increases monotonically with the increase of Te content.

Another parameter related to the density, namely the molar volume (V_m) was determined from the density data by the equation

$$V_m = \frac{1}{\rho}\sum_i x_i M_i \qquad (5.3)$$

where M_i is the molecular weight of the ith component and x_i is the atomic percentage of the same element in the sample. The values of V_m for the prepared compositions are listed in Table 5.1. The molar volume was found to increase with Te content, which is a result of substituting Se atoms with the heavier and larger Te atoms in the glass network.

5.4   Compactness

The compactness (δ) of the structure of the glasses is determined from the measured densities of the glasses. The compactness δ was calculated using the relation [10-12]

$$\delta = \frac{\sum_i \frac{c_i A_i}{\rho_i} - \sum_i \frac{c_i A_i}{\rho}}{\sum_i \frac{c_i A_i}{\rho}} \qquad (5.4)$$

where c_i is the atomic fraction, A_i is the atomic weight, ρ_i is the atomic density of the ith element of the glass and ρ is the measured density of the glass. Thus, δ is a measure of the normalized change of the mean atomic volume due to chemical interactions of the elements forming the network of a given solid [13].

Consequently, it is more sensitive to changes in the structure of the glass network as compared to the mean atomic volume. The compositional variation of compactness, characterized by *m* of the investigated glassy alloys is shown in figure 5.4.1. From the figure, it is evident that the compactness increases with the increase of coordination number while a little kink is observed at $m = 2.4$, which may be considered in light of constraint theory and rigidity percolation concept [6,14,15].
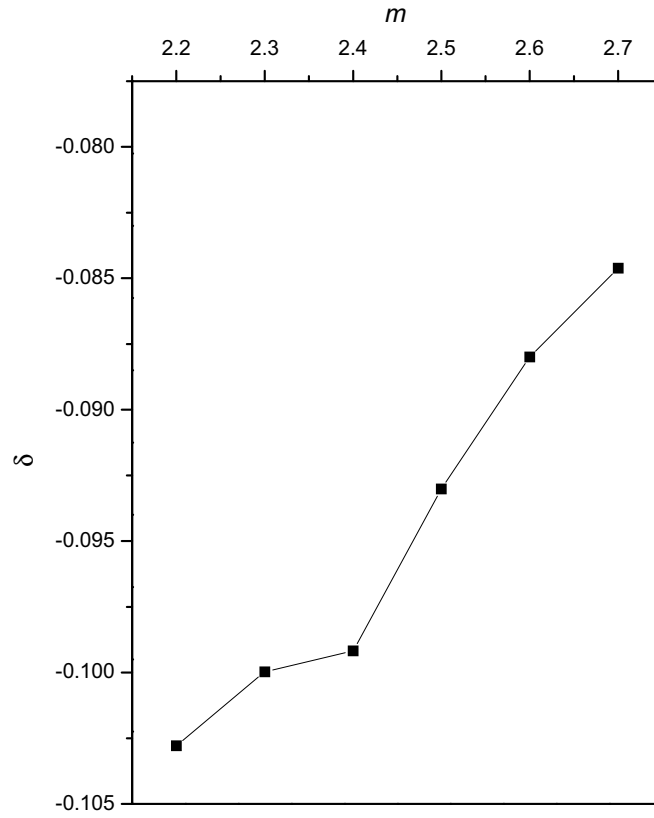
Figure 5.4.1 Plot of compactness vs. average coordination number for $Ge_{10}Se_{90-x}Te_x$ (x = 0, 10, 20, 30, 40, 50) system.

Thus with the increase of Te content in Ge-Se system the system becomes more compact i.e. the prepared compositions are becoming more rigid in structure.

5.5   Lone pair of electrons and glass forming ability

Most of the substances which can solidify in the vitreous state are found to possess structural 'bridges', that give rise to tri-dimensional, bi-dimensional or linear heteropolymeric formation. In most glasses, the bridges are formed of elements of group VI and VII. The chalcogen (S, Se, Te) atoms in glass structures have two pairs of lone-pair electrons. The existence of bridging atoms with lone-pair electrons can eliminate the strain force caused by the formation of amorphous materials. In terms of the viewpoint proposed by Pauling [16], the chemical bonds with lone-pair electrons have a character of flexibility. Increasing the number of lone-pair electrons decreases the strain energy in a system, and structures with large numbers of lone-pair electrons favor glass formation. The lone pair of electrons is calculated using the relation

$$L = V - m \tag{5.5}$$

where L is the number of lone pair electrons, V is the valance electron which is equal to unshared lone-pair electrons and m is the average coordination number. The values of L for different m are listed in table 5.2.

Figure 5.5.1 shows the variation of lone pair electrons with Te content. It is seen from the figure that the number of lone-pair electrons decreases continuously with the increase of Te in the system. This is caused by the interaction between the Te ion and the lone pair electrons of a bridging Se atom. The interaction decreases the role of lone-pair electrons in the glass formation. Liang [17] introduced a simple criterion for computing the ability of a chalcogenide system to retain its vitreous state; the criterion contains the number of lone-pair electrons which is necessary for obtaining the system in its vitreous state. For a binary system the number of lone-pair electrons must be larger than 2.6 and for ternary system it must be larger than 1. This is clear from the table that the minimum value of lone pair of electrons in present study is 3.1 leading to conclude that the system under study is a good glass former.

Table 5.2 Values of lone pair of electrons (L) for $Ge_{10}Se_{90-x}Te_x$ ($x = 0$, 10, 20, 30, 40, 50) glassy alloys.

Composition	m	V	$L = V - m$
$Ge_{10}Se_{90}$	2.2	5.8	3.6
$Ge_{10}Se_{80}Te_{10}$	2.3	5.8	3.5
$Ge_{10}Se_{70} Te_{20}$	2.4	5.8	3.4
$Ge_{10}Se_{60} Te_{30}$	2.5	5.8	3.3
$Ge_{10}Se_{50} Te_{40}$	2.6	5.8	3.2
$Ge_{10}Se_{40} Te_{50}$	2.7	5.8	3.1
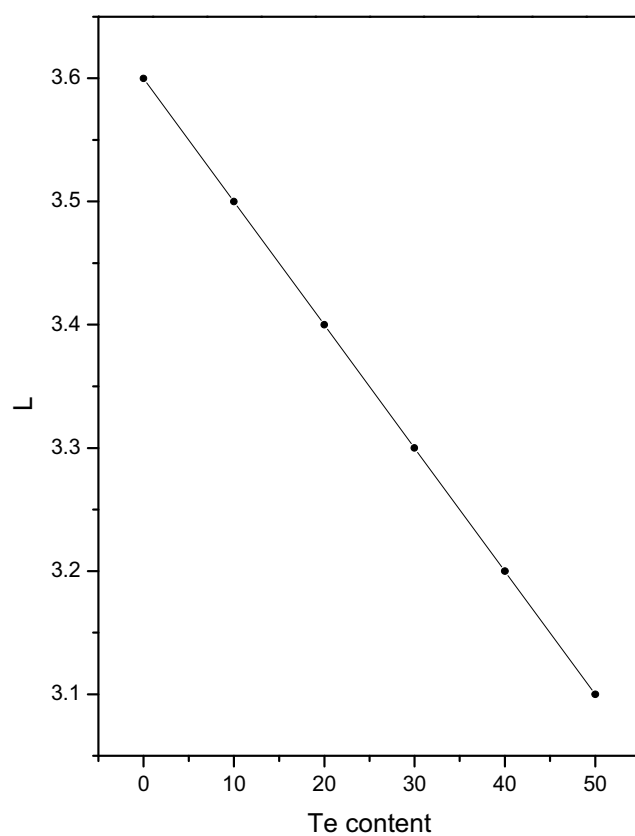
Figure 5.5.1 Variation of lone pair of electrons (L) with the Te content.

5.6   Optical band gap

The variation of energy gap with composition in amorphous alloys can be calculated using relation [18]

$$E_g(AB)(Y) = YE_g(A) + (1-Y)E_g(B) \tag{5.6}$$

where Y is the volume fraction of element A, $E_g(A)$ and $E_g(B)$ are the optical gaps for A and B elements, respectively. The conversion from atomic composition (at%) or molecular composition (mol %) to volume fraction Y is made using atomic or molecular mass and density. Figure 5.6.1 shows the variation of theoretically calculated and experimentally observed band gap for $a\text{-}Ge_{10}Se_{90-x}Te_x$ thin films. In conclusion both the optical gap $E_{g,th}^{opt}$ for $a\text{-}Ge_{10}Se_{90-x}Te_x$ determined by volume fraction and the optical gap $E_{g,exp}^{opt}$ calculated using the experimental data decrease with the increase of Te content leading to the conjecture that a modified virtual crystal approach for mixed crystals is acceptable for an amorphous system. The decrease of optical band gap with the increase of Te content is discussed in detail in chapter 4 section 4.3.

5.7   Average heat of atomization

In chalcogenide glasses containing a high concentration of group VI element, the lone-pair form the top of the valence band and the antibonding band forms the bottom conduction band [19]. The optical gap corresponds closely to the energy difference between the top of the valence band and the bottom of the conduction band. Metal atoms can form a dative bond with group VI atoms (lone pair with empty orbital) without any cost of energy, due to the presence of high-energy lone pair on the latter. Dative bonds have corresponding (empty) antibonding levels which could give localized acceptors states in the gap [20].

It is interesting to relate the optical band gap with the chemical bond energy. For this purpose we calculate the heat of atomization. According to Pauling [16], the heat of atomization $H_s(A-B)$ at standard temperature and pressure of a binary semiconductor formed from atoms A and B is the sum of heat of formation ΔH and
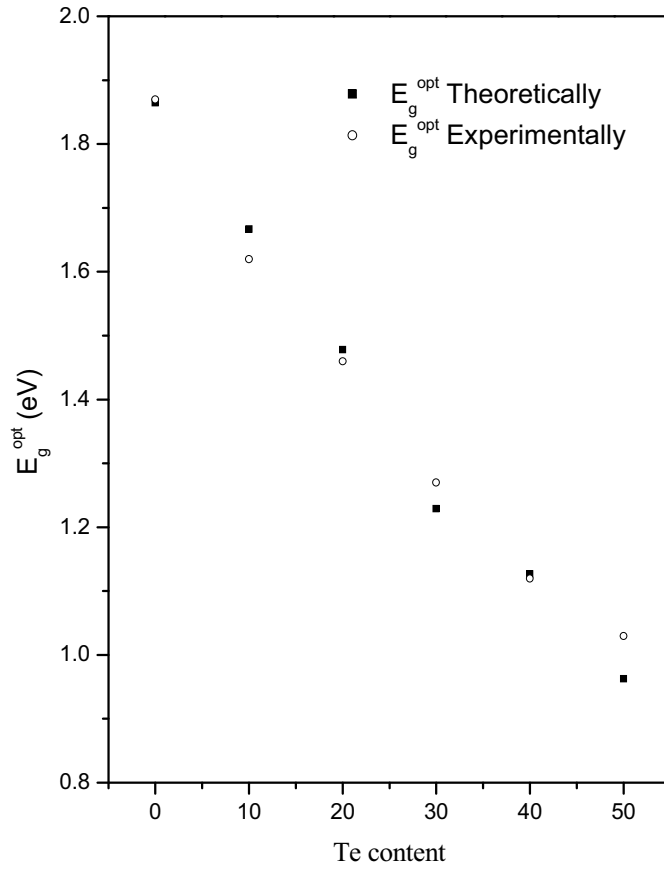
Figure 5.6.1 Plot of optical band gap (theoretical and experimental) vs. Te content for $Ge_{10}Se_{90-x}Te_x$ (x = 0, 10, 20, 30, 40, 50) system.

the average heats of atomization H_s^A and H_s^B that corresponds to the average non-polar bond energy of the two atoms

$$H_s(A-B) = \Delta H + \frac{1}{2}\left(H_s^A + H_s^B\right) \qquad (5.7)$$

The first term in above equation is proportional to the square of the difference between the electronegativities χ_A and χ_B of the two atoms

$$\Delta H \quad \alpha \quad \left(\chi_A - \chi_B\right)^2 \qquad (5.8)$$

In order to extend this idea to ternary and higher order semiconductor compounds, the average heat of atomization $\overline{H}_s$ (in kcal per gram-atom) is defined for a compound $A_\alpha B_\beta C_\gamma$ as a direct measure of the cohesive energy and thus of average bond strength, as

$$\overline{H}_s = \frac{\alpha H_s^A + \beta H_s^B + \gamma H_s^C}{\alpha + \beta + \gamma} \qquad (5.9)$$

Obviously the $\overline{H}_s$ values do not contain the heat of formation (ΔH) as part of cohesive energy; however $\overline{H}_s$ is useful parameter for correlating the physical properties of semiconducting compounds. In case of chalcogenide glasses the heat of formation contributes very little towards the average heat of atomization because the electronegativities of the constituent elements *i.e.* Ge, Se, Te are very similar and in most of the cases of chalcogenide glasses the heat of formation is unknown. In few materials for which heat of formation is known it accounts only 10% of the heat of atomization and is therefore neglected. Hence for binary chalcogenide glasses $H_s(A-B)$ is given by

$$H_s(A-B) = \frac{1}{2}\left(H_s^A + H_s^B\right) \qquad (5.10)$$

whereas for ternary and higher order compounds, $\overline{H}_s$ is given by the equation (5.9). The heat of atomization for Ge, Se, Te elements [21] and average heat of atomization $\overline{H}_s$ (kcal/g-atom) and average single bond energy $(\overline{H}_s/m)$ are given in Table 5.3, where *m* is the average coordination number calculated in section 5.1. From the Table 5.3 it is found that the heat of atomization decreases with the increase of Te content *i.e.* the average single bond energy decreases. This decrease in the average single bond

Table 5.3 Values of average coordination number (*m*), average heat of atomization $(\overline{H}_s)$, average single bond energy $(\overline{H}_s/m)$ and heat of atomization for Ge, Se, Te elements in $Ge_{10}Se_{90-x}Te_x$ (*x=0, 10, 20, 30, 40, 50*) system.

x	*m*	$\overline{H}_s$ (kcal/g-atom)	$(\overline{H}_s/m)$ (kcal/g-atom)	Element	Heat of atomization (kcal/g-atom)
0	2.2	53.46	24.30	Ge	90
10	2.3	53.12	23.09	Se	49.4
20	2.4	52.78	21.99	Te	46
30	2.5	52.44	20.98		
40	2.6	52.10	20.04		
50	2.7	51.76	19.17		

energy with the increase of Te content may be the cause of the decrease in optical band gap.

5.8   Cohesive energy and electronegativity

Using the chemical bond approach (CBA) method [22], the cohesive energy (CE) (the stabilization energy of an infinitely large cluster of material per atom) for investigated samples has been calculated. According to CBA, the bonds are formed in the sequence of decreasing bond energy until the available valence of atoms is satisfied and the bond energies are assumed to be additive. Thus the cohesive energies were calculated by summing the bond energies over all bonds expected in the material. Consequently, bonds between like atoms will only occur if there is an excess of certain type of atoms. In the present compositions, the Ge-Se bonds with the highest possible energy (49.1 kcal/mol) are expected to occur first, followed by Se-Te bonds (40.6 kcal/mol). In all the compositions Ge is saturated by Se as compare to Te since Ge-Se bonds (49.1 kcal/mol) are stronger than Ge-Te bonds (37.4 kcal/mol). Up to x = 20 at. % composition there is still unsatisfied Se which must be satisfied by Se-Se defect homopolar bonds. For x > 20 at. % Te becomes excessive and remain unsatisfied which must be satisfied by Te-Te defect homopolar bonds. Calculated values of CE along with the distribution of chemical bond for all the compositions are tabulated in table 5.4. The results show the decrease in CE of these glassy alloys. Therefore, it can be concluded that the decrease of optical band gap [23,24] with increasing Te content (Fig. 5.7.1) is most probably due to the reduction of the average stabilization energy by Te content. The decrease of CE of the Ge–Se–Te system tends to decrease the energy of the conduction band edge causing a reduction in the gap between bonding (σ) and antibonding (σ^*) orbitals and thus resulting a decrease in optical band gap. It should be mentioned that the approach of the chemical bond neglects dangling bond and other valence defects as a first approximation. Also Vander Walls interactions are neglected, which can provide a means for further stabilization by the formation of much weaker links than regular covalent bonds. According to Yamaguchi [21] average single bond energy $(\overline{H_s}/m)$, where $\overline{H_s}$ is average heat of atomization and m is average coordination number, is a direct measure of cohesive energy. This is reported in
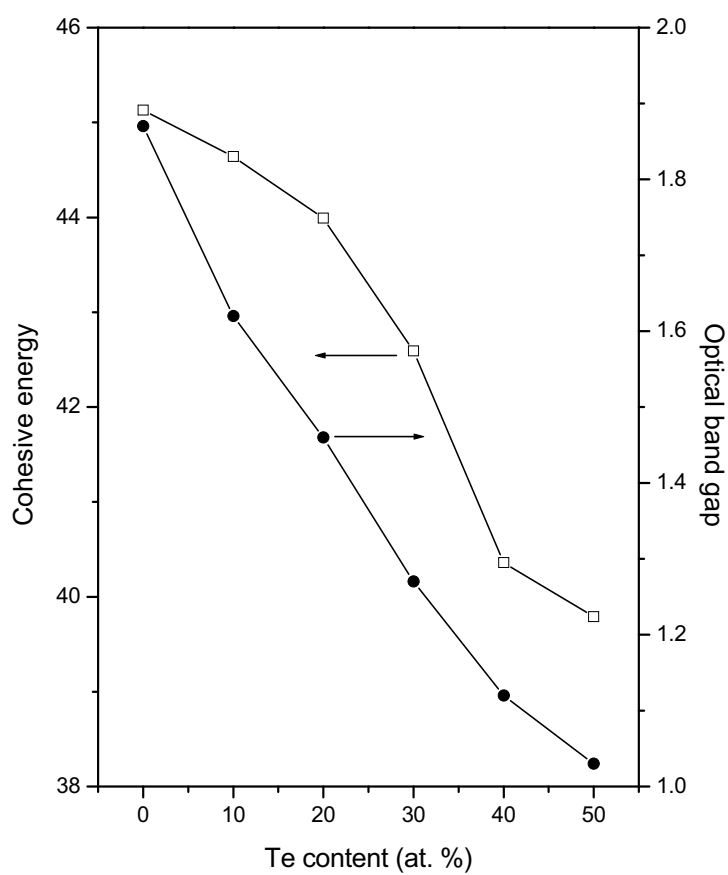
Figure 5.8.1 Variation of cohesive energy (kcal/mol) and optical band gap (eV) with Te content (at. %) for $Ge_{10}Se_{90-x}Te_x$ (x = 0, 10, 20, 30, 40, 50) glassy alloys.

Table 5.4 Values of electronegativity (χ), optical band gap (E_g^{opt}), distribution of chemical bonds and cohesive energy (C.E.) for $Ge_{10}Se_{90-x}Te_x$ (x = 0, 10, 20, 30, 40, 50) glassy alloys.

x	χ	E_g^{opt} (eV)	Distribution of Chemical bonds				C.E.(kcal/ mol)
			Ge-Se	Se-Te	Se-Se	Te-Te	
0	2.489	1.87	0.2222	-	0.7778	-	45.13
10	2.442	1.62	0.2500	0.1875	0.5625	-	44.64
20	2.394	1.46	0.2857	0.4286	0.2857	-	43.99
30	2.348	1.27	0.3333	0.5556	-	0.1111	42.59
40	2.303	1.12	0.2424	0.4546	-	0.3030	40.36
50	2.259	1.03	0.3061	0.2449	-	0.4490	39.79

section 5.6 that there is a decrease in average single bond energy with the increase of Te content. So it is interesting to correlate the optical band gap with cohesive energy for Ge-Se-Te glassy alloys.

Thus, both cohesive energy and average single bond energy supports for the decrease in optical band gap with the increase of Te content in $Ge_{10}Se_{90-x}Te_x$ system. Moreover the decrease in optical band gap is also confirmed by the decrease of electronegativity which is calculated using Sanderson's principle [25]. According to this principle electronegativity of the alloy is the geometric mean of electronegativity of its constituent elements. It is evident from the table 5.4 that optical band gap decreases as electronegativity decreases with the increasing content of Te.

5.9   Conclusion

The average coordination number, density, molar volume, compactness, lone pair of electrons, theoretical optical band gap and average heat of atomization is studied for $Ge_{10}Se_{90-x}Te_x$ (x = 0, 10, 20, 30, 40, 50) glassy alloys. The coordination number increases with the addition of Te on replacing Se. The density and molar volume increases monotonically with the increasing content of Te. Compactness has been found to increase with the increase of Te content showing that structure is becoming rigid. The number of lone pair of electrons decreases with the addition of Te but still, in the present study, has a minimum value 3.1 which is much more than 1 as suggested by Liang for good glass former indicating that the compositions under investigation are good glass forming. The theoretical optical band gap has also been found to decrease with the increase of Te content and is in concordance with the experimental optical band gap. Average heat of atomization ($\overline{H}_s$) which is a measure of the average binding energy decreases with increase of Te content. The decrease of optical band gap may be correlated with the decrease of average binding energy of the system.

References

1. Streem A N, Varshneya A K and Swiler D R 1991 *J. Non-Cryst. Solids* **128** 294 and **130** 225

2. Mahadevan S, Giridhar A and Singh A K 1994 *J. Non-Cryst. Solids* **169** 133

3. Vateva E, Arsova D, Skordeva E and Savova E 1995 *Series Electronic Mat.* (UK: British Academic Press) 604

4. Lucovsky G, Galeener F, Keezer R and Six H 1974 *Phys. Rev. B* **10** 5134

5. Tronc P, Bensoussan M, Brenac A and Sebenne C 1973 *Phys. Rev. B* **8** 5947

6. Phillips J C 1981 *J. Non-Cryst. Solids* **43** 37

7. Phillips J C and Thorpe M F 1985 *Solid State Commun.* **53** 699

8. Tanaka K 1989 *Phys. Rev. B* **39** 1270

9. Mahadevan S and Giridhar A 1989 *J. Non-Cryst. Solids* **110** 118

10. Vlcek M and Frumar M 1987 *J. Non-Cryst. Solids* **97&98** 1223

11. Savova E, Skordeva E and Vateva E 1994 *J. Phys. Chem. Solids* **55** 575

12. Skordeva E and Arsova D 1995 *J. Non-Cryst. Solids* **192&193** 665

13. Tichy L and Ticha H 1995 *J. Non-Cryst. Solids* **189** 141

14. Phillips J C 1979 *J. Non-Cryst. Solids* **34** 153

15. He H and Thorpe M F 1985 *Phys. Rev. Lett.* **54** 2107

16. Pauling L 1960 *The Nature of the Chemical Bond 3rd Ed.* (New York: Cornell University Press)

17. Zhenhua L 1991 *J. Non-Cryst. Solids* **127** 298

18. Andriesh A M and Iovu M S 2003 *Moldavian J. of the Physical Sciences* **2** 3

19. Kastner M 1972 *Phys. Rev. Lett.* **28** 355

20. Ovshinsky S R 1982 *Disordered Materials Science and Technology* Ed. D. Adler (USA: Amorphous Institute Press) 83

21. Yamaguchi M 1985 *Philosophical Magazine B* **41(6)** 651

22. Biecerano J and Ovshinsky S R 1985 *J. Non-Cryst. Solids* **74** 75

23. Sharma P and Katyal S C 2007 *Thin Solid Films* **515** 7966

24. Sharma P and Katyal S C 2007 *J. Optoelectron. and Adv. Mater.* **9** 1994

25. Sanderson R T 1971 *Inorganic Chemistry* (New Delhi: Affliated East-West Press PUT)

CHAPTER VI[*]

Optical Properties of As-Se-Ge Thin Films

[*] • **Pankaj Sharma** and S. C. Katyal, "*Determination of Optical Parameters of a-(As$_2$Se$_3$)$_{90}$Ge$_{10}$ Thin Film*" **Journal of Physics D: Applied Physics** Vol 40 (2007) 2115.

• **Pankaj Sharma** and S. C. Katyal, "*Effect of tin addition on the optical parameters of thermally evaporated As-Se-Ge thin Films*" **Materials Physics and Chemistry** (2007) [Under Review].

• **Pankaj Sharma** and S. C. Katyal, "*A study of metal impurities on the optical properties of (As$_2$Se$_3$)$_{90}$Ge$_{10}$ thin films*" **Vacuum** (2007) [Under review].

The optical properties of As-Se-Ge thin films and the influence of metal additives, (bismuth (Bi), cadmium (Cd), tin (Sn) and lead (Pb), on these is discussed in this chapter. The first section of this chapter deals with the study of optical properties of $(As_2Se_3)_{90}Ge_{10}$ thin film deduced from transmission spectrum. Some of the results of $(As_2Se_3)_{90}Ge_{10}$ thin film are compared with similar material compositions $As_{30}Se_{60}Ge_{10}$ and $Ge_{10}As_{15}Se_{75}$. The second section deals with the effect of metal additives on the optical properties of $(As_2Se_3)_{90}Ge_{10}$ thin films.

6.1   Optical properties of As-Se-Ge thin films

6.1.1 Introduction

The optical parameters of amorphous semiconductors have been extensively studied on As-Se system. As_2Se_3 is a widely studied material for its electrical and optical properties. The coordination number of As_2Se_3 is 2.4 i.e. the system is in floppy mode [1-3], but when As_2Se_3 is alloyed with 10 at. % of Ge the coordination number increases to 2.56 leading the system to rigid mode [1]. Alloying As_2Se_3 chalcogenide glassy semiconductor with Ge is an effective way to control the electrical and optical properties of glasses in the desired direction [4]. The optical properties of amorphous solids are determined by the structural bonding between the neighboring atoms. The bonding in the case of chalcogen (Se) gives rise to one dimensional structural stability of the amorphous materials. The degree of disorder and defects present in amorphous structure changes during the transition from amorphous to crystalline state. The increase of disorder and defects concentration is known to reduce the width of the optical gap shown by the model of Mott and Davis [5].

6.1.2 Experimental details

Bulk glassy alloy of $(As_2Se_3)_{90}Ge_{10}$ was prepared by melt quenching technique (chapter 3). Materials (99.999% purity) were weighed according to their atomic percentages and sealed in an evacuated (at $\sim 10^{-4}$ Pa) quartz ampoule. The sealed ampoule was kept inside a furnace where the temperature was increased up to 950^0C at a heating rate of 3-4 ^0C/min. The ampoule was frequently rocked for 24 h at the highest temperature to make the melt homogeneous. The quenching was done in ice-

cold water. Thin film of $(As_2Se_3)_{90}Ge_{10}$ glassy alloy was deposited on cleaned glass substrates by thermal evaporation at $\sim 10^4$ Pa base pressure. Bulk sample as well as its thin film were characterized by X-ray diffraction technique and found to be amorphous in nature as no prominent peak was observed in their spectra. The transmission spectra of the thin film in the spectral range 400-1500 nm were taken using a double beam ultraviolet-visible-near infrared spectrophotometer (Hitachi-330). The spectrophotometer was set with a slit width of 1 nm. Therefore it was unnecessary to make slit width corrections because of small slit width value in comparison with different line widths [6]. All the measurements reported were taken at room temperature.

6.1.3 Results and discussion

6.1.3.1 Refractive index and extinction coefficient

Using the experimental data of optical transmittance of $(As_2Se_3)_{90}Ge_{10}$ thin film the refractive index and extinction coefficient have been calculated. The homogeneous film has thickness (d) and complex refractive index $n^* = n - ik$, where n is the refractive index and k is the extinction coefficient. The thickness of the substrate is several times larger than the thickness of the film. If the thickness of the film is constant, interference effect will give rise to oscillating curves as shown in figure 6.1.1. Optical parameters are deduced from the fringes pattern in the transmittance spectrum using Swanepoel method [7] described in chapter 2. The calculated value of thickness (d) for the thin film under investigation has been found to be 1674 nm. The spectral distribution of refractive index and extinction coefficient is shown in figure 6.1.2.

Both refractive index and extinction coefficient have been found to decrease with the increase of wavelength for the thin film under investigation which may be correlated with the increase of transmittance and decrease of absorption coefficient. The decrease in the value of refractive index with wavelength shows the normal dispersion behaviour of the material. The decrease of extinction coefficient with
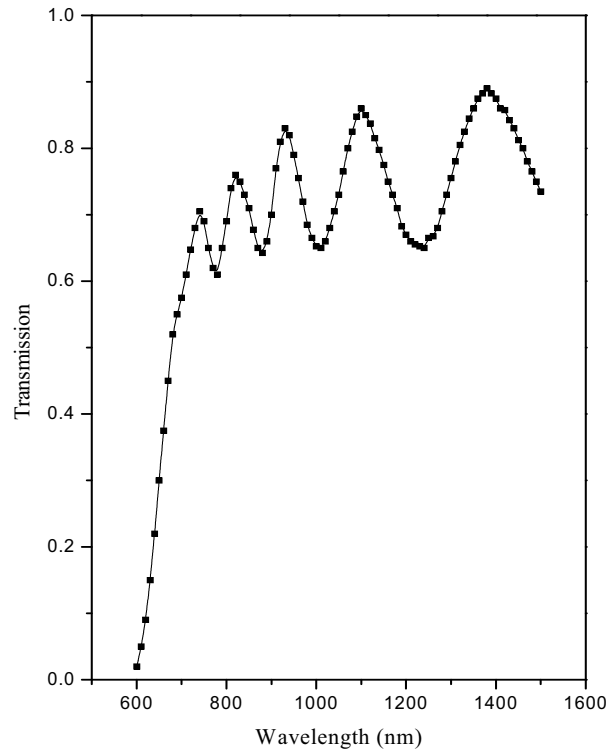
Figure 6.1.1 Plot of optical transmission versus wavelength for $(As_2Se_3)_{90}Ge_{10}$ thin film.
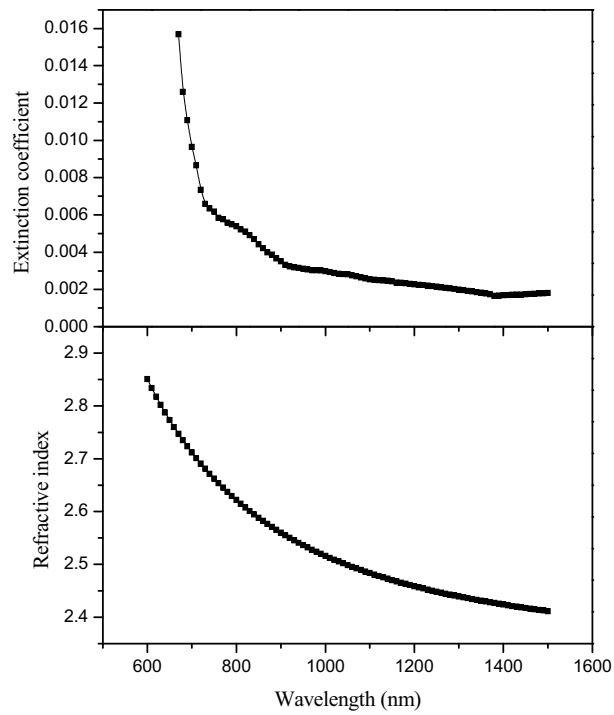
Figure 6.1.2 Plots of Refractive index and Extinction coefficient vs. wavelength for $(As_2Se_3)_{90}Ge_{10}$ thin film.

127

increase of wavelength shows that the fraction of light lost due to scattering and absorbance decreases. These results are very much similar to the results of Marquez et.al. [8] and have similar trend as shown by El-Sayed et.al. [4]. On comparing the variation of refractive index with wavelength for As-Se-Ge [4,8] thin films, we may presume that the material obeys normal dispersion behaviour.

## 6.1.3.2 Dispersion energy, oscillator strength and static refractive index from Wemple-DiDomenico model

The high frequency properties of $(As_2Se_3)_{90}Ge_{10}$ thin film could be treated as single oscillator. According to the single-effective oscillator model proposed by Wemple and DiDomenico [9,10] the optical data could be described to an excellent approximation by the following relation

$$n^2 - 1 = \frac{E_d E_0}{E_0^2 - (h\nu)^2} \qquad (6.1)$$

where $h\nu$ is the photon energy, n is refractive index, E_0 is the single oscillator energy also called average energy gap and E_d is the dispersion energy which is a measure of the average strength of the interband optical transitions. Plotting $(n^2 - 1)^{-1}$ against $(h\nu)^2$ allows us to determine the oscillator parameters by fitting a straight line to the points. Figure 6.1.3 shows the plot of $(n^2 - 1)^{-1}$ versus $(h\nu)^2$. The values of E_0 and E_d can directly be determined from the slope $(E_0 E_d)^{-1}$ and the intercept on the vertical axis (E_0/E_d). The calculated values of E_0 and E_d are given in the inset of figure 6.1.3 and also compared with [4,8] in table 6.1. The straight line equation corresponding to least square fit is $(n^2 - 1)^{-1} = 0.1872 - 0.0183(h\nu)^2$. The value of static refractive index (n_0) is calculated by extrapolating the Wemple-DiDomenico dispersion equation to $h\nu \rightarrow 0$. The value of n_0 is found to be 2.518 and the comparative values of n_0 from [4,8] are given in table 6.1. The high frequency dielectric constant [11] $\varepsilon_\infty = (n_0)^2$ is 6.34. Moreover an important achievement of Wemple-DiDomenico model is that it relates the dispersion energy E_d to other physical parameters of the material through a simple empirical relation
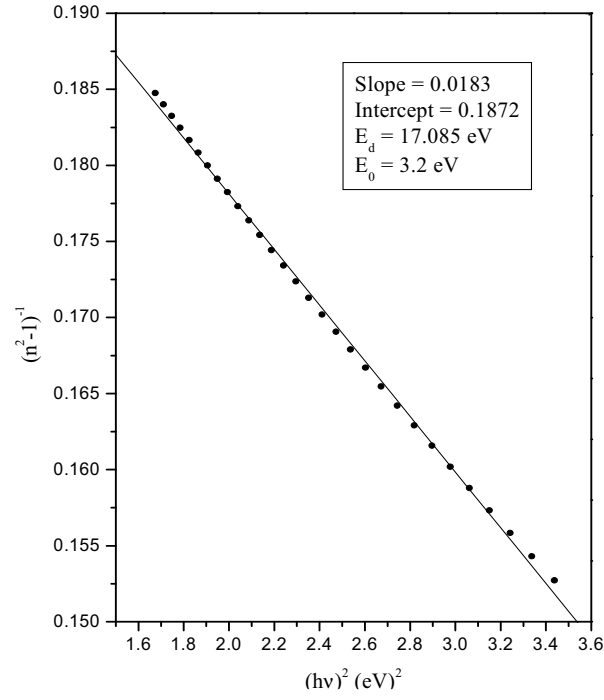
Figure 6.1.3 Plot of refractive index factor $(n^2-1)^{-1}$ versus $(h\nu)^2$ for $(As_2Se_3)_{90}Ge_{10}$ thin film.
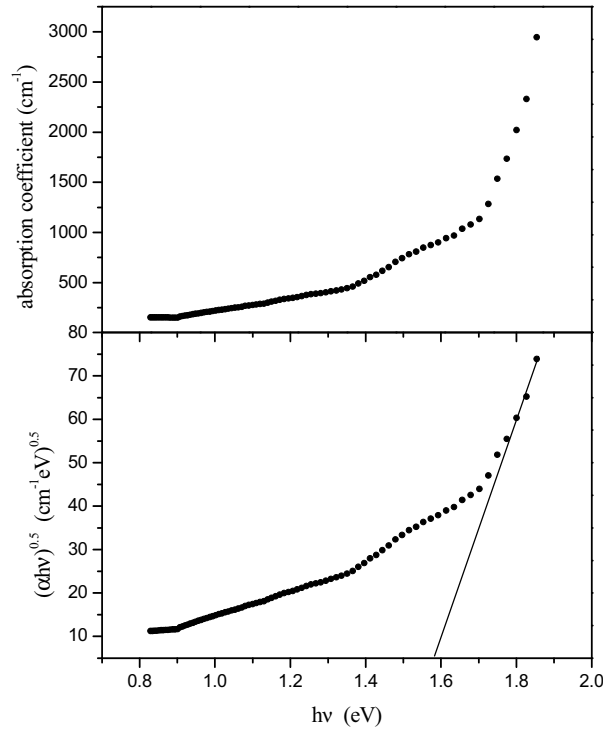
Figure 6.1.4 Plots of absorption coefficient and $(\alpha h\nu)^{0.5}$ versus $h\nu$ for $(As_2Se_3)_{90}Ge_{10}$ thin film.

$$E_d = \beta N_c Z_a N_e \tag{6.2}$$

where N_e is effective number of valence electrons per anion, N_c is effective coordination number of the cation nearest neighbour to the anion, Z_a is the chemical valency of the anion and β is a two valued constant with either an ionic or covalent value (for ionic materials $\beta = 0.26 \pm 0.03$ eV and for covalent materials $\beta = 0.37 \pm 0.04$ eV [9]). The values of N_e and N_c for composition under study are calculated and found to be 9.48 and 2.44 respectively.

Furthermore an approximate value of optical band gap (E_g^{opt}) can also be derived from the Wemple-DiDomenico dispersion parameter E_0 according to the relation [12-14] $E_g^{opt} = E_0/2$ giving an alternative value which is $1.60 \pm 0.01\,\text{eV}$. This value is in good agreement with that determined from Tauc's extrapolation *i.e.* 1.58 ± 0.01 eV calculated later.

6.1.3.3 Absorption coefficient and optical band gap

The absorption coefficient of $(As_2Se_3)_{90}Ge_{10}$ films can be calculated using equation (2.23). Figure 6.1.4 shows the plot of absorption coefficient versus photon energy. For many amorphous materials an exponential dependence of the absorption coefficient is found to hold over a wide range of the photon energy and α takes the form [15,16]

$$\alpha = \alpha_0 \exp(h\nu/E_e) \tag{6.3}$$

where ν is the frequency of the radiation, α_0 is a constant, h is Planck's constant and E_e is an energy which is often interpreted as the width of the tail of localized states in the gap region. This relation was first proposed by Urbach [16] to describe the absorption edge in alkali halide crystals at high absorption levels. The relation has been found to hold for many amorphous or glassy materials. Tauc [17] believed its origin from electronic transitions between localized states in the band edge tails, the density of which is assumed to fall off exponentially with energy. Davis and Mott [5] were uncertain about the precise explanation of the exponential dependence and suggested that the slopes of the observed exponential edges obtained from

Table 6.1 Values of thickness (d), static refractive index (n_0), single oscillator energy (E_0), dispersion energy (E_d) and optical band gap (E_g^{opt}) for $(As_2Se_3)_{90}Ge_{10}$, $Ge_{10}As_{15}Se_{75}$ [9] and $As_{30}Se_{60}Ge_{10}$ [4] thin films.

Composition	d (nm)	n_0	E_0 (eV)	E_d (eV)	E_g^{opt} (eV)
$(As_2Se_3)_{90}Ge_{10}$	1674	2.518	3.20	17.085	1.58 ± 0.01
$Ge_{10}As_{15}Se_{75}$	1476 ± 30	2.566 ± 0.001	3.72 ± 0.01	20.77 ± 0.5	1.88 ± 0.01
$As_{30}Se_{60}Ge_{10}$	300	-	4.825	-	1.81

equation 6.3 are very much same in many semiconductors and the value of E_e for a range of amorphous semiconductors [18] lies between 0.045 and 0.67 eV.

In the high absorption region from which the optical band gap is determined, the absorption is characterized by Tauc's relation [17]

$$\alpha h\nu = B\left(h\nu - E_g^{opt}\right)^n \tag{6.4}$$

where $h\nu$, E_g^{opt} and B denotes the photon energy, the optical gap and band tailing parameter respectively. In the above equation $n = 1/2$ for a direct allowed transition, $n = 3/2$ for a direct forbidden transition, $n = 2$ for an indirect allowed transition and $n = 3$ for an indirect forbidden transition. The value of E_g^{opt} and B can be readily calculated from the plot of $(\alpha h\nu)^{0.5}$ as a function of $h\nu$ (figure 6.1.4). $B^{1/2}$ calculated from the slope was found to be 188.43 $cm^{-1/2}eV^{-1/2}$. The value of E_g^{opt} can be estimated by the intercept of the extrapolations to zero absorption with the photon energy axis $(\alpha h\nu)^{1/2} \to 0$. The obtained value of E_g^{opt} for indirect allowed transition in amorphous $(As_2Se_3)_{90}Ge_{10}$ thin film is $1.58 \pm 0.01\,eV$. The comparison of optical band gap with compositions $As_{30}Se_{60}Ge_{10}$ [4] and $Ge_{10}As_{15}Se_{75}$ [8] is given in table 6.1.

6.1.3.4   Dielectric constants and optical conductivity

Figure 6.1.5 shows the plot of real and imaginary dielectric constants versus photon energy for $(As_2Se_3)_{90}Ge_{10}$ thin film. The knowledge of real and imaginary part of dielectric constant provides information about the loss factor which is the ratio of imaginary part of dielectric constant to real part of dielectric constant i.e. larger the imaginary part of dielectric constant or smaller the real part of dielectric constant, larger is the loss factor. The real and imaginary parts of the dielectric constant were determined using the relations derived from complex refractive index [19],

$$\varepsilon_r = n^2 - k^2 \tag{6.5}$$

and

$$\varepsilon_i = 2nk \tag{6.6}$$
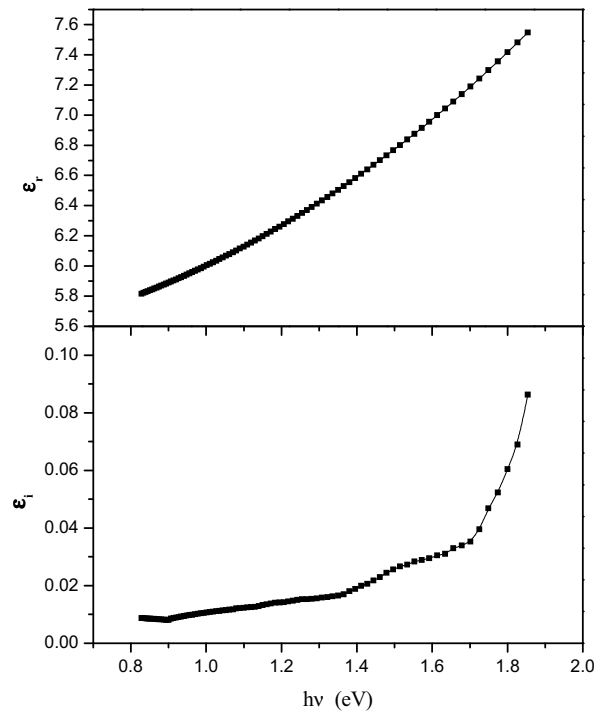
Figure 6.1.5 Plots of real (ε_r) and imaginary (ε_i) part of dielectric constant for $(As_2Se_3)_{90}Ge_{10}$ thin film.

Figure 6.1.6 Plot of optical conductivity (σ) versus $h\nu$ for $(As_2Se_3)_{90}Ge_{10}$ thin film.

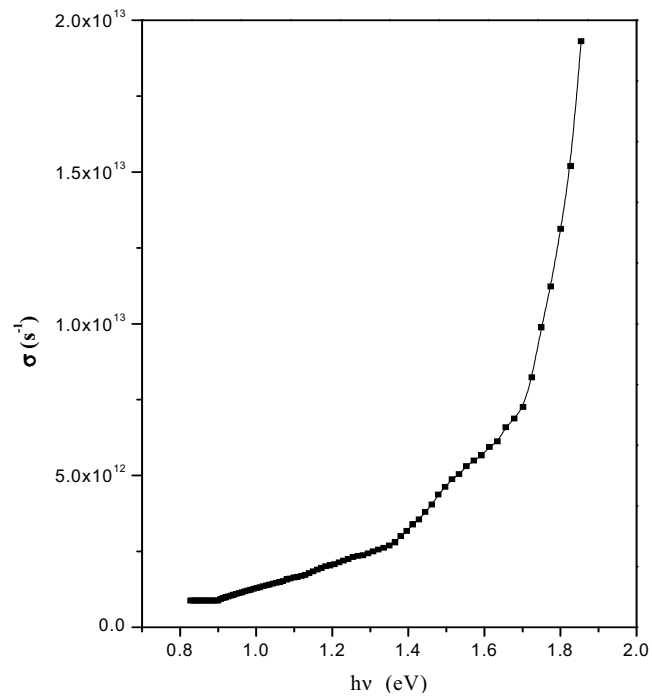Both the real and imaginary parts of dielectric constant are found to increase with increase of energy, the real part of dielectric constant increases sharply with increase of energy whereas the imaginary part increases slowly in the lower energy part but in higher energy part it increases abruptly.

The optical response of a material is most conveniently studied in terms of the optical conductivity. It has dimensions of frequency which is valid only in Gaussian system of units. The optical conductivity (σ) has been determined from relation [20]

$$\sigma = \alpha n c / 4\pi \qquad (6.7)$$

where c is the velocity of light, α is absorption coefficient and n is the refractive index. Figure 6.1.6 shows the plot of optical conductivity versus photon energy. The optical conductivity directly depends on the absorption coefficient and refractive index of the material and is found to follow the same trend as that of absorption coefficient and refractive index with increasing wavelength

6.1.4 Conclusion

Transmission spectrum of $(As_2Se_3)_{90}Ge_{10}$ thin film has been analyzed in the spectral range of 400-1500 nm for the calculation of optical parameters. Refractive index and extinction coefficient decrease with the increase of wavelength indicating the normal dispersion behaviour of thin film.. The optical band gap obtained by Tauc's extrapolation is $1.58 \pm 0.01\,eV$. This is in good agreement with the optical band gap *i.e.* $1.60 \pm 0.01\,eV$ found by Wemple-DiDomenico single oscillator model. The value of static refractive index is found to be 2.518. The real and imaginary parts of dielectric constant increase with the increase of photon energy. The optical conductivity increases sharply for higher energy values and its maximum value is found to be 1.93×10^{13} s^{-1} at 1.85 eV.

6.2   Effect of metal impurities on the optical properties of As-Se-Ge thin films

The optical parameters of amorphous semiconductors have been extensively studied on As-Se-Ge system [21-23] because of the fact that Ge, As and Se are the elements of same period in groups IV-VI and brings about the covalent character of

the interaction between their atoms. This results in a broad glass formation region in As-Se-Ge system [24] among all investigated three component chalcogenide systems. In this section we have reported the influence of addition of metal impurities (Bi, Cd, Sn and Pb) on the optical properties of $(As_2Se_3)_{90}Ge_{10}$ system.

6.2.1 Introduction

Previously, it was believed that chalcogenide glasses are insensitive to added impurities but in recent research scenario, it has been observed that chalcogenide glasses are sensitive to composition, impurities and deposition parameters like thickness, substrate type and substrate temperature [11,25-28]. Recent experiments [28,29] reveal that the addition of impurities likes Bi and Pb have produced a remarkable change in the optical and electrical properties of chalcogenide glasses. In As-Se-Ge system the addition of Bi, Cd, Sn and Pb impurities, which have a large electronegativity difference with As, Se and Ge atoms, are supposed to modify the structure of As-Se-Ge system and thus it's electrical and optical properties. The electrical properties of these impurities added As-Se-Ge system have been reported [30] but not the optical properties. This is conjectured that the addition of metal impurities in $(As_2Se_3)_{90}Ge_{10}$ thin films may change its optical properties remarkably. Thus, a thorough study of optical properties is considered crucial to have better understanding of the system.

6.2.2 Experimental details

Glasses of $[(As_2Se_3)_{90}Ge_{10}]_{95}M_5$, where M = Bi, Cd, Sn and Pb, were prepared by the melt quenching technique. Thin films of the prepared bulk glasses were deposited on the glass substrate using thermal evaporation method. The rate of evaporation of deposited thin films under investigation is given in table 6.2. Thickness of the films has been measured by thickness monitor (Model DTM-101). The amorphous nature of bulk compositions as well as their thin films was examined by the X-ray powder diffraction method using Philips PW 1710 X-ray diffractometer (The radiation used was CuKα). The lack of any sharp peaks indicates the glassy nature of the materials prepared. The transmission spectra of the films in the spectral
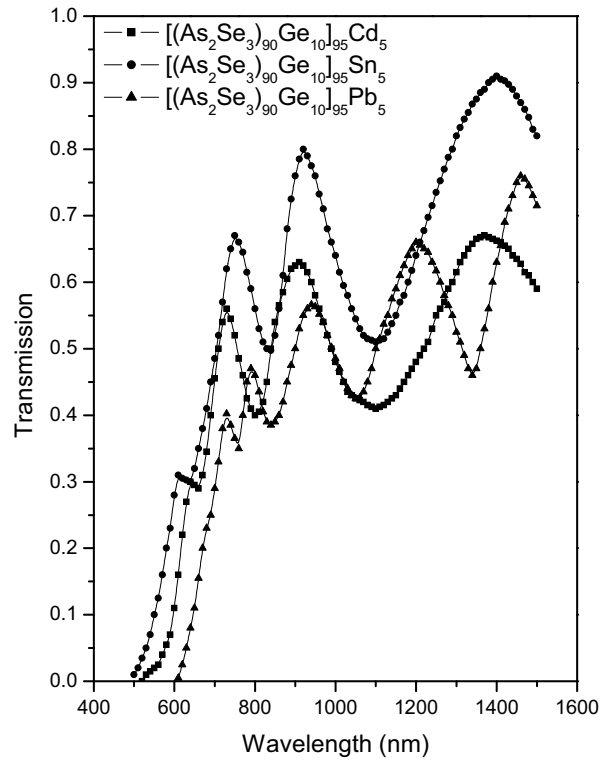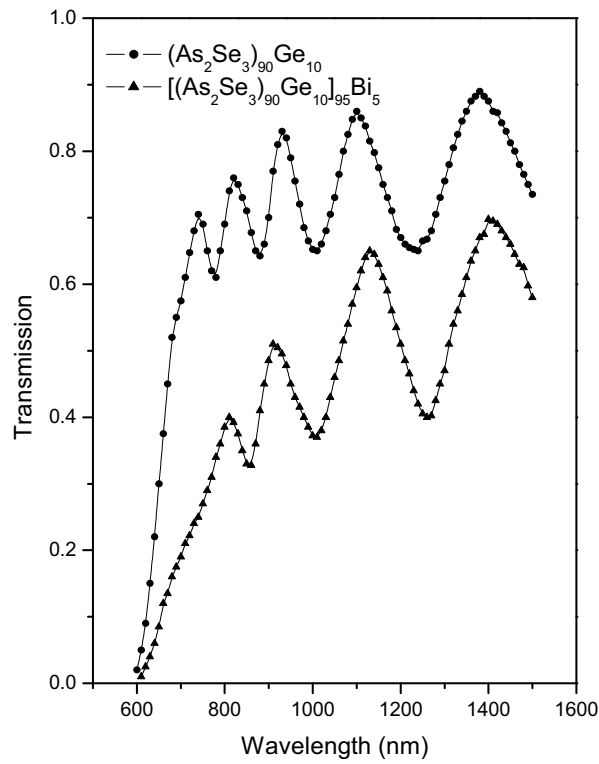
Figure 6.2.1 Transmission spectra for a-$[(As_2Se_3)_{90}Ge_{10}]_{95}M_5$ (M = Bi, Cd, Sn & Pb) thin films.

range 400 – 1500 nm were obtained using a double beam ultraviolet - visible - near infrared spectrophotometer (Hitachi-330).

6.2.3 Results

Optical transmission (T) is a very complex function and is strongly dependent on the absorption coefficient (α). Figure 6.2.1 shows the transmission spectra of amorphous $[(As_2Se_3)_{90}Ge_{10}]_{95}M_5$, (M = Bi, Cd, Sn & Pb) thin films. Refractive index (n) and extinction coefficient (k) have been calculated using Swanepoel technique given in chapter 2. The spectral distribution of refractive index and extinction coefficient is shown in figure 6.2.2. The values of n at 800 nm are given in table 6.2. The thickness of the thin films under investigation has been calculated using equation (2.22) and is given in table 6.2. The difference in thickness measured from thickness monitor and calculated from equation (2.22) lies with in ± 25 nm for all the films prepared.

According to single oscillator model proposed by Wemple-DiDomenico (WDD model) [9,10], the optical data could be described to an excellent approximation by the following expression

$$n^2(h\nu) = 1 + \frac{E_0 E_d}{E_0^2 - (h\nu)^2} \tag{6.8}$$

where $h\nu$ is photon energy, E_0 is single oscillator energy and E_d is dispersion energy which is a measure of the average strength of interband optical transitions. Plotting refractive index factor $(n^2 - 1)^{-1}$ against $(h\nu)^2$ allows us to determine the oscillator parameters by fitting a straight line to the points, as shown in figure 6.2.3. It is worth emphasizing the goodness of the fits to the large wavelength experimental data. The values of WDD dispersion parameters, E_0 and E_d, for all thin films were directly determined from the slope $(E_0 E_d)^{-1}$ and the intercept on the vertical axis (E_0 / E_d) of their corresponding least square straight lines. The values of these dispersion parameters are given in table 6.2. Nevertheless, it must be noted that the WDD model is only valid in transparent region, where the absorption coefficient of chalcogenide thin films takes values $\alpha \approx 0$. The detailed analysis of the dispersion of
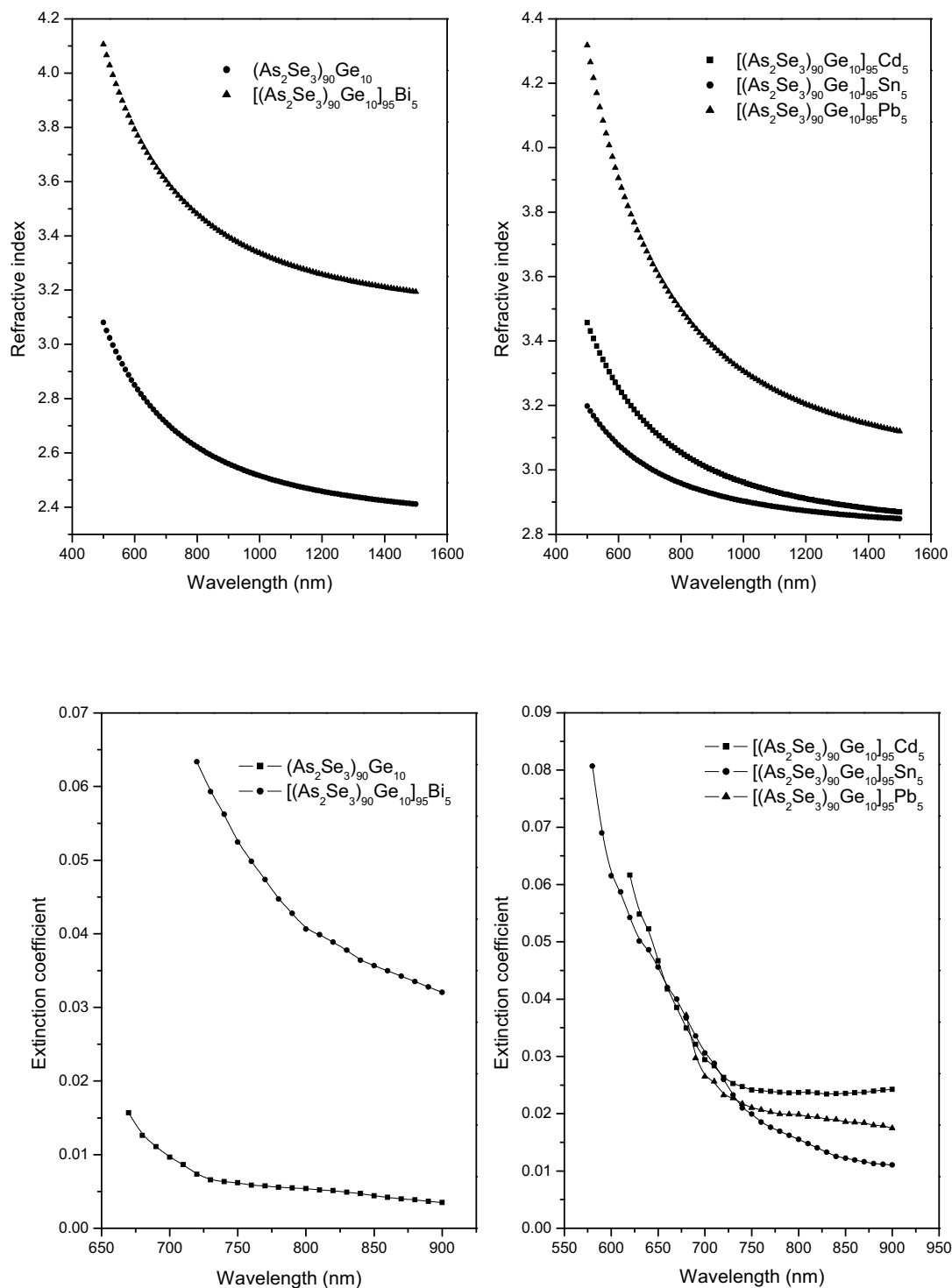
Figure 6.2.2 Plots of refractive index and extinction coefficient vs. wavelength (nm) for $[(As_2Se_3)_{90}Ge_{10}]_{95}M_5$ (M = Bi, Cd, Sn & Pb) thin films.
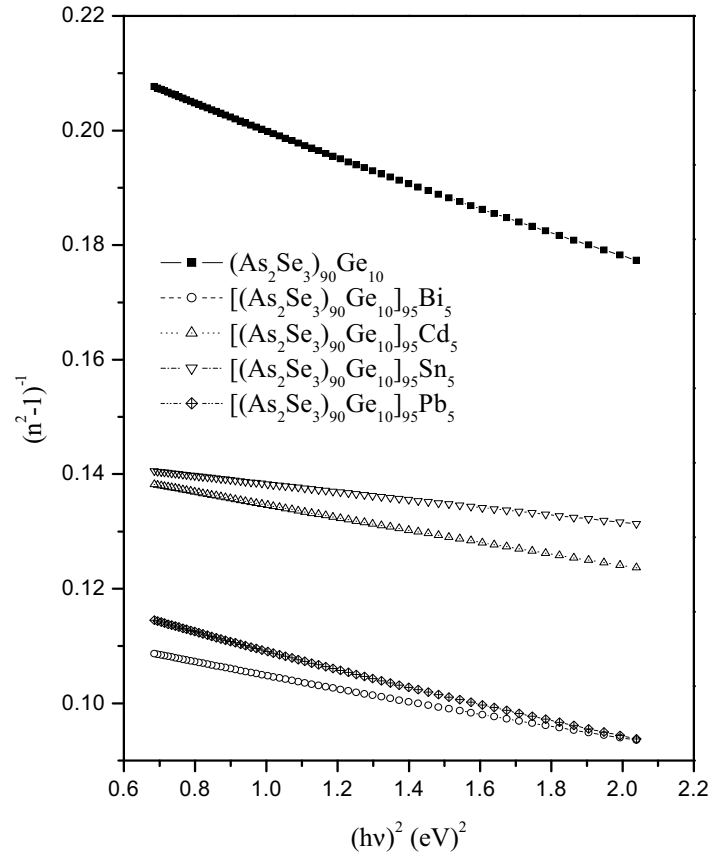
Figure 6.2.3 Plot of refractive index factor $(n^2 - 1)^{-1}$ versus $(h\nu)^2$ for $[(As_2Se_3)_{90}Ge_{10}]_{95}M_5$, (M = Bi, Cd, Sn & Pb), thin films.

refractive index, in terms of WDD model, throws very valuable light on the structure of material through the values of the dispersion energy parameter E_d. The parameter E_d is related to other physical parameters by the simple empirical relation proposed by WDD, i.e. $E_d = \beta N_c Z_a N_e$, where β is a two valued constant [9,10] with either an ionic or covalent value (for ionic materials $\beta = 0.26 \pm 0.03 \, eV$ and for covalent materials $\beta = 0.37 \pm 0.04 \, eV$), N_c is effective coordination number of cation nearest neighbour to anion, N_e is the effective number of valence electrons per anion.

The values for the static refractive index n_0 have been calculated from WDD dispersion parameters E_0 and E_d by using the formula

$$n_0 = \left(1 + \frac{E_d}{E_0}\right)^{1/2} \tag{6.9}$$

The values of n_0 are calculated by extrapolating the WDD dispersion equation to $h\nu \to 0$ {equation (6.8)} and are given in table 6.2. The high frequency dielectric constant (ε_∞) has been calculated from the relation $\varepsilon_\infty = (n_0)^2$ [11] and the obtained values are reported in table 6.2.

The absorption coefficient (α) for the thin films can be calculated using well-known relation (2.23). The variation of absorption coefficient with photon energy for $[(As_2Se_3)_{90}Ge_{10}]_{95}M_5$, (M = Bi, Cd, Sn and Pb), films is shown in figure 6.2.4. The optical band gap has been estimated from absorption coefficient data as a function of wavelength by using the Tauc relation [17]

$$\alpha h\nu = B(h\nu - E_g^{opt})^n \tag{6.10}$$

where B is the slope of Tauc edge called band tailing parameter that depends on the width of localized states in the band gap which are attributed to homopolar bonds in chalcogenide glasses. In the above equation $n = 1/2$ for a direct allowed transition, $n = 3/2$ for a direct forbidden transition, $n = 2$ for an indirect allowed transition and $n = 3$ for an indirect forbidden transition. E_g^{opt} is the optical band gap. This relationship allows us to estimate the value of optical band gap. Figure 6.2.5 shows the plot of $(\alpha h\nu)^{0.5}$ against $h\nu$. The values of E_g^{opt} can readily be calculated from the plot of
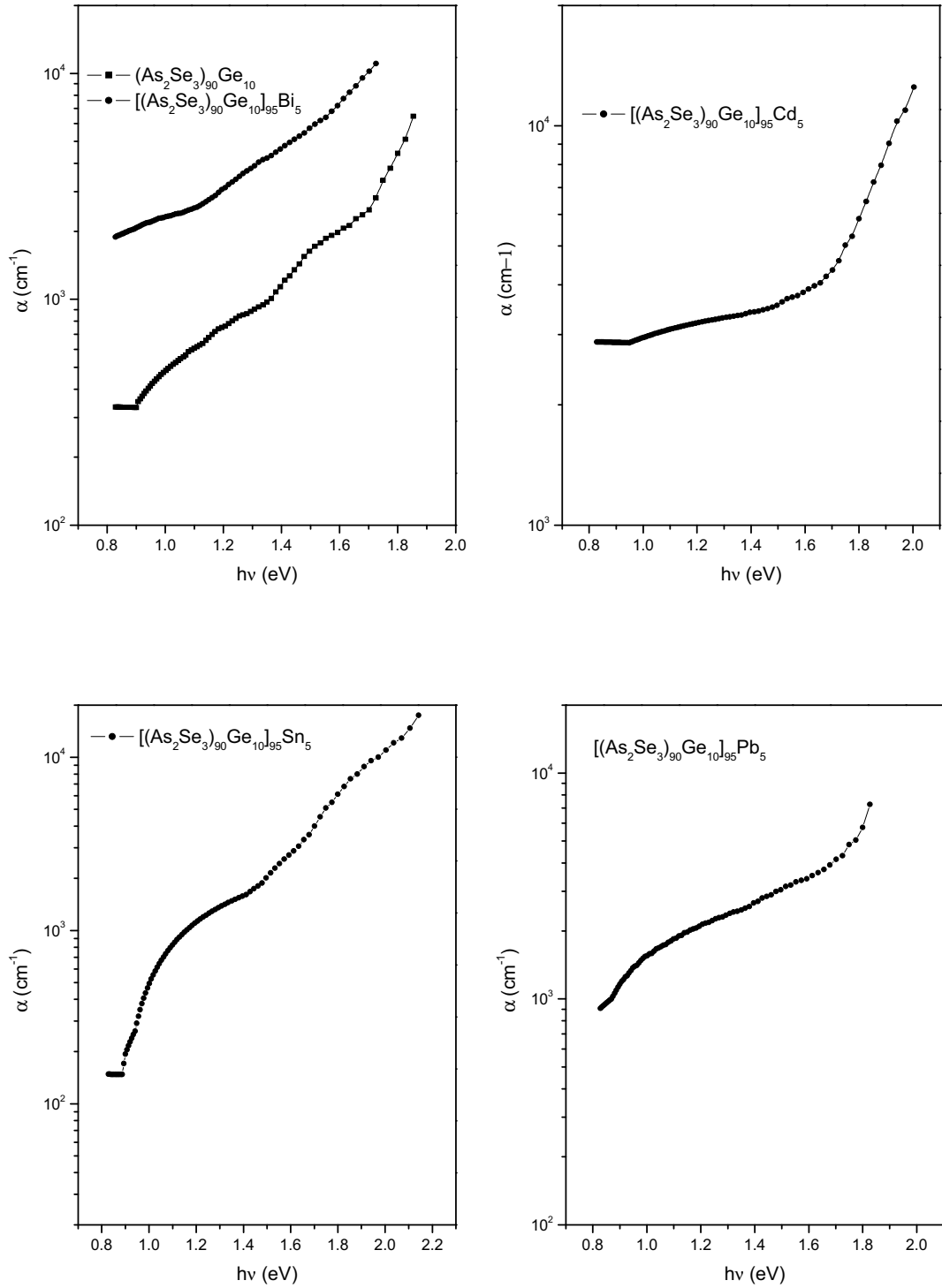
Figure 6.2.4 Plot of absorption coefficient (α) vs. $h\nu$ for a-[(As$_2$Se$_3$)$_{90}$Ge$_{10}$]$_{95}$M$_5$, (M = Bi, Cd, Sn & Pb), thin films.
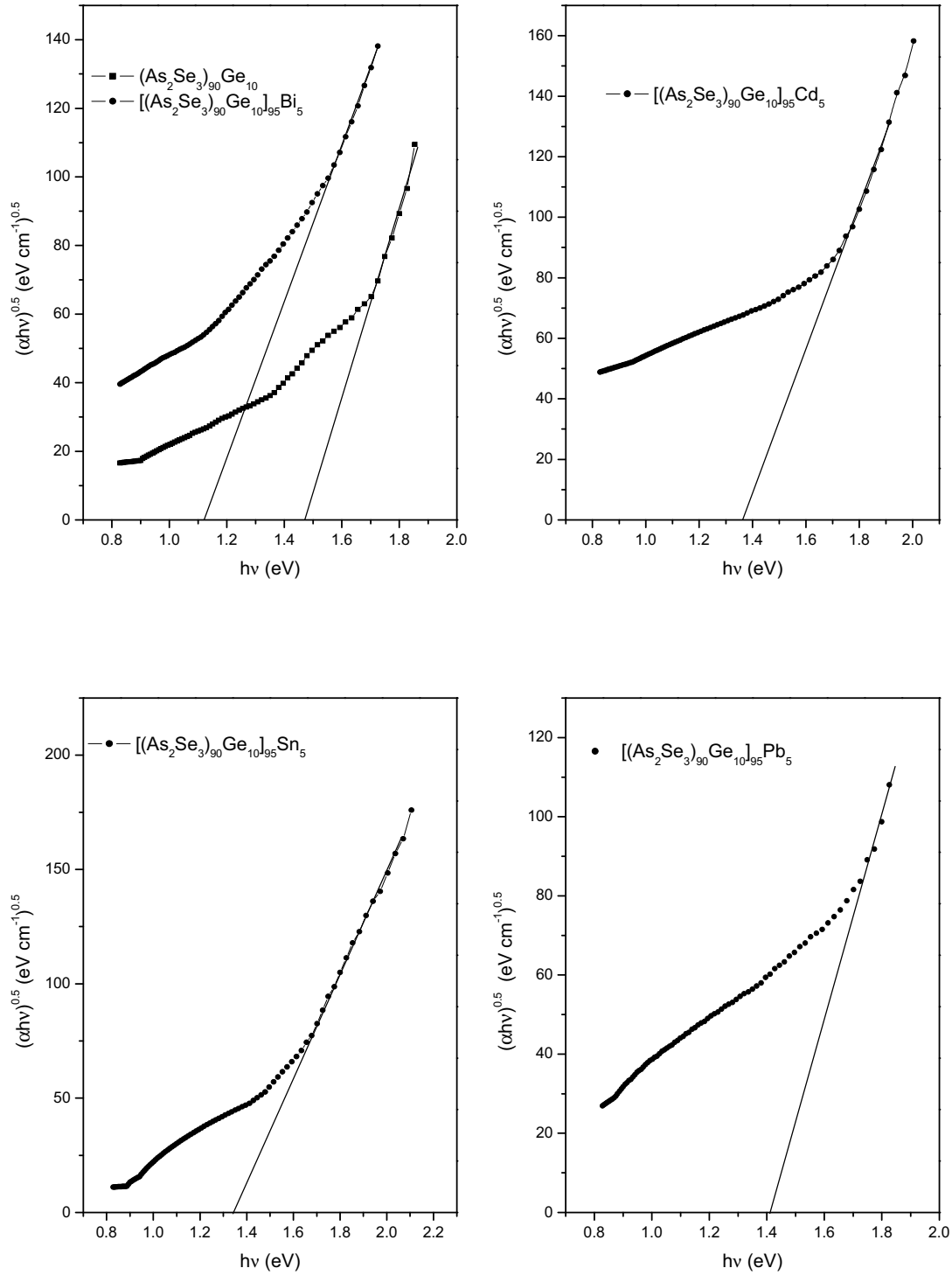
Figure 6.2.5 Plot of $(\alpha h\nu)^{1/2}$ vs. $h\nu$ for a-$[(As_2Se_3)_{90}Ge_{10}]_{95}M_5$ (M = Bi, Cd, Sn & Pb) thin films.
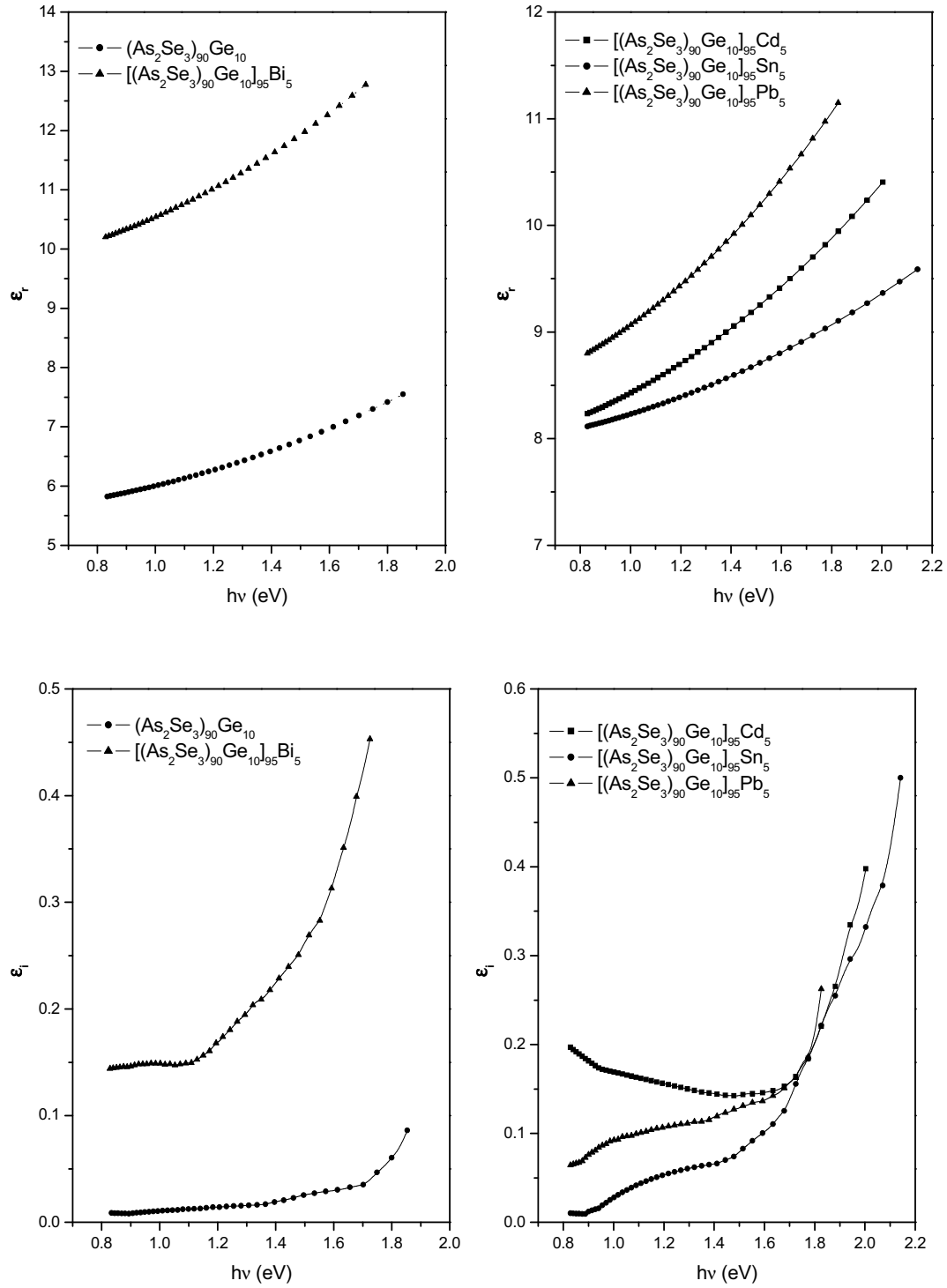
Figure 6.2.6 Plot of real part of dielectric constant (ε_r) and imaginary part of dielectric constant (ε_i) vs. $h\nu$ for a-[(As$_2$Se$_3$)$_{90}$Ge$_{10}$]$_{95}$M$_5$, (M = Bi, Cd, Sn & Pb), thin films.
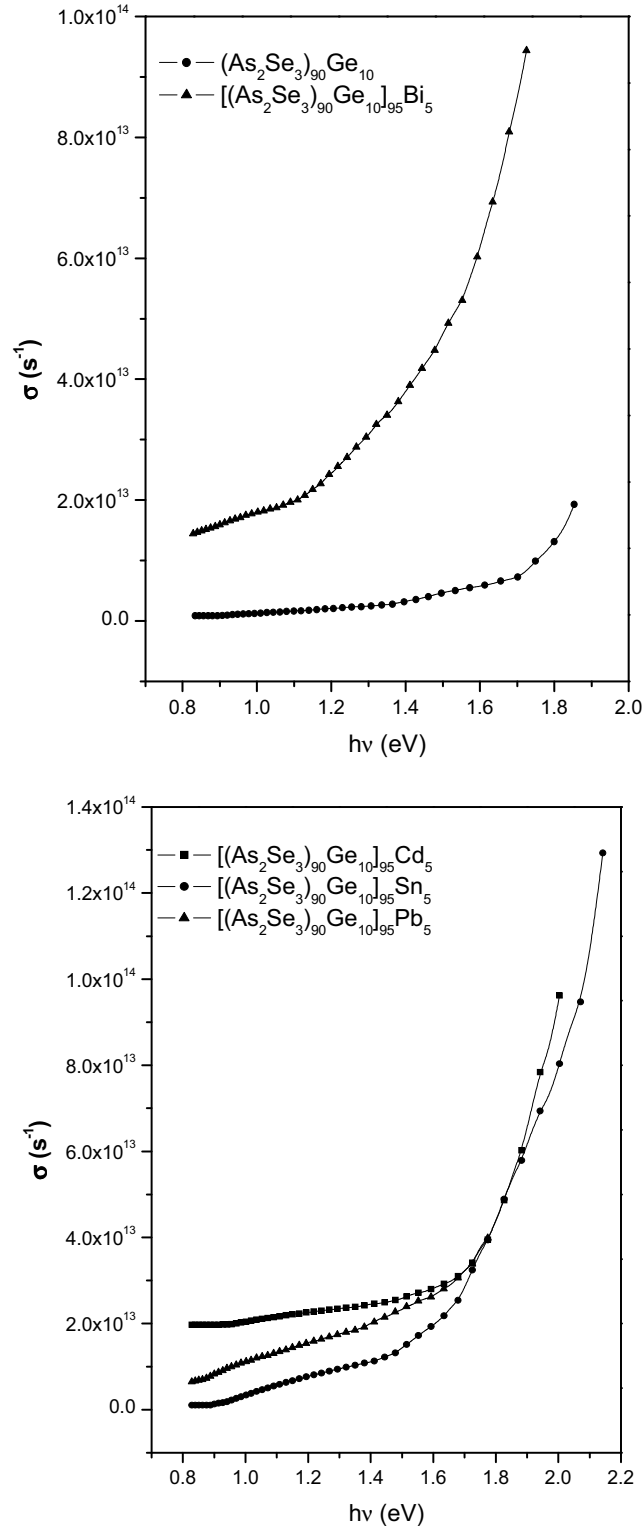
Figure 6.2.7 Plot of optical conductivity (σ) vs. $h\nu$ for *a*-$[(As_2Se_3)_{90}Ge_{10}]_{95}M_5$ (M = Bi, Cd, Sn & Pb) thin films.

$(\alpha h \nu)^{0.5}$ as a function of $h\nu$. The value of E_g^{opt} can be estimated by the intercept of the extrapolations to zero absorption with the photon energy axis $(\alpha h \nu)^{0.5} \rightarrow 0$. The obtained values of E_g^{opt} for indirect allowed transitions for the thin films under investigation are given in table 6.3.

Figure 6.2.6 shows the plot of dielectric constants (real and imaginary). The dielectric constant of $[(As_2Se_3)_{90}Ge_{10}]_{95}M_5$, where M = Bi, Cd, Sn and Pb, thin films can be calculated with the help of refractive index (n) and extinction coefficient (k) [19]. The real dielectric constant ε_r can be calculated from the relation $\varepsilon_r = n^2 - k^2$ and the imaginary dielectric constant ε_i can be calculated from the following relation $\varepsilon_i = 2nk$. The variation of both real and imaginary parts of dielectric constant with wavelength follows the same trend as that of refractive index and extinction coefficient. The optical parameters i.e. n, k, ε_r and ε_i decrease with increasing wavelength.

Figure 6.2.7 shows the variation of optical conductivity in terms of photon energy. The optical conductivity directly depends on the absorption coefficient and refractive index and has been determined from the relation [20]

$$\sigma = \alpha n c / 4\pi \qquad (6.11)$$

where c is the velocity of light, α is absorption coefficient and n is the refractive index.

6.2.4 Discussion

Spectral distribution of refractive index in figure 6.2.2 inferred that refractive index decreases with the increase of wavelength for the thin films under investigation. The decrease of refractive index with the increase of wavelength may be correlated with decrease of absorption coefficient. The decrease in the value of refractive index with wavelength shows the normal dispersion behaviour of the material. On the part of metal impurities addition to $(As_2Se_3)_{90}Ge_{10}$ thin films the refractive index has been found to have higher values.

This increase in the refractive index may be ascribed to increase of disorder in the structure, change in stoichiometry and internal strain caused by the addition of

Table 6.2 Values of rate of deposition (r), thickness (d), refractive index (n) at 800 nm, oscillator strength (E_0), dispersion energy (E_d), static refractive index (n_0) and high frequency dielectric constant (ε_∞) for a-$[(As_2Se_3)_{90}Ge_{10}]_{95}M_5$, where M = Bi, Cd, Sn & Pb, thin films.

Composition	r $(\overset{o}{A}/s)$	d (nm)	n	E_d (eV)	E_o (eV)	n_o	ε_∞
$(As_2Se_3)_{90}Ge_{10}$	13.2	900	2.64	15.07	3.01	2.45	6.01
$[(As_2Se_3)_{90}Ge_{10}]_{95}Bi_5$	13.7	700	3.48	24.05	2.56	3.22	10.4
$[(As_2Se_3)_{90}Ge_{10}]_{95}Cd_5$	13.0	846	3.06	19.74	2.76	2.86	8.18
$[(As_2Se_3)_{90}Ge_{10}]_{95}Sn_5$	12.8	711	2.96	22.05	2.82	2.97	8.82
$[(As_2Se_3)_{90}Ge_{10}]_{95}Pb_5$	13.4	929	3.49	22.72	2.84	3.00	9.00

Table 6.3 Values of optical band gap (E_g^{opt}), real part of dielectric constant (ε_r), imaginary part of dielectric constant (ε_i) and optical conductivity (σ) for a-$[(As_2Se_3)_{90}Ge_{10}]_{95}M_5$, where M = Bi, Cd, Sn & Pb, thin films at 800 nm.

Composition	E_g^{opt} (eV)	ε_r	ε_i	σ (s^{-1}) x 10^{13}
$(As_2Se_3)_{90}Ge_{10}$	1.46 ± 0.01	6.97	0.062	1.2
$[(As_2Se_3)_{90}Ge_{10}]_{95}Bi_5$	1.12 ± 0.01	12.11	0.283	5.3
$[(As_2Se_3)_{90}Ge_{10}]_{95}Cd_5$	1.36 ± 0.01	9.328	0.145	2.7
$[(As_2Se_3)_{90}Ge_{10}]_{95}Sn_5$	1.34 ± 0.01	8.75	0.092	1.7
$[(As_2Se_3)_{90}Ge_{10}]_{95}Pb_5$	1.41 ± 0.01	12.23	0.139	2.6

metal impurities. The individual increase in different metal added thin films may be explained on the basis of polarizability. Larger the atomic radius of the atom larger will be its polarizability and consequently according to Lorentz-Lorenz relation between refractive index and polarizability larger will be the refractive index. Lorentz-Lorenz relation [31] is

$$\frac{n^2 - 1}{n^2 + 2} = \frac{1}{3\varepsilon_0} \sum_i N_i \alpha_{pi} \qquad (6.12)$$

where ε_0 is the vacuum permittivity, N_i is the number of polarizable units of type i per unit volume with polarizability α_{pi}. The atomic radii of different metals are Bi (1.52 Å), Cd (1.41 Å), Sn (1.40 Å) and Pb (1.54 Å) [32]. This is clear from table 6.2 that refractive index follows the same trend as that of the atomic radii for different impurity metals.

The dispersion of refractive index (spectral dependence) has been analyzed in terms of WDD model which is based on single effective oscillator approach. The high frequency properties of thin films under investigation could be treated as single oscillator. The calculated WDD parameters E_0 and E_d are in good agreement with the earlier reported results [9,10]. This has been observed that the single oscillator parameter , E_0, is in concord to the relation i.e. $E_0 \approx 2 \times E_g^{opt}$ obtained by Tanaka [12] when studying vitreous films having a composition As_xS_{100-x}, and which subsequently hold for other vitreous chalcogenide thin films [13,14].

Analysis of the optical absorption spectra is one of the most productive tools for understanding and developing the energy band diagram of both crystalline and amorphous materials. It is well known that the optical gap of amorphous semiconducting alloys strongly depends on their composition. Optical absorption in solids or liquids can occur by several different mechanisms, all of which involve coupling of the electric field vector of the incident radiation to dipole moments in the material and hence a consequent transfer of energy.

The excitation of electrons from filled to empty states by photon absorption is of primary importance in semiconductors. In crystals, the transition can be "direct" or "indirect", the later being phonon-assisted. The form of the absorption edge depends on the symmetry of the wave functions and the effective masses of electrons and holes

147

at the edges of the valence and conduction bands. In present study, as there is no sharp increase in the absorption coefficient near the fundamental absorption edge it indicates an indirect band transition in forbidden gap [33]. The optical band gap has been estimated by Tauc's extrapolation and found to decrease with the addition of metal impurities. In the fundamental absorption region, the absorption is due to the transition from the top of valence band to the bottom of the conduction band. Addition of metal impurities in $(As_2Se_3)_{90}Ge_{10}$ thin films may cause an increase in the density of states in the valence band. The addition of metal impurities may also create localized states in the band gap [34]. This will lead to a shift in the absorption edge towards lower photon energy and consequently decrease in the optical energy gap can be explained by the increased tailing [35] of the conduction band edge into the gap due to the addition of metal impurities.

Optical response of the material is most conveniently studied in terms of optical conductivity (σ). It has the dimensions of frequency which are valid only in Gaussian system of units. With the addition of metal impurities the optical conductivity shifts towards the lower photon energy side. This may be due to the fact that optical conductivity directly depends on the absorption coefficient of the thin film. The optical conductivity found has higher values for impurity added thin films; the Bi added thin film having the largest value.

6.2.5 Conclusion

The optical properties of amorphous $[(As_2Se_3)_{90}Ge_{10}]_{95}M_5$ thin films (M = Bi, Cd, Sn and Pb), prepared by thermal evaporation, have been determined from their corresponding transmission spectra taken at normal incidence in the spectral range 400-1500 nm. Swanepoel's envelop method has been employed to measure the thickness and refractive index of the thin films. This has been found that refractive index increases with the addition of metal impurities to $(As_2Se_3)_{90}Ge_{10}$ thin films. The increase of refractive index has been explained on the basis of increase in the polarizability by larger metal atoms. The dispersion of refractive index has been analyzed using Wemple-DiDomenico single oscillator model. Dispersion parameter E_0 is in concordance with Tanaka's relation. The transition in band gap has been found to be of indirect type and optical band gap has been determined from the

Tauc's extrapolation method. The optical band gap has been found to decrease with the addition of metal impurities. The decrease in the optical band gap has been explained on the basis of increase in the density of states in the valence band. The dielectric constant and optical conductivity have been determined and for metal added thin films these are having higher values.

References

1. Phillips J C, Thorpe M F 1985 *Solid State Commun.* **53** 699

2. Thorpe M F and Tichy L 2001 *Properties and Applications of Amorphous Materials* (London: Kluwer academic Publishers)

3. Boolchand P, Feng X and Bresser W J 2001 *J. Non-Cryst. Solids* **293-295** 348

4. El-Sayed S M, Amin G A M 2001 *Vacuum* **62** 353

5. Mott N F, Davis E A 1979 *Electronic Processes in Non-Crystalline Materials* (Oxford : Clarendon Press)

6. Marquez E, Ramirez-Malo J, Villares P, Jimenez-Garay R, Ewen, P J S and Owen A E 1992 *J. Phys. D: Appl. Phys.* **25** 535

7. Swanepoel R 1983 *J. Phys. E : Sci. Instrum* **16** 1214

8. Marquez E, Bernal-Oliva A M, Gonzalez-Leal J M, Prieto-Alcon R, Ledesma A, Jimenez-Garay R, Martil I 1999 *Materials Chemistry and Physics* **60** 231

9. Wemple S H and DiDomenico M 1971 *Phys. Rev. B* **3** 1338

10. Wemple S H 1973 *Phys. Rev. B* **7** 3767

11. Tigau N, Ciupina V, Rusu G I, Prodan G, Vasile E 2005 *Rom. Journ. Phys.* **50** 859

12. Tanaka K 1980 *Thin Solid Films* **66** 271

13. Gonzalez-Leal J M, Ledesma A, Bernal-Oliva A M, Prieto-Alcon R, Marquez E, Angel J A and Carabe J 1999 *Material Letters* **39** 232

14. Kosa T I, Wagner T, Ewen P J S and Owen A E 1995 *Philo. Mag. B* **71** 311

15. Urbach R 1953 *Phys Rev* **92** 1324

16. Al-Ani S K J, Al-Hassany I H O and Al-Dahan Z T 1995 *J. Mater. Sci.* **30** 3720

17. Tauc J 1970 *The optical properties of solids* (Amsterdam: North-Holland)

18. Abdelghany A, Elsayed S N, Abou El Ela A H and Mousa N H 1996 *Vacuum* **47** 243

19. Goswami A 2005 *Thin Film Fundamental* (New Delhi: New Age International) p.413

20. Pankove J I 1975 *Optical Processes in Semiconductors* (New York: Dover)

21. Wang R P, Rode A V, Madden S J, Zha C J, Jarvis R A and Luther-Davies B 2007 *J. Non-Cryst. Solids* **353** 950

22. El-Nahass M M, El-Deeb A F, El-Sayed H E A and Hassanien A M 2006 *Optics & Laser Technology* **38** 146

23. Skordeva E, Christova K, Tzolov M and Dimitrova Z 1998 *Appl. Phys. A* **66** 103

24. Borisova Z U 1981 *Glassy Semiconductors* (New York: Plenum Press)

25. Ahmed E, Tomlinson R D, Pilkington R D, Hill A E, Ahmed W, Nasar Ali and Hassan I U 1998 *Thin Solid Films* **335** 54

26. Parlak M and Ercelebi C 1998 *Thin Solid Films* **322** 334

27. Pathinettam Padiyan D, Marikani A and Murali K R 2004 *Materials Chemistry and Physics* **88** 250

28. El-Samanoudy M M, 2003 *Thin Solid Films* **423** 201

29. Pattanaik A K and Srinivasan A 2004 *Semicond. Sci. Technol.* **19** 157

30. Katyal S C, Okano, Bando T and Suzuki M 1987 *J. Non-Cryst. Solids* **97 & 98** 1195

31. Gonzalez-Leal J M, Prieto-Alcon R, Angel J A and Marquez E 2003 *J. Non-Cryst. Solids* 315 134

32. Rao C N R, George M V, Mahanty J and Narasiman P T 1970 *A Handbook of Chemistry and Physics* (New Delhi: Affiliated East-West Press)

33. Venkata Subbaiah Y P, Pratap P, Reddy K T R, Mangalaraj D, Kim K and Junsin Y. 2007 *J. Phys. D: Appl. Phys.* **40** 3683

34. Barreau N, Marsillac S, Bernede J C, Ben nasrallah T and Belgacem S 2001 *Phys. Status Solidi (a)* **184** 179

35. Nagels P, Tichy L, Tiska A and Ticha H 1983 *J. Non-Cryst. Solids* **59–60** 1015

CHAPTER VII

Summary

Chalcogenide glasses form an important class of materials which are used in various solid state devices and in infrared optics. Here we have presented two chalcogenide glassy systems viz. $Ge_{10}Se_{90-x}Te_x$ (x = 0, 10, 20, 30, 40, 50) and $[(As_2Se_3)_{90}Ge_{10}]_{95}M_5$ (M = Bi, Cd, Pb, Sn). These two glassy systems were studied for their optical properties using UV-Vis-NIR spectroscopy. Moreover bonding arrangements in Ge-Se-Te system was studied using far-infrared transmission spectra. Ge-Se-Te system has also been studied for its physical properties and this is found that physical properties support the optical results.

Ge-Se-Te system has been studied for its structural properties using far-infrared transmission spectra. The addition of Te to $Ge_{10}Se_{90}$ shows that the far-IR transmission spectra shift a little towards the lower wavenumber side. The addition of Te in $Ge_{10}Se_{90}$ has shown the appearance of $GeTe_2$ and $GeTe_4$ molecular units and vibrations of Se-Te bond in $Se_{8-x}Te_x$ mixed rings. The results were explained in terms of the vibrations of the isolated molecular units. This has been observed that some of the Ge-Se and Se-Se bonds disappear leading to the formation of Se-Te and Ge-Te bonds. The existence of Ge-Ge bonds has not been observed as the compositions under study were chalcogen rich. The absorption peaks at 150 cm^{-1} (for *x ≥ 20* at. %) confirms the formation of Te-Te bonds. However these appear for higher Te content compositions. The least formation of Te-Te bonds may be attributed to their lower relative probability of formation and also to excess of Te-Te bonds according to CBA.

Different parameters related to optical properties were calculated for vacuum evaporated thin films of $Ge_{10}Se_{90-x}Te_x$ glassy alloy. UV-Vis-NIR spectroscopy (transmission spectrum) has been used for the analysis of optical properties of Ge-Se-Te system. Transmission spectra show that with the addition of Te content there is red shift in the transmission. Envelop method has been employed for the calculation of refractive index. Refractive index has been found to decrease with the increase of wavelength showing that material exhibits normal dispersion. The refractive index increases sharply for higher content of Te addition. Absorption coefficient lies in the range 10^{-3} – 10^{-4} cm^{-1}. Optical band gap has been calculated from Tauc's extrapolation method and found to decrease with the increase of Te content. The optical band gap changes from 1.87 eV to 1.03 eV for x = 0 to x = 50 respectively in $Ge_{10}Se_{90-x}Te_x$ thin films. The decrease of optical band gap has been explained on the

basis of decrease of bond energy of the system and electronegativity concept. Dielectric constants (real and imaginary) and optical conductivity has been calculated using values of n, k and α. Dielectric constants were found to decrease with the increase of wavelength and similar for optical conductivity.

The effect of deposition parameters viz. thickness, substrate type and substrate temperature have been studied for the optical properties of $Ge_{10}Se_{90-x}Te_x$ thin films. With the increase of thickness (500 nm - 1100 nm) the optical band gap has been found to increase while no significant change has been observed for refractive index with in experimental errors. For different substrate used in deposition of thin films the refractive index follows the order as $n_{mica} > n_{microscopic\ glass} > n_{quartz}$. The optical band gap for mica substrate is the smallest whereas no significant change has been observed for microscopic glass and quartz substrate. With the increase of substrate temperature (i.e. from 303 K – 423 K) refractive index remains unchanged while optical band gap decreases.

The average coordination number, density, molar volume, compactness; lone pair of electrons, theoretical optical band gap and average heat of atomization, have been calculated for $Ge_{10}Se_{90-x}Te_x$ glassy alloys. The coordination number increases with the addition of Te on replacing Se. The density and molar volume increases monotonically with the increasing content of Te. Compactness has been found to increase with the increase of Te content showing that structure is becoming rigid. The number of lone pair of electrons decreases with the addition of Te but still, in the present study, has a minimum value 3.1 which is much more than 1 as suggested by Liang for good glass former indicating that the compositions under investigation are good glass forming. The theoretical optical band gap has also been found to decrease with the increase of Te content and is in concordance with the experimental optical band gap. Average heat of atomization ($\overline{H_s}$) which is a measure of the average binding energy decreases with increase of Te content. The decrease of optical band gap may be correlated with the decrease of average binding energy of the system.

The optical properties of vacuum evaporated $[(As_2Se_3)_{90}Ge_{10}]_{95}M_5$ (M = Bi, Cd, Sn and Pb) thin films have been determined from their corresponding transmission spectra using UV-Vis-NIR spectroscopy. Swanepoel's envelop method

has been employed to measure the thickness and refractive index of the thin films. This has been found that refractive index increases with the addition of metal impurities to $(As_2Se_3)_{90}Ge_{10}$ thin films. The increase of refractive index has been explained on the basis of increase in the polarizability by larger metal atoms. The dispersion of refractive index has been analyzed using Wemple-DiDomenico single oscillator model and this has been found that dispersion parameter E_0 is in concordance with Tanaka's empirical relation. The transition in band gap has been found to be of indirect type and optical band gap has been determined from the Tauc's extrapolation method. The optical band gap has been found to decrease with the addition of metal impurities. The decrease in the optical band gap has been explained on the basis of increase in the density of states in the valence band. The dielectric constant and optical conductivity have been determined and these are having higher values for metal added thin films.